Author's personal copy

CHAPTER THREE

Some Recent Developments in the Simplest-Level Electron Nuclear Dynamics Method: Theory, Code Implementation, and Applications to Chemical Dynamics

Christopher Stopera, Thomas V. Grimes, Patrick M. McLaurin, Austin Privett, Jorge A. Morales[1]

Department of Chemistry and Biochemistry, Texas Tech University, Lubbock, Texas, USA
[1]Corresponding author: e-mail address: jorge.morales@ttu.edu

Contents

Advances in Quantum Chemistry, Volume 66
ISSN 0065-3276
http://dx.doi.org/10.1016/B978-0-12-408099-7.00003-9

© 2013 Elsevier Inc.
All rights reserved.

Author's personal copy

Abstract

Electron nuclear dynamics (END) is a time-dependent, variational, direct, and nonadiabatic dynamics method that treats nuclei and electrons simultaneously. While admitting a hierarchy of realizations, the simplest-level END (SLEND), which adopts nuclear classical dynamics and an electronic Thouless single-determinantal state, is the most utilized END version due to its feasibility. SLEND was successfully applied to various gas-phase reactions at intermediate and high energies. However, the SLEND reliance on nuclear classical dynamics alone and/or its lack of dynamical electron correlation *inter alia* impedes its reliable utilization for more challenging systems. With higher level END realizations overcoming those shortcomings at high computational cost, we advocate solutions that retain SLEND's feasibility due to classical dynamics and the single-determinantal representation. Thus, we advance a novel SLEND/density functional theory (DFT) method wherein electron correlation is included within a feasible single-determinantal representation through DFT procedures. Additionally, we extend a coherent states (CS) quantum reconstruction procedure (CSQRP) to recover some quantum effects from the nuclear classical dynamics; CSQRP now features harmonic, Morse, rotational, and electronic CS. Finally, we improve the SLEND performance by incorporating effective core potentials and implementing our models in our cutting-edge code PACE. The latter features parallel programming and an environment for rapid method development. The new SLEND developments are applied to various gas-phase systems at intermediate and high energies including proton–molecule collisions and Diels–Alder, S_N2, and proton cancer therapy reactions.

1. INTRODUCTION

The electron nuclear dynamics (END) theory created by Deumens and Öhrn[1–3] is a time-dependent, variational, nonadiabatic, and direct-dynamics method that treats the nuclear and electronic degrees of freedom concurrently. Direct dynamics is a class of methods that computes the potential energy and forces of a system "on the fly," just during the actual computation of the dynamics.[4–8] This has the benefit of avoiding the costly construction of global potential energy surfaces (PESs) prior to the dynamics' computation, a task required by more traditional dynamics methods such as quasi-classical trajectory (QCT) method[9] and the close-coupling method and its many approximations (e.g., the infinite-order sudden (IOS) approximation).[10] As a nonadiabatic method, END is not, in principle, strictly limited to a single electronic state. This allows for the accurate modeling of electron excitation processes and electron transfer (ET) reactions.

END entails the application of the time-dependent variational principle (TDVP)[11] to a trial wavefunction, $|\Psi_{\mathrm{END}}\rangle$, that describes both the nuclear

Author's personal copy

and the electronic degrees of freedom. Within the TDVP, END dynamical equations are obtained by imposing stationarity on the quantum action A_{END}

$$A_{\mathrm{END}}\left[\Psi_{\mathrm{END}},\Psi^{*}_{\mathrm{END}}\right]=\int_{t_{\mathrm{i}}}^{t_{\mathrm{f}}}L_{\mathrm{END}}\left[\Psi_{\mathrm{END}}(t),\Psi^{*}_{\mathrm{END}}(t)\right]\mathrm{d}t, \tag{3.1}$$

that is $\delta A_{\mathrm{END}}=0$, along with the end-point boundary conditions $\delta|\Psi_{\mathrm{END}}(t_{\mathrm{i}})\rangle=\delta|\Psi_{\mathrm{END}}(t_{\mathrm{f}})\rangle=0$. In Eq. (3.1), L_{END} is the quantum Lagrangian,[11]

$$L_{\mathrm{END}}\left[\Psi_{\mathrm{END}},\Psi^{*}_{\mathrm{END}}\right]=\frac{\langle\Psi_{\mathrm{END}}|\mathrm{i}\frac{\partial}{\partial t}-\hat{H}_{\mathrm{Total}}|\Psi_{\mathrm{END}}\rangle}{\langle\Psi_{\mathrm{END}}|\Psi_{\mathrm{END}}\rangle} \tag{3.2}$$

with the total Hamiltonian $\hat{H}_{\mathrm{Total}}$. This procedure leads to a set of Euler–Lagrange equations for the variational parameters in $|\Psi_{\mathrm{END}}\rangle$ that constitutes the END equations of motion. In its conception, END is a general dynamics framework that admits a hierarchy of methods whose level of sophistication is determined by the choice of the trial wavefunction $|\Psi_{\mathrm{END}}\rangle$.[3] The simplest-level END (SLEND) chooses a trial wavefunction $|\Psi_{\mathrm{SLEND}}\rangle=|\Psi_{\mathrm{N}}\rangle|\Psi_{\mathrm{e}}\rangle$ having nuclear $|\Psi_{\mathrm{N}}\rangle$ and electronic $|\Psi_{\mathrm{e}}\rangle$ parts of single-configurational forms. While that scheme admits various types of functions for $|\Psi_{\mathrm{N}}\rangle$ and $|\Psi_{\mathrm{e}}\rangle$, the standard choices in SLEND are a product of frozen-width Gaussian wave packets and an unrestricted single-determinantal state, respectively. Moreover, the Gaussian wave packets in SLEND are taken in the zero-width limit, which results in a nuclear classical dynamics coupled to the electronic quantum dynamics.

For the propagation of the nuclear dynamics, each SLEND wave packet lends its defining variables, the center position and momentum, as the natural parameters for the TDVP treatment. For the propagation of the electronic dynamics, the SLEND single-determinantal state could be parameterized by the atomic coefficients of its molecular spin orbitals (MSOs). However, since those atomic coefficients can be changed via a unitary transformation among the occupied MSO while leaving the state unchanged, the atomic coefficients are a set of redundant parameters; the latter not only lack a one-to-one mapping with the states but also exhibit numerical instabilities during dynamical evolution.[12–14] For this reason, SLEND adopts a single-determinantal state in the Thouless representation.[15] In that scheme, a single-determinantal state is defined in terms of a set of complex-valued, continuous, and nonredundant (or minimal) parameters that remove the aforesaid numerical instabilities during dynamical evolution. (Details of the Thouless single-determinantal state and its parameterization are given in Section 3.)

Author's personal copy

While a Gaussian wave packet and a Thouless single-determinantal state are different types of functions, both nevertheless belong to a vast category of functions named coherent states (CS). In its most accepted definition,[16] CS are a set of functions that are continuous with regard to a set of (real or complex) parameters and that satisfy the resolution of identity with a positive measure. These two defining properties and their nonzero overlap between two CSs render the CS set overcomplete. Each SLEND Gaussian wave packet is a member of the canonical CS[17] set associated with the harmonic oscillator Hamiltonian; in this case, the wave packet position and momentum are the CS parameters. The Thouless single-determinantal state is a member of the Thouless CS[16] set associated with the electronic Hamiltonian; in this case, the aforesaid Thouless parameters defining the state are the CS parameters. Other types of CS sets of course exist[16] as will be discussed in detail in Section 3 (cf. Fig. 3.1). Due to their overcompleteness in terms of continuous parameters, CS sets have found fruitful use in the mathematical formulation of theories and models in such diverse fields as mathematical physics, condensed matter theory, atomic physics, nuclear physics, and quantum field theory.[16] The use of CS sets in chemical dynamics has been more restrained and mostly limited to employing *only* the canonical CS for the nuclear motion *alone* in a *nondirect-dynamics* context. In that scheme, it is worth mentioning the wave packet semi-classical dynamics by Heller,[18] the canonical CS representation of the semi-classical propagator by Herman and Kluk,[19,20] and the recovery of quantum vibrational excitation probabilities from classical mechanics with the canonical CS in the distribution of exact energy transfer (DECENT) method by Giese and Gentry.[21] In contrast, SLEND has augmented the use of CS in chemical dynamics by merging the traditional canonical CS

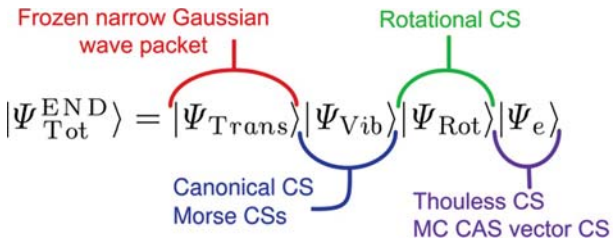

Figure 3.1 Scheme of various types of coherent state (CS) sets that can be associated with an END method having a nuclear classical description. The nuclear part of the total wavefunction is factored out into translational, vibrational, and rotational parts under standard approximations. The electronic Thouless CS corresponds to the SLEND case.

Author's personal copy

for *nuclei* with the less usual Thouless CS for *electrons* to obtain a *direct-dynamics* method in the TDVP framework. However, the originality of SLEND with CS is by no means limited to an ingenious utilization of the canonical and Thouless CS to represent trial wavefunctions under TDVP. For instance, as stated earlier, SLEND acquires a nuclear classical dynamics through the zero-width limit applied to its Gaussian wave packets, now reinterpreted as canonical CS. However, at any time of a SLEND evolution, the finite-width wave packets (or canonical CS) that would correspond to the SLEND nuclear classical mechanics can be reconstructed so that their quantum effects faded out by the zero-width limit can be recovered. When such a CS quantum reconstruction procedure (CSQRP)[22] is applied to the vibrational degrees of freedom in the harmonic approximation, the above-mentioned DECENT method is rigorously obtained from the SLEND framework.[22–24] Moreover, that CSQRP can be further expanded by calling into play other types of CS for anharmonic vibrations[25] and for the rotations.[22,26] Such a general CSQRP to recover some quantum rotational and vibrational effects will be discussed in detail in Section 3.

Despite its deceiving simplicity, SLEND has been successfully applied to a multitude of scattering systems and chemical reactions in the gas phase. Due to its nuclear description, SLEND is mostly successful at intermediate ($10\,\text{eV} \leq E_{\text{Lab}} \leq 100\,\text{eV}$) and high ($100\,\text{eV} < E_{\text{Lab}}$) collision energies, where classical mechanics is mostly accurate and where some relevant quantum effects can be recovered accurately with the CSQRP. Additionally, the SLEND Thouless single-determinantal state provides a satisfactory quantum description for the electrons that can capture all the basic events in reactive processes (bond formations and breakings, electron excitations, electron transfers, etc.). In that manner, SLEND has been applied to proton–molecule ($H^+ + H_2$,[23,24] $H^+ + CH_4$,[27] $H^+ + H_2O$,[28] $H^+ + C_2H_2$,[29,30] $H^+ + HF$,[31] $H^+ + CF_4$,[32] $H^+ + N_2$,[33] $H^+ + CO$,[34] and $H^+ + NO$[25]), hydrogen–molecule ($H + D_2$[35] and $H + HOD$[36]), and molecule-molecule reactions ($D_2 + NH_3$,[37] S_N2, Diels–Alder, and proton cancer therapy reactions—see Section 5 for the last three cases), *inter alia*. The SLEND dynamical properties predicted for the above systems showed good agreement with their experimental counterparts and include rainbow scattering angle predictions,[24,25,27,30,33,34] nonelectron-transfer (NET) proton–molecule vibrational energy transfers,[24,28,33] NET total differential cross sections (DCSs),[27,28,30] NET state-to-state vibrational DCSs,[24,25,33,34] NET projectile energy loss spectra,[25,33] and total ET DCSs[28] and integral cross sections (ICSs).[24,27,30]

Author's personal copy

While accurate with the aforesaid systems, SLEND may perform unsatisfactorily in situations that are more challenging. In regard to the electronic part, the insufficient inclusion of electron correlation effects[38] (especially of dynamical correlation) in the SLEND single-determinantal wavefunction $|\Psi_e\rangle$ should be corrected if a very accurate chemical description is sought. Therefore, efforts[39–43] have been made to move END beyond the SLEND single-determinantal representation by adopting more sophisticated electronic wavefunctions $|\Psi_e\rangle$ that progressively include higher degrees of electron correlation. Such an approach lays out the ladder of END realizations[3] from the lowest SLEND to the highest fully correlated END rungs. That scheme parallels wavefunction-based approaches in time-independent electronic structure that systematically include electron correlation through clearly defined procedures for wavefunctions' improvement.[38] Thus, while still keeping a nuclear classical description, the electronic multiconfiguration (MC) complete-active-space (CAS)[38] END (MCCASEND)[3,39] and the coupled-cluster (CC)[44] END (CCEND)[43] methods have been proposed. (CCEND required a modification of the TDVP due to the use of the CC ansatz.) In regard to the nuclear part, SLEND classical dynamics, even augmented with the CSQRP, is incapable of describing classically forbidden phenomena such as nuclear tunneling. In that case, the SLEND nuclear wavefunction $|\Psi_N\rangle$ comprising frozen-width Gaussian wave packets should be substituted by a nuclear wavefunction analogous to the electronic wavefunction of MCCASEND or CCEND but now containing nuclear molecular orbitals (cf. Refs. 45–47). Thus, by employing MC wavefunctions for both nuclei and electrons, the total multiconfiguration electron nuclear dynamics (MCEND)[40–42] method has been formulated and implemented.

Undoubtedly, the discussed high-level END realizations beyond SLEND have the potential of providing exceedingly accurate chemical descriptions. However, those realizations are difficult to implement and expensive to compute (for instance, total MCEND has been applied only to the small LiH molecule,[40] whereas electronic MCCASEND and CCEND remain unimplemented and therefore unapplied to any system). The limited feasibility of the high-level END realizations bodes ill in view of the great potential of END for studying high-energy chemical reactions involving large biochemical molecules, as is the case in proton cancer therapy[48] just to mention one example. While we keep a keen interest in the high-level END realizations, we also realize that feasible END applications to large systems will be mostly (if not only) possible within an improved SLEND framework. For that reason, we have concentrated our recent

Author's personal copy

research efforts to further enhance SLEND in order to overcome or at least mitigate its aforesaid shortcomings and make SLEND applicable to more challenging systems. For instance, in regard to the SLEND deficiency in electronic correlation, we have implemented the novel END/density functional theory (DFT) method,[49] where electron correlation effects are incorporated into END through established time-dependent Kohn–Sham (KS) DFT (TDKSDFT) procedures[50] while preserving a feasible single-determinantal representation like that of SLEND. In regard to the SLEND nuclear classical dynamics, we have further developed, and continue to develop, the CSQRP procedure to extend its scope of applications to nuclear anharmonic vibrations,[25] nuclear rotations,[22,26] and even the electronic degrees of freedom[51] (however, nuclear tunneling remains intractable with SLEND). Moreover, to facilitate further methods' programming and increase computer performance with large systems, we have implemented all our SLEND developments in our new parallel code PACE (Python Accelerated Coherent-states Electron nuclear dynamics)[52] that benefits from several cutting-edge technologies in computer science and atomic integral evaluation.[53] All our new SLEND developments are presented and discussed in full detail in the following sections. We sincerely hope that our new SLEND efforts will contribute to the enrichment of the END theory and inaugurate a new epoch of fruitful END application to challenging systems.

This chapter is organized as follows: in Section 2, we present the theoretical background of END, generally, and of SLEND, specifically, along with our theoretical advances; in Section 3, we present a discussion about various types of CS sets and their new involvement in SLEND and the CSQRP; in Section 4, we provide details about our new code PACE[52]; in Section 5, we present various applications of our discussed SLEND developments to a vast array of chemical reactions; and finally, in Section 6, we present some final remarks.

2. NEW DEVELOPMENTS IN THE SLEND THEORY

2.1. END and SLEND

As SLEND is one realization of the END theory,[1–3] it is helpful to briefly review END in general. END, as previously mentioned, involves the application of the TDVP[11] to a trial wavefunction. With a trial total wavefunction $|\Psi_{\mathrm{END}}\rangle$ parameterized by a set of generally complex parameters, $|\Psi_{\mathrm{END}}\rangle = |\boldsymbol{\lambda}\rangle$, where $\boldsymbol{\lambda} = (\lambda_1,\lambda_2,\lambda_3,\lambda_4,\ldots,\lambda_i,\ldots)$ and $\lambda_i = \lambda_i(t)$, the quantum Lagrangian L_{END} in Eq. (3.2) can be written as

Author's personal copy

$$L[\boldsymbol{\lambda},\boldsymbol{\lambda}^*] = \frac{\langle \boldsymbol{\lambda} | \mathrm{i}\frac{\partial}{\partial t} - \hat{H} | \boldsymbol{\lambda} \rangle}{\langle \boldsymbol{\lambda} | \boldsymbol{\lambda} \rangle} \tag{3.3}$$

In analogy with Hamilton's principle in classical mechanics,[54] the TDVP[11] states that a system evolves along a path in the parameter space whose quantum action A_{END} is stationary to a first-order variation in the parameters $\boldsymbol{\lambda}$,

$$\delta A_{\mathrm{END}}[\boldsymbol{\lambda},\boldsymbol{\lambda}^*] = \delta \int_{t_\mathrm{i}}^{t_\mathrm{f}} \mathrm{d}t L_{\mathrm{END}}[\boldsymbol{\lambda}(t),\boldsymbol{\lambda}^*(t)] = 0 \tag{3.4}$$

with end-point boundary conditions $\delta\,|\,\boldsymbol{\lambda}(t_\mathrm{i})\rangle = \delta\,|\,\boldsymbol{\lambda}(t_\mathrm{f})\rangle = 0$. The resultant Euler–Lagrange equations are of the form[1,2,11]:

$$\begin{aligned} \mathrm{i}\sum_a C_{ab}\dot{\lambda}_a &= \frac{\partial E_{\mathrm{Total}}}{\partial \lambda_b^*} \\ -\mathrm{i}\sum_a C_{ab}^*\dot{\lambda}_a^* &= \frac{\partial E_{\mathrm{Total}}}{\partial \lambda_b} \end{aligned} \tag{3.5}$$

where $E_{\mathrm{Total}} = \langle \boldsymbol{\lambda} | \hat{H}_{\mathrm{Total}} | \boldsymbol{\lambda} \rangle / \langle \boldsymbol{\lambda} | \boldsymbol{\lambda} \rangle$ is the total energy and $\mathbf{C}$ is a Hermitian matrix with elements

$$C_{ab} = \frac{\partial^2 \ln S}{\partial \lambda_a^* \partial \lambda_b} \tag{3.6}$$

and where S is the overlap, $S = \langle \boldsymbol{\lambda}\,|\,\boldsymbol{\lambda} \rangle$. Equation (3.5) can be rewritten in matrix form as

$$\begin{pmatrix} \mathrm{i}\mathbf{C} & 0 \\ 0 & -\mathrm{i}\mathbf{C} \end{pmatrix} \begin{pmatrix} \dot{\boldsymbol{\lambda}} \\ \dot{\boldsymbol{\lambda}}^* \end{pmatrix} = \begin{pmatrix} \partial E/\partial \dot{\boldsymbol{\lambda}}^* \\ \partial E/\partial \boldsymbol{\lambda} \end{pmatrix} \tag{3.7}$$

It can be proved[1,11] that Eq. (3.7) is the quantum generalization of the classical Hamilton equation in symplectic form[54] with conjugate variables $\mathbf{q}$ and $\mathbf{p}$ and classical Hamiltonian $H(\mathbf{q},\mathbf{p})$

$$\begin{pmatrix} \mathbf{I} & 0 \\ 0 & -\mathbf{I} \end{pmatrix} \begin{pmatrix} \dot{\mathbf{q}} \\ \dot{\mathbf{p}} \end{pmatrix} = \begin{pmatrix} \partial H/\partial \mathbf{p} \\ \partial H/\partial \mathbf{q} \end{pmatrix} \Rightarrow \begin{pmatrix} 0 & \mathbf{I} \\ -\mathbf{I} & 0 \end{pmatrix} \begin{pmatrix} \partial H/\partial \mathbf{q} \\ \partial H/\partial \mathbf{p} \end{pmatrix} = \begin{pmatrix} \dot{\mathbf{q}} \\ \dot{\mathbf{p}} \end{pmatrix} \tag{3.8}$$

More specifically, $\boldsymbol{\lambda}$ and $\boldsymbol{\lambda}^*$ are the complex quantum conjugate variables of Eq. (3.7), analogous to the real classical conjugate variables $\mathbf{q}$ and $\mathbf{p}$ of Eq. (3.8). Similarly, the complex matrix $\mathrm{i}\begin{pmatrix} \mathbf{C} & 0 \\ 0 & -\mathbf{C} \end{pmatrix}$ in Eq. (3.7) is the

Author's personal copy

quantum generalization of the real classical matrix $\begin{pmatrix} \mathbf{I} & 0 \\ 0 & -\mathbf{I} \end{pmatrix}$ in Eq. (3.8). The analogy between the quantum dynamical equation (3.7) and the classical Hamilton equation (3.8) is not surprising in view of the analogy between the quantum TDVP[11] and the classical Hamilton principle[54] that generate Eqs. (3.7) and (3.8), respectively. This analogy can be made even more apparent if the complex parameterization in terms of complex conjugate variables $\boldsymbol{\lambda}$ and $\boldsymbol{\lambda}^*$ is substituted by an equivalent parameterization in terms of real conjugate variables proportional to $\mathrm{Re}(\boldsymbol{\lambda})$ and $\mathrm{Im}(\boldsymbol{\lambda})$. That will be illustrated more conveniently when discussing the SLEND equations shortly.

The discussed parameterization does not impose any significant limitations on $|\Psi_{\mathrm{END}}\rangle = |\boldsymbol{\lambda}\rangle$. Indeed, it permits END to admit a hierarchy of methods dependent on the form of $|\Psi_{\mathrm{END}}\rangle = |\boldsymbol{\lambda}\rangle$. For instance, in the electronic MCCASEND,[39] the variational parameters of the electronic part $|\Psi_{\mathrm{e}}\rangle$ of $|\Psi_{\mathrm{END}}\rangle = |\boldsymbol{\lambda}\rangle$ are the linear coefficients of the configuration states and the parameters of the MSO within each configuration state. Similarly, in CCEND,[43] the variational parameters of the electronic part $|\Psi_{\mathrm{e}}\rangle$ in $|\Psi_{\mathrm{END}}\rangle = |\boldsymbol{\lambda}\rangle$ are the CC amplitudes.[43] These MCCAS and CC wavefunctions can be used for parameterizing the nuclear part $|\Psi_{\mathrm{N}}\rangle$ of $|\Psi_{\mathrm{END}}\rangle = |\boldsymbol{\lambda}\rangle$ as well. Yet, the predominant treatment of $|\Psi_{\mathrm{END}}\rangle$ is that of SLEND: a single-configuration description for both nuclei and electrons whose nuclear part $|\Psi_{\mathrm{N}}\rangle$ is a product of frozen-width Gaussian wave packets and whose electronic part $|\Psi_{\mathrm{e}}\rangle$ is a single-determinantal state.[1–3]

Propagation of the dynamics using Eq. (3.5) requires the inversion of the matrix $\mathbf{C}$: an operation that is impossible when $\mathbf{C}$ becomes singular as a result of two or more parameters $\boldsymbol{\lambda}$ becoming linearly dependent.[12–14] While linear dependency among SLEND nuclear wave packets' parameters is improbable, that situation is certainly likely among the parameters of an electronic single-determinantal state if those are not chosen carefully. In that situation, it is possible to use a pseudo-inverse of $\mathbf{C}$ to avoid numerical instabilities; however, this can result in integration errors growing without bound.[12,13] An alternative approach that avoids the latter problem is to parameterize the electronic trial wavefunction in such a way that its parameters remain linearly independent throughout the dynamics simulation. As anticipated in Section 1, that convenient feature and other advantages are achieved in SLEND by adopting the Thouless representation of a single-determinantal state[55] that involves a set of continuous and nonredundant parameters λ, usually referred to as the Thouless parameters $\mathbf{z}$.[1] Due precisely to those parameters' nonredundancy, the SLEND Thouless

Author's personal copy

single-determinantal state remains free of linear dependencies in its constituent molecular orbitals throughout its dynamics; in that way, the dynamics integration will not stumble upon numerical instabilities due to the inversion of $\mathbf{C}$. The nonredundant Thouless parameters also provide solutions to other problems closely related to that of the singularity; namely, they provide a one-to-one mapping with distinct nonequivalent single-determinantal states by excluding equivalent states generated by unitary transformation among the occupied molecular orbitals. In addition, the continuous nature of the Thouless parameters makes possible the expression of the generalized symplectic structure of Eq. (3.7) and ensures sufficient flexibility for the electronic wavefunction to vary smoothly and continuously during the simulation of taxing chemical reactions.

As discussed earlier, the SLEND trial total wavefunction $|\Psi_{\mathrm{SLEND}}\rangle$ is separated into single-configuration nuclear $|\Psi_{\mathrm{N}}\rangle$ and electronic $|\Psi_{\mathrm{e}}\rangle$ parts: $|\Psi_{\mathrm{SLEND}}\rangle = |\Psi_{\mathrm{N}}\rangle\,|\Psi_{\mathrm{e}}\rangle$. Having N_{N} nuclei, $|\Psi_{\mathrm{N}}\rangle$ is the direct product of $3N_{\mathrm{N}}$ 1D frozen-width Gaussian wave packets centered at the nuclear positions $\mathbf{R}$ with nuclear momenta $\mathbf{P}$, $|\Psi_{\mathrm{N}}\rangle = |\mathbf{R},\mathbf{P}\rangle$, each nucleus taking three 1D wave packets for its three position/motion variables. In configuration space with coordinates $\mathbf{X}$, $\langle\mathbf{X}|\Psi_{\mathrm{N}}\rangle$ is[56]:

$$\begin{aligned}\langle\mathbf{X}|\Psi_{\mathrm{N}}\rangle &= \langle\mathbf{X}|\mathbf{R},\mathbf{P}\rangle \\ &= \prod_{i=1}^{3N_{\mathrm{N}}}\langle X_i|R_i\,P_i\rangle \\ &= \prod_{i=1}^{3N_{\mathrm{N}}}\exp\left[-\left(\frac{X_i-R_i}{2\Delta R_i}\right)^2+\mathrm{i}P_i(X_i-R_i)\right]\end{aligned} \tag{3.9}$$

where $\mathbf{X}=(X_i)$, $\mathbf{R}=(R_i)$, and $\mathbf{P}=(P_i)$, $1\le i\le 3N_{\mathrm{N}}$; $\{\Delta R_i\}$ are the widths of the Gaussian wave packets. The nuclear positions $\mathbf{R}$ and momenta $\mathbf{P}$ are the variational parameters of $|\Psi_{\mathrm{N}}\rangle = |\mathbf{R},\mathbf{P}\rangle$ forming pairs of real conjugate variables $\{R_i,P_i\}$. For computational convenience, SLEND takes the zero-width limit in Eq. (3.9), $\Delta R_i \to 0\,\forall\, i$, after constructing the SLEND quantum Lagrangian, L_{SLEND}, thus rendering the nuclear dynamics as classical mechanics.

The SLEND electronic wavefunction $|\Psi_{\mathrm{e}}\rangle$ is a Thouless single-determinantal state[15] $|\Psi_{\mathrm{e}}\rangle = |\mathbf{z};\mathbf{R}\rangle$ parameterized in terms of the complex Thouless coefficients $\mathbf{z}$ and having an extra dependency upon $\mathbf{R}$ as explained shortly. Having N_{e} electrons in a basis of rank $K > N_{\mathrm{e}}$, the Thouless single-determinantal state $\langle\mathbf{x}|\Psi_{\mathrm{e}}\rangle$ in configuration space with coordinates $\mathbf{x}$ is:

Author's personal copy

$$\begin{aligned}\langle \mathbf{x}|\Psi_{\mathrm{e}}\rangle &= \langle \mathbf{x}|\mathbf{z};\mathbf{R}\rangle \\ &= \langle \mathbf{x}|\exp\left(\sum_{p=N_{\mathrm{e}}+1}^{K}\sum_{h=1}^{N_{\mathrm{e}}} z_{ph}b_p^{\dagger}b_h\right)|0\rangle \\ &= \det[\chi_h(x_h;\mathbf{z},\mathbf{R})]\end{aligned} \tag{3.10}$$

where the dynamical spin orbitals (DSOs), χ_h, are defined in terms of N_{e} occupied, ψ_h, and $K-N_{\mathrm{e}}$ virtual, ψ_p, reference MSOs[1–3]:

$$\chi_h(x_h;\mathbf{z},\mathbf{R}) = \psi_h(x_h;\mathbf{R}) + \sum_{p=N_{\mathrm{e}}+1}^{K} z_{ph}\psi_p(x_h;\mathbf{R}), \quad 1 \le h \le N_{\mathrm{e}} \tag{3.11}$$

In Eq. (3.10), $\langle \mathbf{x}\,|\,\Psi_{\mathrm{e}}\rangle$ is generated with the MSO particle–hole (virtual-occupied) operators $b_p^{\dagger}b_h$ from the Fermi reference single-determinantal state $|0\rangle$ having N_{e} occupied MSOs $\{\psi_h\}$: $|0\rangle = |\psi_1 \ldots \psi_h \ldots \psi_{N_{\mathrm{e}}}\rangle$. The Thouless coefficients $\mathbf{z}$ and $\mathbf{z}^*$ are the variational parameters of $|\,\Psi_{\mathrm{e}}\rangle = |\,\mathbf{z};\mathbf{R}\rangle$ forming pairs of complex conjugate variables $\{z_{ph},z_{ph}^*\}$. The MSOs $\{\psi_h,\psi_p\}$ are constructed with K standard atomic basis set functions $\{\phi_i(x_i;R_i)\}$ centered at the nuclear positions $\mathbf{R}=(R_i)$, usually through a time-independent Hartree–Fock (HF) calculation as explained shortly. For that reason, $\{\psi_h,\psi_p\}$, $\{\chi_h\}$, and $|\,\Psi_{\mathrm{e}}\rangle = |\,\mathbf{z};\mathbf{R}\rangle$ acquire a dependency upon $\mathbf{R}$. While the MSOs are orthogonal among themselves, the DSOs are not as can be easily proved from their definition in Eq. (3.11). The MSOs and DSOs are unrestricted with respect to spin blocks, and therefore, $|\,\Psi_{\mathrm{e}}\rangle = |\,\mathbf{z};\mathbf{R}\rangle$ is an unrestricted single-determinantal state. As such, $|\,\Psi_{\mathrm{e}}\rangle = |\,\mathbf{z};\mathbf{R}\rangle$ has some degree of nondynamical correlation that allows an adequate description of bond-forming and bond-breaking processes, at least qualitatively.

The SLEND quantum Lagrangian, L_{SLEND}, is obtained by setting $|\,\Psi_{\mathrm{SLEND}}\rangle = |\,\Psi_{\mathrm{N}}\rangle\,|\,\Psi_{\mathrm{e}}\rangle$ into Eq. (3.3) (cf. Eq. 3.2). Taking the zero-width limit in the wave packets of $|\,\Psi_{\mathrm{N}}\rangle$, Eq. (3.9), L_{SLEND} becomes (3.2)

$$\begin{aligned}L_{\mathrm{SLEND}}[\mathbf{R},\mathbf{P},\mathbf{z},\mathbf{z}^*] &= \sum_{j=1}^{3N_{\mathrm{N}}}\left[P_j + \frac{\mathrm{i}}{2}\left(\frac{\partial \ln S}{\partial R_j} - \frac{\partial \ln S}{\partial R'_j}\right)\right]\dot{R}_j \\ &\quad + \frac{\mathrm{i}}{2}\sum_{p=N_{\mathrm{e}}+1}^{K}\sum_{h=1}^{N_{\mathrm{e}}}\left(\frac{\partial \ln S}{\partial z_{ph}}\dot{z}_{ph} - \frac{\partial \ln S}{\partial z_{ph}^*}\dot{z}_{ph}^*\right) - E_{\mathrm{Total}}[\mathbf{R},\mathbf{P},\mathbf{z},\mathbf{z}^*]\end{aligned} \tag{3.12}$$

Author's personal copy

where the electronic overlap is $S = \langle \mathbf{z}', \mathbf{R}' | \mathbf{z}, \mathbf{R} \rangle$ and the total energy E_{Total} is

$$\begin{aligned} E_{\text{Total}}[\mathbf{R},\mathbf{P},\mathbf{z},\mathbf{z}^*] &= \langle \Psi_{\text{SLEND}} | \hat{H}_{\text{Total}} | \Psi_{\text{SLEND}} \rangle / \langle \Psi_{\text{SLEND}} | \Psi_{\text{SLEND}} \rangle \\ &= \sum_{i=1}^{N_{\text{N}}} \frac{\mathbf{P}_i^2}{2M_i} + \sum_{\substack{i=1 \\ j>1}}^{N_{\text{N}}} \frac{Z_i Z_j}{|\mathbf{R}_i - \mathbf{R}_j|} + E_{\text{e}}[\mathbf{R},\mathbf{z},\mathbf{z}^*] \end{aligned} \tag{3.13}$$

whose consecutive terms are the nuclear kinetic energy, $\sum_{i=1}^{N_{\text{N}}} \mathbf{P}_i^2 / 2M_i$, the nuclear repulsion potential energy, $\sum_{i=1, j>i}^{N_{\text{N}}} Z_i Z_j / |\mathbf{R}_i - \mathbf{R}_j|$, and the purely electronic energy, $E_{\text{e}}[\mathbf{R},\mathbf{z},\mathbf{z}^*] = \langle \Psi_{\text{e}} | \hat{H}_{\text{e}} | \Psi_{\text{e}} \rangle / \langle \Psi_{\text{e}} | \Psi_{\text{e}} \rangle$ (M_i and Z_i are the nuclear masses and charges and $\hat{H}_{\text{e}}$ is the purely electronic Hamiltonian). Using $\{\mathbf{R}(t), \mathbf{P}(t), \mathbf{z}(t), \mathbf{z}^*(t)\}$ as the SLEND variational parameters, application of the TDVP to the SLEND quantum action $A_{\text{SLEND}}[\mathbf{R},\mathbf{P},\mathbf{z},\mathbf{z}^*]$ associated with $L_{\text{SLEND}}[\mathbf{R},\mathbf{P},\mathbf{z},\mathbf{z}^*]$, Eq. (3.4), renders the SLEND dynamical equations as a set of Euler–Lagrange equations in matrix form[1–3]

$$\begin{bmatrix} \mathrm{i}\mathbf{C} & \mathbf{0} & \mathrm{i}\mathbf{C}_{\mathbf{R}} & \mathbf{0} \\ \mathbf{0} & -\mathrm{i}\mathbf{C}^* & -\mathrm{i}\mathbf{C}_{\mathbf{R}}^* & \mathbf{0} \\ \mathrm{i}\mathbf{C}_{\mathbf{R}}^\dagger & -\mathrm{i}\mathbf{C}_{\mathbf{R}}^{\mathrm{T}} & \mathbf{C}_{\mathbf{RR}} & -\mathbf{I} \\ \mathbf{0} & \mathbf{0} & \mathbf{I} & \mathbf{0} \end{bmatrix} \begin{bmatrix} \frac{\mathrm{d}\mathbf{z}}{\mathrm{d}t} \\ \frac{\mathrm{d}\mathbf{z}^*}{\mathrm{d}t} \\ \frac{\mathrm{d}\mathbf{R}}{\mathrm{d}t} \\ \frac{\mathrm{d}\mathbf{P}}{\mathrm{d}t} \end{bmatrix} = \begin{bmatrix} \frac{\partial E_{\text{Total}}}{\partial \mathbf{z}^*} \\ \frac{\partial E_{\text{Total}}}{\partial \mathbf{z}} \\ \frac{\partial E_{\text{Total}}}{\partial \mathbf{R}} \\ \frac{\partial E_{\text{Total}}}{\partial \mathbf{P}} \end{bmatrix} \tag{3.14}$$

where the metric matrices: $\mathbf{C}$, $\mathbf{C}_{\mathbf{R}}$, and $\mathbf{C}_{\mathbf{RR}}$ are defined as[1–3]

$$\begin{aligned} \mathbf{C} &= \left. \frac{\partial^2 \ln S(\mathbf{z}^*,\mathbf{R},\mathbf{z},\mathbf{R}')}{\partial \mathbf{z}^* \partial \mathbf{z}} \right|_{\mathbf{R}'=\mathbf{R}} \\ \mathbf{C}_{\mathbf{R}} &= \left. \frac{\partial^2 \ln S(\mathbf{z}^*,\mathbf{R},\mathbf{z},\mathbf{R}')}{\partial \mathbf{z}^* \partial \mathbf{R}} \right|_{\mathbf{R}'=\mathbf{R}} \\ \mathbf{C}_{\mathbf{RR}} &= -2\mathrm{Im} \left. \frac{\partial^2 \ln S(\mathbf{z}^*,\mathbf{R},\mathbf{z},\mathbf{R}')}{\partial \mathbf{R} \partial \mathbf{R}'} \right|_{\mathbf{R}'=\mathbf{R}} \end{aligned} \tag{3.15}$$

The matrices $\mathbf{C}_{\mathbf{R}}$ and $\mathbf{C}_{\mathbf{RR}}$ couple the nuclear and the electronic degrees of freedom and are the SLEND equivalents to the standard nonadiabatic coupling terms. Noticeably, those nuclear–electronic coupling terms are

Author's personal copy

retained in SLEND despite the zero-width limit in the nuclear wave packets in $|\Psi_N\rangle$.[2] Comparison of Eq. (3.14) with Eq. (3.7) reveals that the former is a generalization of the classical Hamilton's equations in symplectic form[54] that express the coupled nuclear classical and electronic quantum dynamics in terms of pairs of real $\{R_i(t), P_i(t)\}$ and complex $\{z_{ph}(t), z^*_{ph}(t)\}$ conjugate variables, respectively.

In a SLEND simulation, the total wavefunction at initial time t_i, $|\Psi_{SLEND}(t_i)\rangle$, is defined by the initial positions and momenta of the reactants' nuclei, $\{\mathbf{R}(t_i), \mathbf{P}(t_i)\} \Rightarrow |\Psi_N(t_i)\rangle = |\mathbf{R}(t_i), \mathbf{P}(t_i)\rangle$, as well as by the initial Thouless parameters of the reactant's electronic wavefunction, $\{\mathbf{z}(t_i), \mathbf{z}^*(t_i)\} \Rightarrow |\Psi_e(t_i)\rangle = |\mathbf{z}(t_i); \mathbf{R}(t_i)\rangle$. The latter's construction depends upon the selection of the MSOs $\{\psi_h, \psi_p\}$ and the reference state $|0\rangle$ (cf. Eq. 3.10). In most SLEND simulations including those presented herein, the MSOs $\{\psi_h, \psi_p\}$ are obtained at t_i through a time-independent unrestricted HF calculation on the reactants' supermolecule at the initial configuration $\mathbf{R}(t_i)$. In all the SLEND simulations discussed in Section 5, the reactants' supermolecule at t_i is in its electronic ground state, which at the HF level corresponds to the reference Fermi single-determinantal state $|0\rangle$ having N_e occupied HF MSOs $\{\psi_h\}$: $|0\rangle = |\psi_1 \ldots \psi_h \ldots \psi_{N_e}\rangle$. In that situation, the initial Thouless parameters assume the value $\mathbf{z}(t_i) = 0$ so that $\chi_h(t_i) = \psi_h$ and $|\Psi_e(t_i)\rangle = |\mathbf{z}(t_i) = 0; \mathbf{R}(t_i)\rangle = |0\rangle$ (cf. Eqs. 3.10 and 3.11). From these described initial conditions, a SLEND simulation starts and the successive values of the dynamical variables $\{\mathbf{R}(t), \mathbf{P}(t), \mathbf{z}(t), \mathbf{z}^*(t)\}$ are calculated by integrating the SLEND equation (3.14). As time progresses, the Thouless parameters may evolve into nonzero values $\mathbf{z}(t) \neq 0$ and if so, virtual HF MSOs $\{\psi_p\}$ are eventually included into the dynamical orbitals $\{x_h(t)\}$ and the electronic wavefunction $|\mathbf{z}(t); \mathbf{R}(t)\rangle$ (cf. Eqs. 3.10 and 3.11); that virtual space inclusion is usually indicative of a nonadiabatic behavior. During evolution, $|\Psi_e(t)\rangle = |\mathbf{z}(t); \mathbf{R}(t)\rangle$ departs from the HF ground state at the nuclear configuration $\mathbf{R}(t)$ as the dynamics ventures into the nonadiabatic regime. It is worth mentioning that, after performing the initial HF optimization to define the MSOs and initial electronic wavefunction, no additional HF optimizations are necessary during a SLEND simulation because the dynamical variables $\{\mathbf{R}(t), \mathbf{P}(t), \mathbf{z}(t), \mathbf{z}^*(t)\}$ are obtained from the solution of SLEND equation (3.14). The evolving electronic wavefunction $|\Psi_e(t)\rangle = |\mathbf{z}(t); \mathbf{R}(t)\rangle$ is still expressed in terms of the initial (static) HF MSOs $\{\psi_h, \psi_p\}$ but changes temporally in terms of its evolving dynamical variables $\{\mathbf{R}(t), \mathbf{z}(t), \mathbf{z}^*(t)\}$. If the simulated dynamics is too violent, the situation described by the initial HF MSOs $\{\psi_h, \psi_p\}$ may differ too much from the

Author's personal copy

actual situation described by $|\Psi_e(t)\rangle$ so that those MSOs become an inadequate basis to express $|\Psi_e(t)\rangle$. That is signaled by large absolute values of the Thouless parameters $\{\mathbf{z}(t), \mathbf{z}^*(t)\}$ that make the SLEND equation (3.14) ill-conditioned. If that situation is reached, the following actions are taken to overcome such an ill-conditioned state: (1) The SLEND simulation is stopped; (2) a new reference basis is constructed; (3) $|\Psi_e(t)\rangle = |\mathbf{z}(t); \mathbf{R}(t)\rangle$ is re-expressed in terms of the new basis; and (4) the SLEND simulation is restarted from that better-conditioned state. The described procedure to find a better reference state during a simulation is performed automatically by our SLEND codes whenever necessary. In the SLEND simulations discussed in Section 5, that procedure happened only once during a particular simulation in very few cases (1% of the simulations, approximately). At the completion of a SLEND simulation at time t_f, the final values of the dynamical variables $\{\mathbf{R}(t_f), \mathbf{P}(t_f), \mathbf{z}(t_f), \mathbf{z}(t_f)^*\}$ define the final total wavefunction $|\Psi_{SLEND}(t_f)\rangle$. Various dynamical properties are calculated by analyzing $|\Psi_{Total}(t_f)\rangle$. For instance, probability amplitudes for electronic excitations and electron transfers from the described initial conditions are obtained by projecting the final electronic wavefunction $|\Psi_e(t_f)\rangle = |\mathbf{z}(t_f); \mathbf{R}(t_f)\rangle$ on the HF electronic states at the final nuclear configuration $\mathbf{R}(t_f)$.[24,57] Those HF states are readily obtained by a single HF calculation at that configuration. In addition, probability amplitudes for nuclear vibrational and rotational excitations from the described initial conditions are obtained by applying the CSQRP to the final nuclear variables $\{\mathbf{R}(t_f), \mathbf{P}(t_f)\}$. With those electronic and nuclear amplitudes, various dynamical properties can be calculated (energy loss spectra, state-to-state DCSs and ICSs, etc.). Further details about those properties' calculations are discussed in Sections 2.4 and 3.

The SLEND dynamical equation (3.14) contains the much simpler Born–Oppenheimer direct-dynamics (BODD) method as a particular case. To downgrade SLEND into BODD, two drastic approximations should be introduced in the former. In the first approximation, the electronic wavefunction $|\Psi_e\rangle$ and the electronic energy E_e in E_{Total}, Eq. (3.13), are obtained as the ground-state HF wavefunction and energy through a HF optimization at each nuclear configuration $\mathbf{R}(t)$. In that scheme, the Thouless parameters $\{\mathbf{z},\mathbf{z}^*\}$ are determined by a HF optimization rather than by the TDVP simultaneously with the other dynamical variables, Eq. (3.14). (Standard BODD methods do not employ an electronic optimization in terms of Thouless parameters but an equivalent procedure in terms of ordinary MSOs' atomic coefficients.) For this reason, in the BODD limit, the Thouless parameters cease being genuine dynamical variables and along

Author's personal copy

with their related matrix $\mathbf{C}$, Eq. (3.15), vanish from Eq. (3.14). In the second approximation, the nuclear–electronic coupling terms are directly neglected (i.e., $\mathbf{C_R} = \mathbf{C_{RR}} = 0$). With those two approximations, the SLEND equation (3.14) reduces to their BODD counterparts:

$$\begin{bmatrix} 0 & -\mathbf{I} \\ \mathbf{I} & 0 \end{bmatrix} \begin{bmatrix} \frac{d\mathbf{R}}{dt} \\ \frac{d\mathbf{P}}{dt} \end{bmatrix} = \begin{bmatrix} \frac{\partial E_{\text{Total}}}{\partial \mathbf{R}} \\ \frac{\partial E_{\text{Total}}}{\partial \mathbf{P}} \end{bmatrix} \Rightarrow \begin{bmatrix} 0 & \mathbf{I} \\ -\mathbf{I} & 0 \end{bmatrix} \begin{bmatrix} \frac{\partial E_{\text{Total}}}{\partial \mathbf{R}} \\ \frac{\partial E_{\text{Total}}}{\partial \mathbf{P}} \end{bmatrix} = \begin{bmatrix} \frac{d\mathbf{R}}{dt} \\ \frac{d\mathbf{P}}{dt} \end{bmatrix} \tag{3.16}$$

where E_{Total} now contains the HF-optimized E_e. The BODD equation (3.16) is nothing but the classical Hamilton's equation in symplectic form for the nuclear variables $\{\mathbf{R}(t), \mathbf{P}(t)\}$ with the BODD total energy E_{Total}.[54] Strictly speaking, SLEND contains BODD/HF as a particular case. Other END realizations contain their corresponding BODD particular cases: SLEND/KSDFT contains BODD/DFT and MCCASEND contains BODD/MCCAS. All those BODD methods have dynamical equations like those in Eq. (3.16) with the electronic energy E_e in the total energy E_{Total} at the DFT, MCCAS, etc., level. Each of those BODD methods completely lacks the nonadiabatic features of its END counterpart due to the obvious fact that the BODD electronic wavefunction and energy are confined to those of the ground state throughout the whole dynamics. Therefore, BODD methods are only adequate to simulate low-energy reactions ($E_{\text{Lab}} < 50\,\text{eV}$, approximately) that remain on or very close to the ground state and that do not undergo electronic excitations and/or ET processes predominantly. Even when appropriately applied to ground-state processes, the BODD nuclear dynamics is still approximate due to its neglect of the nuclear–electronic coupling terms (cf. Ref. 58).

Having reviewed the END and SLEND theories in their original forms, we can now proceed to explain our new theoretical developments in SLEND to make it more accurate and more feasible. Following the preliminary discussion in Section 1, we present in the following sections solutions to increase the degree of electronic correlation in SLEND, to decrease the SLEND computational cost, and to extend the SLEND CSQRP to calculate a larger variety of dynamical properties. Those solutions come in the forms of the SLEND/KSDFT method (Section 2.2), the effective core potential (ECP) implementations in SLEND and SLEND/KSDFT (Section 2.3), and the

Author's personal copy

SLEND protocol to calculate dynamical properties in general and reconstruct quantum nuclear effects with the CSQRP in particular (Sections 2.4 and 3).

2.2. The SLEND/KSDFT method

SLEND, being a single-determinantal method, lacks a proper inclusion of electron correlation effects. As explained in Section 2.1, the SLEND unrestricted single-determinantal electronic wavefunction $|\Psi_e(t)\rangle = |\mathbf{z}(t); \mathbf{R}(t)\rangle$ does include an adequate degree of nondynamical correlation so that SLEND can satisfactorily describe bond-forming and bond-breaking processes. However, that electronic wavefunction totally lacks dynamical correlation, a more essential type of correlation that determines the accuracy of various critical features of chemical systems and reactions. From a SLEND perspective, those features include the reaction's energetics (critical for determining the likelihood and extent of a reaction), the nuclear vibrational motions and frequencies (critical for the accuracy of the vibrational CSQRP), and the actual electron–electron interactions (critical for determining ET processes), *inter alia*. As previously discussed in Section 1, high-level realizations of END (MCCASEND, MCEND, CCEND, etc.) acquire considerable degrees of electron correlation, both nondynamical and dynamical, by adopting wavefunctions beyond the single-determinantal representation, but at very high computational costs. To overcome the latter, we have put forward a far more feasible approach[49] that involves retaining the less demanding SLEND single-determinantal wavefunction and including electron correlation via the TDKSDFT.[50,59–61] The novel method resulting from that approach, SLEND/KSDFT,[49] was in part stimulated by the TDKSDFT direct-dynamics method developed by Theilhaber two decades ago.[62] However, the latter method was not formulated in the END framework, and therefore, it only provided us a general inspiration to develop a TDKSDFT version of SLEND. The main theoretical details of our novel SLEND/KSDFT method and its derivation from SLEND and TDKSDFT are presented in the following paragraphs. Further details can be found in Ref. 49.

TDDFT has its foundation in the Runge and Gross (RG) theorem.[50] That theorem asserts that there is a one-to-one correspondence between the TD external potential $v_{ext}(\mathbf{r},t)$ and the electron density $\rho(\mathbf{r},t)$ of a time-evolving system. That one-to-one mapping implies that the TD electron density $\rho(\mathbf{r},t)$ completely determines the TD electronic wavefunction $|\Psi_e[\rho](t)\rangle$

Author's personal copy

and all the properties of a system. The foundational role of the RG theorem in TDDFT is analogous to that of the first Hohenberg and Kohn theorem in time-independent DFT.[63] While the RG theorem legitimizes TDDFT, it does not provide by itself a practical formulation of TDDFT leading to applications to systems of interest. However, in analogy to the time-independent KS DFT[64] again, TDDFT adopts a formulation with practical consequences when it is cast into a time-dependent KS (TDKS) form.[59–61] Like its time-independent counterpart, that approach invokes an auxiliary system of N_e noninteracting electrons described by the KS single-determinantal wavefunction $|\Phi_{KS}\rangle$: $\langle \mathbf{r}|\Phi_{KS}\rangle = \Phi_{KS}(\mathbf{r}_1,\ldots,\mathbf{r}_{N_e},t) = \det\left[\psi_i^{KS}(\mathbf{r}_i,t)\right]/\sqrt{N_e!}$, involving orthonormal KS MSOs $\{\psi_i^{KS}(\mathbf{r}_i,t)\}$. This auxiliary system is subjected to an effective external potential $v_s[\rho](\mathbf{r},t)$ (unique by the RG theorem) so that its electron density $\rho(\mathbf{r},t)$

$$\rho(\mathbf{r},t) = \sum_{i=1}^{N_e} \left|\psi_i^{KS}(\mathbf{r},t)\right|^2 \tag{3.17}$$

is assumed to be identical to the electron density of the actual system of N_e-interacting electrons. In that scheme, the time evolution of $\rho(\mathbf{r},t)$ is determined by the time evolution of the KS MSOs, each of them obeying a TD Schrödinger equation with the potential $v_s[\rho](\mathbf{r},t)$[50,59,60]:

$$\begin{gathered}\left[-\frac{1}{2}\nabla^2 + v_s[\rho](\mathbf{r},t)\right]\psi_j^{\mathbf{KS}}(\mathbf{r},t) = \mathrm{i}\frac{\partial}{\partial t}\psi_j^{\mathbf{KS}}(\mathbf{r},t)(1 \le j \le N_e) \\ v_s[\rho](\mathbf{r},t) = v_{ext}(\mathbf{r},t) + \int \mathrm{d}\mathbf{r}'\frac{\rho(\mathbf{r}',t)}{|\mathbf{r}-\mathbf{r}'|} + v_{xc}[\rho](\mathbf{r},t)\end{gathered} \tag{3.18}$$

where $v_{ext}(\mathbf{r},t)$ is the external potential on the actual system, $\int \mathrm{d}\mathbf{r}'\rho(\mathbf{r}',t)/|\mathbf{r}-\mathbf{r}'|$ the Coulombic potential, and $v_{xc}[\rho](\mathbf{r},t)$ the exchange-correlation potential.[50,59,60] Equation (3.18) is currently considered as the fundamental TDKSDFT equation after former TDKSDFT formulations in terms of a DFT quantum action $A_{DFT}[\rho(\mathbf{r},t)]$ were proved problematic.[60,61,65,66] The crucial component in Eq. (3.18) is the exchange-correlation potential $v_{xc}[\rho](\mathbf{r},t)$ that introduces electron exchange and correlation effects into an equation that without $v_{xc}[\rho](\mathbf{r},t)$ would be a sort of uncorrelated TD Hartree equation. Further progress in any TDKSDFT effort depends upon obtaining an expression for $v_{xc}[\rho](\mathbf{r},t)$, a term unknown in its exact form, but for which various approximations have been proposed.[59–61] However, the formulation

Author's personal copy

of genuine TD potentials $v_{xc}[\rho](\mathbf{r},t)$ without resorting to their many time-independent DFT counterparts has proved extremely difficult. Therefore, the simplest and most widespread approximation to $v_{xc}[\rho](\mathbf{r},t)$ is the adiabatic approximation[59–61]:

$$v_{xc}[\rho](\mathbf{r},t) \approx v_{xc}^{\text{adia.}}[\rho](\mathbf{r},t) = v_{xc}^{gs}[\widetilde{\rho}](\mathbf{r})\big|_{\widetilde{\rho}(\mathbf{r})=\rho(\mathbf{r},t)};$$
$$v_{xc}^{gs}[\widetilde{\rho}](\mathbf{r}) = \frac{\delta E_{xc}^{gs}[\widetilde{\rho}(\mathbf{r})]}{\delta[\widetilde{\rho}(\mathbf{r})]} \tag{3.19}$$

where $v_{xc}^{gs}[\widetilde{\rho}](\mathbf{r})$ and $E_{xc}^{gs}[\widetilde{\rho}(\mathbf{r})]$ are selected ground-state, time-independent, KSDFT exchange-correlation potential and energy functional, respectively. The adiabatic approximation is extensively used in linear-response TDKSDFT calculations of excitation energies[59–61] and also in Theilhaber's TDKSDFT direct-dynamics method,[62] in both cases producing satisfactory results. The adiabatic approximation is supposed to work well with slow-evolving electron densities that remain near the ground state. However, previous TDKSDFT experience[60,61] suggests that this approximation may work acceptably well even with processes beyond the slow and near-ground-state regime, as is the case in many chemical reactions. For all those reasons, the adiabatic approximation has been adopted in our SLEND/KSDFT implementation.

The formulation of SLEND/KSDFT starts by considering Eqs. (3.14) and (3.15) as the fundamental SLEND dynamical equations, just as TDKSDFT considers Eq. (3.18) as its fundamental dynamical equation. Then, the SLEND electronic single-determinantal wavefunction $|\Psi_e\rangle = |\mathbf{z};\mathbf{R}\rangle$ is reformulated (or reinterpreted) as a KS wavefunction in the Thouless representation, $|\Psi_e\rangle = |\mathbf{z};\mathbf{R}\rangle \rightarrow |\Phi_{KS}\rangle$, by substituting its reference time-independent HF MSOs $\{\psi_h,\psi_p\}$ for analogous time-independent KSDFT MSOs $\{\psi_h^{KS},\psi_p^{KS}\}$ (cf. Eqs. 3.10 and 3.11). Notice that the SLEND $|\Psi_e\rangle = |\mathbf{z};\mathbf{R}\rangle$ is an approximate electronic wavefunction for the actual system that provides an approximate electron density $\rho(\mathbf{r},t)$. In contrast, the SLEND/KSDFT $|\Psi_e\rangle = |\mathbf{z};\mathbf{R}\rangle$ acts as an auxiliary electronic KS wavefunction that can provide the exact electron density $\rho(\mathbf{r},t)$ if the exchange-correlation potential $v_{xc}[\rho](\mathbf{r},t)$ occurring in the SLEND/KSDFT equations is known exactly. It is worth emphasizing that the SLEND/KSDFT formulation of the electronic KS wavefunction as a Thouless single-determinantal wavefunction confers to the former all the discussed numerical advantages of the Thouless representation to integrate dynamical equations. Those valuable numerical features are absent in the typical

Author's personal copy

TDKSDFT formulations, Eq. (3.18), which employ standard Slater single-determinantal wavefunctions.

Having assimilated the SLEND electronic wavefunction as a KS wavefunction, the SLEND/KSDFT electron density $\rho(\mathbf{r},t)$ is obtained as

$$\rho\{\mathbf{r};\mathbf{z}(t),\mathbf{z}^*(t),\mathbf{R}(t)\} = \int \mathrm{d}s\, \gamma_1\{\mathbf{r}',s',\mathbf{r},s;\mathbf{z}(t),\mathbf{z}^*(t),\mathbf{R}(t)\}|_{\mathbf{r}'=\mathbf{r},s'=s} \tag{3.20}$$

where the one-electron reduced density matrix $\gamma_1(\mathbf{x}',\mathbf{x})$[67,68] is

$$\begin{aligned}\gamma_1\{\mathbf{r}',s',\mathbf{r},s;\mathbf{z}(t),\mathbf{z}^*(t),\mathbf{R}(t)\} &= \sum_{i,j}^{K} \psi_i\{\mathbf{r}',s';\mathbf{R}(t)\}\gamma_{ij}^{(1)}\{\mathbf{z}(t),\mathbf{z}^*(t)\}\psi_j^*\{\mathbf{r},s;\mathbf{R}(t)\} \\ \gamma_{ij}^{(1)}\{\mathbf{z}(t),\mathbf{z}^*(t)\} &= \frac{\left\langle \mathbf{z}(t);\mathbf{R}(t)\middle| b_j^\dagger b_i \middle|\mathbf{z}(t);\mathbf{R}(t)\right\rangle}{\langle \mathbf{z}(t);\mathbf{R}(t)|\mathbf{z}(t);\mathbf{R}(t)\rangle} \\ &= \begin{bmatrix}\mathbf{I} \\ \mathbf{z}(t)\end{bmatrix}\left[\mathbf{I}+\mathbf{z}^\dagger(t)\mathbf{z}(t)\right]^{-1}\begin{bmatrix}\mathbf{I} & \mathbf{z}(t)^\dagger\end{bmatrix}\end{aligned} \tag{3.21}$$

where s and s' are spin variables, and $\mathbf{I} = (\delta_{ij}) \in \mathbb{R}^{N_e \times N_e}$ and $\mathbf{z} = (z_{ph}) \in \mathbb{C}^{(K-N_e)\times N_e}$ are the identity and Thouless parameter matrices, respectively.[1] At this point, the electron density $\rho(\mathbf{r},t)$ from Eqs. (3.20) and (3.21) becomes the central property of the SLEND/KSDFT method. Therefore, to obtain the SLEND/KSDFT dynamical equations, all the electronic terms in the SLEND equations (3.14) and (3.15) should be substituted for their corresponding TDKSDFT counterparts, which ultimately are functionals of $\rho(\mathbf{r},t)$. The resulting SLEND/KSDFT dynamical equations have exactly the same form as that of their SLEND counterparts, Eqs. (3.14) and (3.15), but with all their electronic terms changed into their TDKSDFT equivalents. In particular, the electronic energy E_e in the total energy E_{Total}, Eq. (3.13), which occurred in the SLEND equation (3.14), now adopts a corresponding KSDFT expression in the SLEND/KSDFT dynamical equations:

$$\begin{aligned}E_e^{\mathrm{SLEND/KSDFT}}[\mathbf{R},\mathbf{z},\mathbf{z}^*] = &\frac{\langle \mathbf{z};\mathbf{R}|-\frac{1}{2}\nabla^2|\mathbf{z};\mathbf{R}\rangle}{\langle \mathbf{z};\mathbf{R}|\mathbf{z};\mathbf{R}\rangle} + \int \mathrm{d}\mathbf{r}\rho(\mathbf{r};\mathbf{z},\mathbf{z}^*,\mathbf{R})v_{\mathrm{ext}}(\mathbf{r};\mathbf{R}) \\ &+\frac{1}{2}\int\int \mathrm{d}\mathbf{r}\mathrm{d}\mathbf{r}'\frac{\rho(\mathbf{r};\mathbf{z},\mathbf{z}^*,\mathbf{R})\rho(\mathbf{r}';\mathbf{z},\mathbf{z}^*,\mathbf{R})}{|\mathbf{r}-\mathbf{r}'|} \\ &+E_{\mathrm{xc}}^{\mathrm{gs}}[\rho(\mathbf{r};\mathbf{z},\mathbf{z}^*,\mathbf{R})]\end{aligned} \tag{3.22}$$

Author's personal copy

whose terms are the KS kinetic, external-potential, classical self-repulsion, and exchange-correlation energies. The external potential $v_{\text{ext}}(\mathbf{r};\mathbf{R}) = -\sum_{i=1}^{N_N} Z_i|\mathbf{r}-\mathbf{R}_i|^{-1}$ is caused by the moving classical nuclei. The adiabatic approximation is employed in Eq. (3.22) via $E_{\text{xc}}^{\text{gs}}[\rho]$ (cf. Eq. 3.19). The discussed SLEND/KSDFT equations have been implemented in our own END codes as is explained in Section 4. The first ever applications of our novel SLEND/KSDFT method involved molecular vibrations and proton–molecules reactions and were presented in Refs. 22,49. Recent SLEND/KSDFT applications to those types of systems and to Diels–Alder reactions are presented in Section 5.

It is interesting to note that one could have attempted to derive the SLEND/KSDFT dynamical equations not from the preexisting SLEND equations (3.14) and (3.15) but from the TDVP applied to the SLEND/KSDFT quantum action $A_{\text{SLEND/KSDFT}}[\mathbf{R},\mathbf{P},\rho(\mathbf{z},\mathbf{z}^*;\mathbf{R})]$. The latter is obtained by rewriting the SLEND action $A_{\text{SLEND}}[\mathbf{R},\mathbf{P},\mathbf{z},\mathbf{z}^*]$ as a TDKSDFT functional of $\rho(\mathbf{r},t)$. That action approach to SLEND/KSDFT is analogous to the earlier action approach to TDKSDFT in terms of the TDDFT quantum action $A_{\text{DFT}}[\rho(\mathbf{r},t)]$.[50,59] However, we refrained from following that action approach herein because the conventional TDDFT quantum action notoriously exhibits two defective traits.[61,65,66] First, a TDDFT action leads to exchange-correlation kernels $f_{\text{xc}}[\rho](\mathbf{r},t,\mathbf{r}',t') = \delta v_{\text{xc}}[\rho](\mathbf{r},t)/\delta\rho(\mathbf{r}',t')$ that violate the causality condition: $f_{\text{xc}}[\rho](\mathbf{r},t,\mathbf{r}',t') = 0$ for $t' > t$ (the so-called causality paradox). Second, under the RG theorem, an initial TDVP boundary condition $\delta\,|\,\Psi_{\text{e}}[\rho](t_{\text{i}})\rangle = 0$ completely determines a final variation $\delta\,|\,\Psi_{\text{e}}[\rho](t_{\text{f}})\rangle$ so that it is no longer possible to set the final TDVP boundary condition $\delta\,|\,\Psi_{\text{e}}[\rho](t_{\text{f}})\rangle = 0$ independently from the initial one. Various sophisticated solutions have been advanced to solve the aforesaid defects.[65,66,69–71] However, it is unclear if those sophisticated solutions, some of them in terms of the formidable Keldish action in pseudo-time, can be implemented into a computationally feasible method like SLEND/KSDFT. The sole exception seems to be Vignale's solution, which still utilizes the conventional TDDFT action in real time but under a modified TDVP that in essence incorporates a nonzero final-end point variation. Vignale's solution is amenable to formulating a correct action approach to SLEND/KSDFT, which is under consideration in our group. Until that SLEND/KSDFT formulation becomes available, we can safely derive the SLEND/KSDFT dynamical equations from their SLEND counterparts taking the latter as the fundamental SLEND dynamical equations and thus circumventing the SLEND/KSDFT action. This is

Author's personal copy

analogous to TDKSDFT taking Eq. (3.18) as its fundamental dynamical equation and thus circumventing the TDKSDFT action.[60,61] If one insists on obtaining the SLEND/KSDFT dynamical equations from the SLEND/KSDFT action through the conventional TDVP, the result will be the same SLEND/KSDFT dynamical equations discussed earlier, but obtained through a questionable procedure. In fact, Theilhaber derived his TDKSDFT direct-dynamics method in that way,[62] unaware of the defects of the TDKSDFT action; nonetheless, Theilhaber's method proved to be physically meaningful during applications.[62] Finally, it is worth mentioning that the SLEND/KSDFT action adopting the adiabatic approximation through $E_e^{\mathrm{SLEND/KSDFT}}$, Eq. (3.22), inherits an *ad hoc* solution to the causality paradox because the $f_{xc}^{\mathrm{adia.}}[\rho](\mathbf{r},t,\mathbf{r}',t')$ is causal by construction: $f_{xc}^{\mathrm{adia.}}[\rho](\mathbf{r},t,\mathbf{r}',t') = \delta v_{xc}^{\mathrm{adia.}}[\rho](\mathbf{r},t)/\delta\rho(\mathbf{r}',t') = \delta(t-t')\,\delta v_{xc}^{gs}[\tilde{\rho}](\mathbf{r})/\delta\tilde{\rho}(\mathbf{r}')|_{\tilde{\rho}(\mathbf{r})=\rho(\mathbf{r},t)}$.

Some of the first results with the new SLEND/KSDFT are presented in Section 5. They concern vibrational motions of several representative molecules and the simulation of a Diels–Alder reaction. Additional results from ion–molecule reactions are given in Ref. 49.

2.3. SLEND + ECP and SLEND/KSDFT + ECP

In both SLEND and SLEND/KSDFT, the majority of the computational effort lies in the calculation of the quantum electronic nonadiabatic dynamics, wherein the rate-determining steps are the computation of the two-electron atomic integrals and their contribution to the energy gradients with respect to nuclear positions. Those operations have an algorithmic complexity of $O(K^4)$. Undoubtedly, this computational effort becomes prohibitively expensive with the use of the large atomic basis sets that are necessary to obtain very accurate dynamics. The same computational effort becomes burdensome even with modest atomic basis sets if the system being simulated is very large, as are the cases of the biomolecules involved in proton cancer therapy. However, significant computational savings can be obtained if the valence electrons of a system are treated explicitly while the core electrons are modeled by pseudopotentials. Such an approximation is acceptable for chemical reactions because the core electrons only become directly involved in chemical processes at extremely high energies. In that regard, the ECP method[72–74] provides a rigorous and feasible way to achieve the outlined treatment of valence and core electrons, exhibiting a long history of successes in time-independent electronic structure theory calculations.[72–74] Inspired by those traditional ECP efforts, we have recently extended the

Author's personal copy

use of the ECP method to TD dynamics calculations by implementing ECPs into the SLEND and SLEND/KSDFT methods.[75] Those efforts have produced the new SLEND + ECP and SLEND/KSDFT + ECP methods, which are outlined in the following paragraphs.

In any ECP approach, only the valence electrons are treated explicitly. The core electrons are replaced by pseudopotentials $V_{\mathrm{ECP}}(i)$, whose evaluable expressions can be found in the ECP literature.[72–74] One important role for $V_{\mathrm{ECP}}(i)$ is to prevent the so-called variational collapse of the explicit valence electrons (i.e., to prevent basis functions intended to describe valence orbitals from being used to describe core orbitals). That effect is achieved by nonlocal projection operators in terms of spherical harmonics $|lm\rangle$ that are included in $V_{\mathrm{ECP}}(i)$. In that scheme, the total Hamiltonian $\hat{H}_{\mathrm{Total}}$ employed in the SLEND and SLEND/KSDFT dynamical equations and the HF and KS operators $\hat{f}_{\mathrm{HF/KS}}(1)$, employed to calculate the HF and KSDFT states at initial and final times, are substituted for their ECP-formulated equivalents $\hat{H}^{\mathrm{ECP}}_{\mathrm{Total}}$ and $\hat{f}^{\mathrm{ECP}}_{\mathrm{HF/KS}}(i)$, respectively:

$$\begin{aligned}\hat{H}^{\mathrm{ECP}}_{\mathrm{Total}} &= -\frac{1}{2M_i}\sum_{i=1}^{N_{\mathrm{N}}}\nabla^2_{\mathbf{R}_i} + \sum_{\substack{i=1\\ j>i}}^{N_{\mathrm{N}}}\frac{Z_i^{eff}Z_j^{eff}}{|\mathbf{R}_i-\mathbf{R}_j|} - \frac{1}{2}\sum_{i=1}^{N_{\mathrm{e}}^{\mathrm{Val}}}\nabla_i^2 \\ &\quad + \sum_{\substack{i=1\\ j>i}}^{N_{\mathrm{e}}^{\mathrm{Val}}}\frac{1}{|\mathbf{r}_i-\mathbf{r}_j|} - \sum_{i=1}^{N_{\mathrm{N}}}\sum_{j=1}^{N_{\mathrm{e}}^{\mathrm{Val}}}\frac{Z_i^{\mathrm{eff}.}}{|\mathbf{R}_i-\mathbf{r}_j|} + \sum_{i=1}^{N_{\mathrm{e}}^{\mathrm{Val}}}\hat{V}_{\mathrm{ECP}}(i) \\ \hat{f}^{\mathrm{ECP}}_{\mathrm{HF/KS}}(i) &= -\frac{1}{2}\nabla_i^2 + \int\frac{\rho(\mathbf{r}')}{|\mathbf{r}-\mathbf{r}'|}\mathrm{d}\mathbf{r}' + v_{\mathrm{HF/KS}}(i) - \sum_{i=1}^{N_{\mathrm{N}}}\frac{Z_i^{\mathrm{eff}}}{|\mathbf{R}_i-\mathbf{r}|} + \hat{V}_{\mathrm{ECP}}(i)\end{aligned} \tag{3.23}$$

where $N_{\mathrm{e}}^{\mathrm{Val}}$ is the number of valence electrons, $\{Z_i^{\mathrm{eff}}\}$ are the effective nuclear charges experienced by the valence electrons due to the formal removal of the core electrons, and $v_{\mathrm{HF/KS}}(i)$ is either the HF-exchange operator $-\hat{K}(i)$ in SLEND or the KSDFT exchange-correlation potential $v_{\mathrm{xc}}[\rho](\mathbf{r})$ in SLEND/KSDFT. With $\hat{H}^{\mathrm{ECP}}_{\mathrm{Total}}$, the electronic single-determinantal wavefunction in the Thouless representation, $|\Psi_{\mathrm{e}}\rangle = |\mathbf{z};\mathbf{R}\rangle$, is reduced in size as it only contains the $N_{\mathrm{e}}^{\mathrm{Val}}$ valence electrons, $N_{\mathrm{e}}^{\mathrm{Val}} < N_{\mathrm{e}}$. With all these changes, SLEND + ECP and SLEND/KSDFT + ECP reduce the dimensionality of the electron integrals and therefore the computational cost.

Author's personal copy

As discussed in Section 1, SLEND and SLEND/KSDFT have been highly successful in the simulation of chemical reactions at intermediate ($10\,\text{eV} \leq E_{\text{Lab}} \leq 100\,\text{eV}$) and high ($100\,\text{eV} < E_{\text{Lab}}$) collision energies. The appropriateness of applying SLEND + ECP and SLEND/KSDFT + ECP to reactions in that energy regime (especially to reactions in proton cancer therapy) assumes that the core electrons only participate in the electronic quantum nonadiabatic dynamics in a secondary way, for instance, by preventing the aforesaid variational collapse of the valence electrons. This assumption is justified by conventional chemical experience that reveals that more drastic core-electron processes, such as electron excitations and transfers, only occur at exceedingly high energies. Obviously, the implicit core electrons modeled by the ECPs are excluded from participating in collision-induced electronic excitations and ET reactions. Exhaustive comparisons of SLEND and SLEND + ECP simulations of benchmark systems (e.g., H^+ collisions with HCl and CO_2 molecules *inter alia*) have demonstrated that the use of ECPs within SLEND does not significantly affect their reactivity (as measured by product predictions), deflection angle functions $\Theta(b)$, and ET probabilities in collisions with energies up to about 100 keV.[75] Those results finally justify the use of SLEND + ECP and SLEND/KSDFT + ECP for the simulation of many reactions in the above-mentioned energy regime. In light of this observation, the use of SLEND + ECP and SLEND/KSDFT + ECP is found to dramatically reduce the computational cost of a simulation with minimal degradation of accuracy, thus allowing for the accurate treatment of large systems. Some of the first ever simulations with SLEND + ECP are presented in Section 5; they concern the S_N2 reaction $CH_3Br + F^- \rightarrow CH_3F + Br^-$ at $E_{\text{Lab}} = 20\,\text{eV}$ and the reaction $H^+ + (H_2O)_4$ at $E_{\text{Lab}} = 1\,\text{keV}$ that is a prototype for the water radiolysis in proton cancer therapy.

2.4. Dynamical properties calculations

Regardless of the implementation being used (SLEND, SLEND/KSDFT, SLEND + ECP, SLEND/KSDFT + ECP), SLEND simulations of chemical reactions can yield various dynamical properties. The latter include rotational and vibrational energy transfers, vibrationally resolved projectile energy loss spectra, rotational and vibrational state-to-state DCSs, rotational and vibrational state-to-state integral cross sections (ICSs), total ET DCSs, and total ET ICSs, *inter alia*. Those calculated properties can be compared with available experimental results, thus allowing opportunities to test the accuracy of SLEND. Many available experiments measuring the above-mentioned dynamical properties involve intermediate- and high-energy

Author's personal copy

reactions (collisions) between an atomic cation I^q, $q \geq +1$, (the moving projectile) with a molecule M (the initially stationary target) in its ground state:

$$I^q + M\left(n_D^i = 0\right) \rightarrow I^{q'} + M^{q''}\left(n_D^f = 0,1,2\ldots\right); \quad q = q' + q'' \tag{3.24}$$

where $n_D^i(n_D^f)$ is the initial (final) quantum number for an internal degree-of-freedom D, D = rotational, vibrational, and/or electronic, and $n_D^i = 0$ denotes symbolically the ground state of M at initial time. In most experiments, $I^q = H^+$. The key dynamical properties in those reactions are state-to-state and/or total DCSs from which many other properties can be calculated immediately. Since all SLEND implementations feature a classical nuclear dynamics, SLEND relies on established semi-classical approximations[76,77] for the nuclear degrees of freedom in order to calculate state-to-state DCSs.[31] For many scattering situations in the reactions of Eq. (3.24), the state-to-state DCS in the center-of-mass (CM) frame for the transition $n_D^i = 0 \rightarrow n_D^f$, $\dfrac{d\sigma(\theta_{CM})_{n_D^i=0\rightarrow n_D^f}}{d\Omega}$, is obtained from the application of the stationary phase approximation to the DCS partial wave expression yielding[76,77]:

$$\begin{aligned}\frac{d\sigma(\theta_{CM})_{n_D^i=0\rightarrow n_D^f}}{d\Omega} &= \left|\sum_{m=1}^{N} f_m(\theta_{CM})\right|^2 \\ &= \left|\sum_{m=1}^{N} \frac{b_m^{1/2} A_{n_D^i=0\rightarrow n_D^f}(b_m)}{\sin^{1/2}[\theta_{CM}(b_m)]\left|\dfrac{d\Theta_{CM}(b)}{db}\right|_{b=b_m}^{1/2}} \exp[i\delta(b_m)]\right|^2\end{aligned} \tag{3.25}$$

where b is the projectile's impact parameter, θ_{CM}, $0^\circ \leq \theta_{CM} \leq 180^\circ$, is the projectile's scattering angle, $\Theta_{CM}(b)$ is the projectile's deflection function ($|\Theta_{CM}(b)| = \theta_{CM}$ in all the reactions discussed in Section 5), $f_m(\theta_{CM})$ is a scattering amplitude, $\delta(b)$ is the phase shift obtained through $d\delta(b)/db = (k/2)\Theta_{CM}(b)$, where k is the collision wave number, and $A_{n_D^i=0\rightarrow n_D^f}(b)$ is the probability amplitude for the $n_D^i = 0 \rightarrow n_D^f$ target's transition. The sum in m in Eq. (3.25) is over the N branches of $\Theta_{CM}(b)$ contributing to the same θ_{CM} (i.e., the N projectile's classical trajectories ending up into the scattering direction θ_{CM}). At most, $N = 3$ with one repulsive and two attractive

Author's personal copy

branches (trajectories) in all the cases discussed in Section 5. Equation (3.25) refers to the scattering of projectiles I^q starting with varying impact parameters b, $b \geq 0$, and colliding with a target M at a particular initial orientation. The final reported DCS is an average over all the initial orientations of M. Equation (3.25) is expressed in the center-of-mass (CM) frame and requires transforming SLEND variables from their original laboratory frame into the CM frame. The final reported DCS is transformed back into the laboratory frame. $\Theta_{\mathrm{CM}}(b)$, $\dfrac{\mathrm{d}\Theta_{\mathrm{CM}}(b)}{\mathrm{d}b}$, b_m, and $\delta(b_m)$ in Eq. (3.25) are obtained directly from the SLEND classical nuclear trajectories. For state-to-state, $n_{\mathrm{D}}^{\mathrm{i}}=0 \rightarrow n_{\mathrm{D}}^{\mathrm{f}}$, DCSs with $D=$ rotational and vibrational, $A_{n_{\mathrm{D}}^{\mathrm{i}}=0 \rightarrow n_{\mathrm{D}}^{\mathrm{f}}}(b)$ is obtained by applying the rotational and vibrational CSQRP[22] to the final classical nuclear state of M. Such a quantum reconstruction procedure from classical mechanics is explained in detail in Section 3. For a total ET, $n_{\mathrm{D}}^{\mathrm{i}}=0 \rightarrow \mathrm{All}\, n_{\mathrm{D}}^{\mathrm{f}}$, DCS with $D=$ electronic, $A_{n_{\mathrm{D}}^{\mathrm{i}}=0 \rightarrow \mathrm{All}\, n_{\mathrm{D}}^{\mathrm{f}}}(b)$ is obtained by projecting the final electronic wavefunction $|\Psi_{\mathrm{e}}(t_{\mathrm{f}})\rangle = |\mathbf{z}(t_{\mathrm{f}});\mathbf{R}(t_{\mathrm{f}})\rangle$ into HF (SLEND) or KSDFT (SLEND/KSDFT) states corresponding to projectile-target electron transfers at the final nuclear configuration $\mathbf{R}(t_{\mathrm{f}})$.[24,78] Unlike the CSQRP, this projection involves no quantum reconstruction from classical mechanics; it is a standard projection operation involving quantum entities: the final electronic wavefunction projected onto final quantum states. This projection is performed with the auxiliary code Resolve associated to our SLEND codes. Some details of this projection operation and Resolve are given in Sections 3 and 4, respectively.

The DCS equation (3.25) clearly suffers from nonphysical singularities when $\theta_{\mathrm{CM}} = |\Theta_{\mathrm{CM}}(b_{\mathrm{G}})| = 0^\circ$ or 180°, the forward and backward glory scattering angles, and when $\mathrm{d}\Theta_{\mathrm{CM}}(b_{\mathrm{R}})/\mathrm{d}b = 0$, which occurs at the rainbow scattering angles $\theta_{\mathrm{CM\,R}} = |\Theta_{\mathrm{CM}}(b_{\mathrm{R}})|$ corresponding to the critical points of $\Theta_{\mathrm{CM}}(b)$ at b_{R}. Those unphysical singularities not observed in experiments arise in Eq. (3.25) because its underlying stationary phase approximation is inapplicable under the described situations. For instance, that approximation assumes that the branches (trajectories) contributing to the sum of Eq. (3.25) are well separated; however, at rainbow scattering angles $\theta_{\mathrm{CM\,R}}$, two or more branches (trajectories) coalesce rendering the stationary phase approximation useless. More sophisticated semi-classical methods are available to correctly treat situations exhibiting the above singularities[76,77] and all of them can find fruitful applications with SLEND. For the reactions discussed in Section 5, only one type of singularity is of concern: a rainbow singularity arising from the coalescence of the two attractive branches (trajectories) present in their

Author's personal copy

typical $\Theta_{CM}(b)$ (their third repulsive branch remains somewhat separated). That situation can be correctly treated by a proper combination of the uniform and transitional Airy approximations.[76,77] In that approach, the two scattering amplitudes in Eq. (3.25) corresponding to the two attractive coalescing trajectories, say $f_2(\theta_{CM})$ and $f_3(\theta_{CM})$, are replaced with a single scattering amplitude, $f_{23}(\theta_{CM})$, obtained from the uniform Airy approximation if $\theta_{CM} < \theta_{CM\,R}$:

$$f_{23}(\theta_{CM}) = \pi^{1/2} \exp\left[i\left(A_{23} - \frac{1}{4}\pi\right)\right]\left[B_+ \xi_{23}^{1/4} \mathrm{Ai}(-\xi_{23}) - iB_- \xi_{23}^{-1/4} \mathrm{Ai}'(-\xi_{23})\right] \tag{3.26}$$

and from the transitional Airy approximation if $\theta_{CM} \geq \theta_{CM\,R}$:

$$f_{23}(\theta_{CM}) = \left(\frac{2\pi b_R}{k \sin(\theta_{CM})}\right)^{1/2} \frac{\exp\left\{i\left[2\delta(b_R) - k b_R \theta_{CM} - \frac{1}{4}\pi\right]\right\}}{|q_R|^{1/3}} \mathrm{Ai}\left(\frac{\theta_{CM} - \theta_{CMR}}{|q_R|^{1/3}}\right) \tag{3.27}$$

where Ai and Ai′ are the Airy function and its first derivative, $q_R = (1/2k^2)\left|\mathrm{d}^2\Theta_{CM}(b_R)/\mathrm{d}b^2\right|$, $B_\pm = |f_2(\theta_{CM})| \pm |f_3(\theta_{CM})|$, $A_{23} = (1/2)[2\delta(b_3) + 2\delta(b_2) - (b_3 + b_2)\theta_{CM}]$, and $\xi_{23} = \{(3/4)[2\delta(b_3) - 2\delta(b_2) - k(b_3 - b_2)\theta_{CM}]\}^{2/3}$. The use of the two Airy approximations results in the replacement of the rainbow singularity at $\theta_{CM\,R}$ by a bounded rainbow peak, which achieves maximum value at a scattering angle $\theta_{CM\,R}^{Airy}$ that is slightly lower than the classical-mechanics $\theta_{CM\,R}$ and is in better agreement with experiments. The discussed approach to calculate DCSs in the SLEND and SLEND/KSDFT framework has been employed to obtain the vibrational state-to-state DCSs and total ET DCSs presented in Section 5.

Having obtained suitable expressions to calculate DCSs, other properties follow from the latter. For instance, state-to-state ICSs, $\sigma_{n_D^i=0\to n_D^f}$, are obtained by integrating their DCS counterparts in Eq. (3.25) over the solid angle Ω. The resulting expression is:

$$\sigma_{n_D^i=0\to n_D^f} = 2\pi \int_0^\infty b \left|A_{n_D^i=0\to n_D^f}(b)\right|^2 \mathrm{d}b. \tag{3.28}$$

Total ICSs have the same expression in Eq. (3.28) but with the probability $\left|A_{n_D^i=0\to n_D^f}(b)\right|^2$ substituted for a total probability for a given process (e.g. the total target-to-projectile one-electron ET probability). The final reported ICSs are averages over all the target orientations. Vibrational state-to-state ICSs were calculated with SLEND for $H^+ + H_2(v_i = 0) \to H^+ + H_2(v_i = 0-6)$ at $E_{Lab} = 30\,\mathrm{eV}$,[23] while total ET ICS were calculated with SLEND for $H^+ + M \to H + M^+$ at $E_{Lab} = 30\,\mathrm{eV}$ with $M = H_2$,[24]

Author's personal copy

CH_4,[27] and C_2H_2.[30] All those calculated ICS compared well with available experimental results. Finally, the average vibrational energy transferred to the target M, $\langle E_{\mathrm{Vib}}(\theta)\rangle$, from an initial target orientation is given in the laboratory frame as (cf. Refs. 23,24,27):

$$\langle \Delta E_{\mathrm{Vib}}(\theta)\rangle = \frac{\sum_{i=m}^{N}\left[\frac{\mathrm{d}\sigma(\theta)}{\mathrm{d}\Omega}\right]_m \Delta E^m_{\mathrm{Vib}}(\theta)}{\sum_{m=i}^{N}\left[\frac{\mathrm{d}\sigma(\theta)}{\mathrm{d}\Omega}\right]_m} = \frac{\sum_{m=1}^{N}\left[\frac{\mathrm{d}\sigma(\theta)}{\mathrm{d}\Omega}\right]_m \Delta E^m_{\mathrm{Vib}}(\theta)}{\frac{\mathrm{d}\sigma(\theta)_{\mathrm{Total}}}{\mathrm{d}\Omega}} \tag{3.29}$$

where $\Delta E^m_{\mathrm{Vib}}(\theta)$ is the vibrational energy transferred to the target M in the branch (trajectory) m, and $\left[\frac{\mathrm{d}\sigma(\theta)}{\mathrm{d}\Omega}\right]_m = |f_m(\theta)|^2$ with $A_{n^{\mathrm{i}}_{\mathrm{D}}=0\to n^{\mathrm{f}}_{\mathrm{D}}}(b) = 1$ (i.e., $\left[\frac{\mathrm{d}\sigma(\theta)}{\mathrm{d}\Omega}\right]_m$ is the total classical DCS of branch m, cf. Eq. 3.25). The final reported $\langle E_{\mathrm{Vib}}(\theta)\rangle$ is an average over all the target orientations. Some examples of SLEND-calculated $\langle E_{\mathrm{Vib}}(\theta)\rangle$ are discussed in Section 5.

3. THE CS STRUCTURE OF SLEND AND SLEND/KSDFT

3.1. END and the CS theory

In this section, we review our latest CS developments for SLEND and SLEND/KSDFT. For sake of brevity, whenever we refer to SLEND alone in Section 3, we actually mean both SLEND and SLEND/KSDFT as both methods share the same CS structure. As discussed in Section 1, each 1D Gaussian frozen wave packet $|R_i,P_i\rangle$ of the SLEND nuclear wavefunction $|\Psi_{\mathrm{N}}\rangle = |\mathbf{R},\mathbf{P}\rangle$, Eq. (3.9), and the whole SLEND electronic wavefunction $|\Psi_{\mathrm{e}}\rangle = |\mathbf{z};\mathbf{R}\rangle$, Eq. (3.10), are two examples of CSs: each $|R_i,P_i\rangle$ is a member of the canonical CS set[16,17] and $|\mathbf{z};\mathbf{R}\rangle$ is a member of the Thouless CS set.[15,16] As discussed in Sections 1 and 2, the continuous parameters defining those CSs, R_i and P_i in $|R_i,P_i\rangle$ and $\mathbf{z}$ in $|\mathbf{z};\mathbf{R}\rangle$, are convenient parameters for TDVP treatments that produce dynamical equations free of numerical deficiencies in the time integration. However, a meticulous study of the vast corpus of the CS theory[16] reveals that the canonical and Thouless CS sets are by no means the only types of CS sets known and that the use of the various CS sets should not be limited to furnish convenient TDVP parameterizations. For instance,

Author's personal copy

having an END realization with nuclear classical and electronic quantum descriptions (e.g., SLEND, SLEND/KSDFT, MCCASEND[39]), different types of CS sets assuming various roles can be associated with the nuclear and electronic degrees of freedom of the END total wavefunction as shown in Fig. 3.1 (cf. Ref. 22). For instance, the canonical CS set,[16] which is associated with the harmonic oscillator, and several types of Morse CS sets,[79–83] which are associated with the anharmonic Morse oscillator, can be associated with the nuclear vibrational motions of a system.[22–25] Likewise, a rotational CS set[22,26] can be associated with the nuclear rotational motion of a system. Those nuclear CS sets constitute the foundation of the previously discussed CSQRP,[22] which recovers quantum probability amplitudes for rotational and vibrational excitations from the nuclear classical dynamics. While the original 1D Gaussian frozen wave packets of $|\Psi_N\rangle = |\mathbf{R},\mathbf{P}\rangle$ certainly possess quantum features, these features completely fade out when the zero-width limit is applied to those wave packets and a nuclear classical dynamics is obtained. Fortunately, the aforesaid harmonic vibrational and rotational CS sets exhibit the remarkable property of quasi-classical dynamical behavior, exactly in the former and approximately in the latter.[22,56] That property essentially means that the quantum dynamics of some CS averages (average position, average momentum, average angular momentum, etc.) is identical or very close to the classical dynamics of their classical counterparts (classical position, classical momentum, classical angular momentum, etc.) for the same system. Therefore, at any time during a simulation with an END version featuring nuclear classical dynamics, it is possible to construct vibrational and rotational CS so that the dynamics of their property averages match exactly or very closely the dynamics of their classical counterparts from the END simulation.[22] These matched quasi-classical CSs reconstruct some of the quantum features vanished by the zero-width limit applied to the 1D Gaussian frozen wave packets. Having constructed those CSs, the calculation of probability amplitudes for vibrational and rotational excitations with those quantum states follows standard quantum-mechanics prescriptions.[22] In this way, the simulation of the nuclear dynamics can be performed with classical mechanics at a very low computational cost, while the feasible CSQRP can be applied at the (usually few) times when quantum properties should be known. For instance, for the calculation of the vibrational and rotational state-to-state DCSs and ICSs discussed in Section 2.4, the CSQRP should be only applied at the initial and final times, t_i and t_f, of a simulation to obtain the resolution of the vibrational and the rotational parts of $|\Psi_N(t_k)\rangle = |\mathbf{R}(t_k),\mathbf{P}(t_k)\rangle$, $k = i,f$, into the initial and final vibrational and rotational eigenstates.[22] However,

Author's personal copy

not only the vibrational and rotational parts of the nuclear wavefunction are related to CSs but also the complete electronic wavefunction of some END realizations are electronic CSs themselves (cf. Fig. 3.1).[22] In that regard, the electronic wavefunctions of SLEND and SLEND/KSDFT are Thouless CSs, and the electronic wavefunction of MCCASEND[39] is a MC version of a vector CS.[84] Unlike the aforesaid nuclear CSs, these electronic CSs are by no means quasi-classical because they are supposed to provide conveniently parameterized electronic quantum descriptions along the lines of the HF, KSDFT, and MCCAS quantum methods, respectively. Therefore, from those electronic CSs (wavefunctions), quantum probability amplitudes for electronic excitations and electron transfers are obtained directly and without any quantum reconstruction by projecting those CSs into appropriate electronic states. However, in the context of hybrid quantum/classical (Q/C) methods,[85–89] classical electronic descriptions are routinely adopted for the peripheral region of very large systems as a way to reduce computational cost. In some Q/C methods, that classical electronic description entails classical-electrostatic charges *in lieu* of charges obtained from quantum wavefunctions and/or quantum electron densities. For instance, the charge-equilibration (CE) model[90,91] represents the atoms in a molecule as a set of fluctuating charges interacting in a classical-electrostatics fashion. The CE energy is a second-order polynomial in the CE charges having as coefficients the atomic electronegativities,[67] atomic hardnesses,[67] and Coulomb interactions. The optimal CE charges and energy are obtained by minimizing the CE energy with respect to the CE charges,[90,91] a procedure equivalent to applying Sanderson's principle of electronegativity equalization.[67] In that CE context, the construction of a novel quasi-classical electronic CS set based on a quantum valence bond (VB)[38] model has been suggested.[51] This VB CS gives rise to a generalized CE model that can properly describe electron transfers at bond dissociations,[51] a process that the standard CE model describes quite inaccurately. Furthermore, this quasi-classical VB CS set is a link between a quantum electronic description in terms of the VB theory and a classical-electrostatics description in terms of the generalized CE model. However, this Q/C relationship runs in the opposite direction of that of the nuclear CSQRP. That is, with the electronic VB CS, no quantum effects are recovered from a classical description but, conversely, the classical-electrostatics-generalized CE model is obtained from a quantum VB model rigorously. The novel VB CS set is currently under development in our research and will play a key role in incorporating the generalized CE model into Q/C END realizations. In summary, the combined use of all the

Author's personal copy

CSs associated with END total wavefunctions (Fig. 3.1) provides a convenient way to parameterize the END dynamics in the TDVP framework and furnishes accurate and feasible tools to calculate dynamical properties resolved into vibrational, rotational, and electronic (eigen)states.[22]

3.2. Rigorous definition of CS sets and their construction

While a conceptual definition of CS sets was given in Section 1, at this point, it becomes necessary to give a rigorous and formal definition of the CS sets. According to Klauder's initial definition,[16] CSs $\{|\zeta_i\rangle\}$ are states in a Hilbert space that satisfy two properties:

- **Property 1** (**P1**): Continuity,[16] the states $\{|\zeta_i\rangle\}$ are continuous with respect to a set of parameters $\{\zeta_i\}$.
- **Property 2** (**P2**): Resolution of unity,[16] the states $\{|\zeta_i\rangle\}$ attain resolution of unity $\hat{1} = \int \mathrm{d}\mu(\zeta_i)|\zeta_i\rangle\langle\zeta_i|$ with a positive measure $\mathrm{d}\mu(\zeta_i) > 0$. Sometimes, **P2** is relaxed to permit CS sets with measures taking positive and negative values.[26,83]

CS sets admit both real and complex parameterizations, and we will switch between those types of parameterizations whenever it is opportune. In the case of the two primal CSs in SLEND, their more convenient parameterizations for SLEND implementations are: each canonical CS $|R_i(t), P_i(t)\rangle$ in Eq. (3.9) have real parameters $\{\zeta_i\} = \{R_i, P_i\}$,[16] while the Thouless CSs $|\mathbf{z}; \mathbf{R}\rangle$ in Eq. (3.10) have complex parameters $\{\zeta_i\} = \{z_{ph}\}$.[16] However, it is possible to parameterize the canonical CSs in terms of complex parameters (cf. Eq. 3.37) and the Thouless CSs in terms of real parameters. The positive measures $\mathrm{d}\mu(\zeta_i) > 0$ of the canonical and the Thouless CS sets are given in Ref. 16. All the CS sets discussed herein satisfy property **P1** and most of them satisfy property **P2**.

Some authors, including Klauder himself,[92] have included one or more extra properties in the definition of CS sets in addition to the primal properties **P1** and **P2**. Additional CS properties relevant to this investigation include:

- **Property 3** (**P3**): Eigenstate–eigenvalue condition,[16,56,93] the CSs $\{|\xi_i\rangle\}$ with complex parameters $\{\xi_i\}$ are eigenstates of non-Hermitian annihilation operators a_i with complex eigenvalues ξ_i, $a_i|\xi_i\rangle \propto \xi_i|\xi_i\rangle$.
- **Property 4** (**P4**): Minimum uncertainty relationship,[94] the CSs $\{|\xi_i\rangle\}$ satisfy the minimum uncertainty relationship: $\Delta X \Delta P = 1/2$, where ΔX and ΔP are the CS standard deviations ("uncertainties") for generalized position and momentum, respectively.

Author's personal copy

- **Property 5** (**P5**): Temporal stability,[92] when evolving with an associated Hamiltonian $\hat{H}$, the CSs $\{|\gamma_i(t)\rangle\}$ maintain their functional form throughout time, with only its parameter(s) varying in time as follows: $|\gamma_i(t)\rangle = \exp\left(-it\hat{H}\right)|\gamma_i\rangle = |\gamma_i + \omega_i t\rangle$ or $|\gamma_i(t)\rangle = \exp\left(-it\hat{H}\right)|\gamma_i\rangle = |\gamma_i \omega_i t\rangle$, where ω_i is a constant angular velocity.
- **Property 6** (**P6**): Action identity,[92] CSs $\{|J,\gamma\rangle\}$ parameterized with real action-angle[54] variables J and γ, $J \geq 0$ and $-\infty < \gamma < +\infty$, satisfy a general action identity relationship with an associated Hamiltonian $\hat{H}$: $\langle J,\gamma|\hat{H}|J,\gamma\rangle = f(J)$, where $f(J)$ is a function of J alone. While various types of functions $f(J)$ have been proposed,[82,83,92] the ideal form is $f(J) = \omega J$,[92] where ω is the angular velocity associated with γ.
- **Property 7** (**P7**): Quasi-classical behavior in its weak sense,[22–24,33,34,56] the average position $\langle R,P|\hat{X}|R,P\rangle = R$ and momentum $\langle R,P|\hat{P}_x|R,P\rangle = P$ of CSs $|R,P\rangle$ with real parameters R and P evolve with an associated Hamiltonian $\hat{H}$ as the position and momentum of its classical-mechanics analogue with classical Hamiltonian $H(R,P)$.

Properties **P4**–**P7** aim at constructing CSs that evolve with an associated Hamiltonian $\hat{H}$ as classically as possible within quantum mechanics. Properties **P4**–**P7** collectively define the quasi-classical dynamical behavior in its hard sense. The canonical CS satisfies all the additional CS properties **P3**–**P7**, having the boson annihilation operators a and the 1D harmonic oscillator Hamiltonian $\hat{H}_{\mathrm{HO}}$ as its associated annihilation operator (**P3**) and associated Hamiltonian (**P4**–**P7**), respectively. The canonical CS satisfies properties **P4**–**P7** with $\hat{H}_{\mathrm{HO}}$ both under its exact dynamics from the TD Schrödinger equation and under TDVP dynamics, both dynamics being identical in this case. Perfect compliance with properties **P4**–**P7** on part of the canonical CS makes the latter the ideal CS for a CSQRP.

There exist several methods to construct CS sets for specific systems under study. Those methods provide CS sets that at least satisfy the primary CS property **P1**.[16] Four of those CS methods are relevant for SLEND and are therefore reviewed in the following paragraphs.

The predominant method to construct CS sets is the group-theoretical approach.[16] Detailed prescriptions to construct CS sets through group theory have been presented by Perelomov[95] and by Gilmore[96] and have been reviewed by Zhang.[97] (Group-generated CSs were originally called "generalized" CSs because they were constructed as a generalization of the canonical CS that historically was the first CS.[17]). A quantum-mechanical

Author's personal copy

system may be defined by using a complete set of operators $\{\hat{T}_i\}$ that is closed under the commutation relations:

$$[\hat{T}_i, \hat{T}_j] = \sum_k C_{ij}^k \hat{T}_k \tag{3.30}$$

where $\{C_{ij}^k\}$ are the structure coefficients.[98] These commutation relations define a Lie algebra **A** and its associated Lie group **G**.[98] The latter, in general, contains elements $\hat{h}$ that only affect the phase of a state $|\psi\rangle$:

$$\hat{h}|\psi\rangle = e^{i\varphi(h)}|\psi\rangle \tag{3.31}$$

The set of all such elements, $\mathbf{H} = \{\hat{h}\} \subset \mathbf{G}$, forms a subgroup of **G**. The quotient group **G**/**H** is the set of all the left cosets of **H** in **G**. Each $x \in \mathbf{G}/\mathbf{H}$ is an equivalence class of the elements of **G**, that is, $\{x\} = \{\hat{g}\mathbf{H}, \hat{g} \in \mathbf{G}\}$; the members of each x differ only by a phase factor. Then, CSs can be constructed by using representative members from each equivalence class, $\hat{g}'$. If $\hat{T}(\hat{g}')$ is a unitary irreducible representation of $\hat{g}'$ in the Hilbert space V^λ and $|\psi_0\rangle$ is an arbitrary reference state in V^λ, then the CSs $\left\{\left|\psi_{g'}\right\rangle\right\}$ generated from the Lie group **G** are:

$$\left|\psi_{g'}\right\rangle = \hat{T}(\hat{g}')|\psi_0\rangle \tag{3.32}$$

The reference state $|\psi_0\rangle$ in Eq. (3.32) is chosen so as to generate states which are closest to classical states, as described by Perelomov.[95] For compact simple Lie groups, which are those that are important to SLEND, the ground or "vacuum" state satisfies this condition. All the group-generated CS sets relevant for this study have the same general form for $\hat{T}(\hat{g}')$: $\hat{T}(\hat{g}')$ is the product of a phase factor and a displacement operator. The arbitrary phase factor is taken to be equal to one resulting in CSs given by

$$|\psi_a\rangle = \hat{D}(\alpha)|\psi_0\rangle \tag{3.33}$$

where $\hat{D}(\alpha)$ is the displacement operator with a parameter α. The latter becomes the parameter of the CS set. Group-generated CSs constructed in this way are named displacement operator CSs (DOCSs). Group-generated CS sets satisfy the primal CS properties **P1** and **P2** by construction.[16]

Author's personal copy

As an example of a group-generated DOCS set, let us examine the canonical CS set associated with the 1D quantum harmonic oscillator. The latter system is defined by boson creation and annihilation operators $\{\hat{a}^\dagger,\hat{a}\}$ with the commutation relations:

$$\left[\hat{a},\hat{a}^\dagger\right]=\hat{I};\quad \left[\hat{a},\hat{I}\right]=\left[\hat{a}^\dagger,\hat{I}\right]=0 \tag{3.34}$$

where $\hat{I}$ is the identity operator. Additionally, a number operator, $\hat{n}$, can be defined such as

$$\hat{n}=\hat{a}^\dagger\hat{a};\quad \left[\hat{n},\hat{a}^\dagger\right]=\hat{a}^\dagger;\quad [\hat{n},\hat{a}]=-\hat{a};\quad \left[\hat{n},\hat{I}\right]=0 \tag{3.35}$$

Equations (3.34) and (3.35) define the Heisenberg–Weyl Lie algebra and its corresponding Heisenberg–Weyl Lie group $\mathbf{H}_4$.[97] The harmonic-oscillator Hamiltonian $\hat{H}_{\mathrm{HO}}$ can be written in terms of the boson creation and annihilation operators

$$\hat{H}_{\mathrm{HO}}=\omega\left(\hat{a}^\dagger\hat{a}+\frac{1}{2}\right) \tag{3.36}$$

where ω is the oscillator angular frequency. An appropriate reference state for this system is the harmonic-oscillator ground state $|0\rangle$. The set of operators that leave $|0\rangle$ invariant up to a phase factor is $\{\hat{n},\hat{I}\}$, which spans the group $\mathbf{U}(1)\otimes\mathbf{U}(1)$. The displacement operator chosen from the coset space $\mathbf{H}_4/\mathbf{U}(1)\otimes\mathbf{U}(1)$ has the form $\hat{D}(\alpha)=\exp\left(\alpha\hat{a}^\dagger-\alpha^*\hat{a}\right)$, where α is a complex parameter. Then, following Eq. (3.33), a canonical CS set $|\alpha\rangle$ in terms of the complex parameter α is:

$$\begin{aligned}|\alpha\rangle&=\exp\left(\alpha\hat{a}^\dagger-\alpha^*\hat{a}\right)|0\rangle\\&=\exp\left(-\frac{1}{2}|\alpha|^2\right)\exp\left(\alpha\hat{a}^\dagger\right)|0\rangle\\&=\exp\left(-\frac{1}{2}|\alpha|^2\right)\sum_n\frac{\alpha^n}{\sqrt{n!}}|n\rangle\end{aligned} \tag{3.37}$$

where the Baker–Campbell–Hausdorff (BCH) formula[97] has been used from the first to the second lines and $\{|n\rangle;\quad n=0,1,2,\ldots\}$ are the quantum harmonic oscillator eigenstates. The last line of Eq. (3.37) gives the resolution of a canonical CS into the quantum harmonic oscillator eigenstates: a

Author's personal copy

key relationship to perform the harmonic vibrational CSQRP. The boson creation and annihilation operators $\{a^\dagger, a\}$ can be expressed in terms of the position and momentum operators $\hat{X}$ and $\hat{P}$

$$a^\dagger = \sqrt{\frac{m\omega}{2}}\hat{X} - \frac{\mathrm{i}}{\sqrt{2m\omega}}\hat{P}; \quad a = \sqrt{\frac{m\omega}{2}}\hat{X} + \frac{\mathrm{i}}{\sqrt{2m\omega}}\hat{P} \tag{3.38}$$

where m is the oscillator mass. By using the expressions in Eq. (3.38) and by projecting the canonical CS $|\alpha\rangle$ into position space, a closed-form expression for that CS in terms of the real parameters $\langle\hat{X}\rangle_\alpha$ and $\langle\hat{P}\rangle_\alpha$ is obtained:[56]

$$\begin{aligned}\psi_\alpha(X) &= \langle X|\alpha\rangle \\ &= \langle X|\langle\hat{X}\rangle_\alpha\langle\hat{P}\rangle_\alpha\rangle \\ &= \mathrm{e}^{\mathrm{i}\theta_\alpha}\left(\frac{m\omega}{\pi}\right)^{1/4}\exp\left[-\left(\frac{X-\langle\hat{X}\rangle_\alpha}{2\Delta X_\alpha}\right)^2 + \mathrm{i}\langle\hat{P}\rangle_\alpha X\right]\end{aligned} \tag{3.39}$$

where $\langle\hat{X}\rangle_\alpha$ and $\langle\hat{P}\rangle_\alpha$ are the CS average position and average momenta, $\mathrm{e}^{\mathrm{i}\theta_\alpha}$ is a global phase term, and $\Delta X_\alpha = \sqrt{1/2m\omega}$ is the CS standard deviation for the position. The relationship between the complex parameter α and the real parameters $\langle\hat{X}\rangle_\alpha$ and $\langle\hat{P}\rangle_\alpha$ is

$$\alpha = \sqrt{\frac{m\omega}{2}}\langle\hat{\boldsymbol{X}}\rangle_\alpha + \frac{\mathrm{i}}{\sqrt{2m\omega}}\langle\hat{\boldsymbol{P}}\rangle_\alpha \tag{3.40}$$

The canonical CS wavefunction $\psi_\alpha(X)$ in Eq. (3.39) is a normalized 1D Gaussian frozen wave packet with position (center) $\langle\hat{X}\rangle_\alpha$, momentum $\langle\hat{P}\rangle_\alpha$, and width ΔX_α. $\psi_\alpha(x) = \langle X|\langle\hat{\boldsymbol{X}}\rangle_\alpha\langle\hat{\boldsymbol{P}}\rangle_\alpha\rangle$ is identical (up to a normalization constant and a global phase term) to any of the SLEND nuclear wave packets $\langle X_i|R_i,P_i\rangle$ in Eq. (3.9) if one identifies $X = X_i$, $\langle\hat{X}\rangle_\alpha = R_i$, and $\langle\hat{P}\rangle_\alpha = P_i$.

A second method to construct CS sets is the one proposed by Barut and Girardello.[93] These authors sought to construct CS sets that satisfy the CS property **P3** in addition to **P1** and **P2**. Originally, this method was a generalization of the previous group-theoretical approach that would allow for constructing CS sets for noncompact groups when the latter method was unable to do so.[93] However, Perelomov later extended the group-theoretical method to any arbitrary group.[95] Barut and Girardello's original work concerned a specific application to the SO(2,1) group;[93] however, a general presentation was given by Popov et al.[99] For a set of Fock vectors

Author's personal copy

$\{|n;\lambda\rangle\}$, where n is a quantum number and λ is a parameter, and a pair of creation and annihilation operators $\{\hat{a}^\dagger,\hat{a}\}$ defined by

$$\begin{aligned}\hat{a}|n;\lambda\rangle &= \sqrt{e_n(\lambda)}|n-1;\lambda\rangle \\ \hat{a}^\dagger|n;\lambda\rangle &= \sqrt{e_{n+1}(\lambda)}|n+1;\lambda\rangle,\end{aligned} \tag{3.41}$$

where $e_n(\lambda)$ are some functions of λ, Barut and Girardello define as CSs the states $\{|z;\lambda\rangle\}$ that satisfy

$$\hat{\boldsymbol{a}}|z;\lambda\rangle = z|z;\lambda\rangle \tag{3.42}$$

where z is a complex parameter. In other words, the CSs $\{|z;\lambda\rangle\}$ satisfy the CS property **P3**. The CSs $\{|z;\lambda\rangle\}$ can be expanded in the Fock vector basis $\{|n;\lambda\rangle\}$

$$\hat{\boldsymbol{a}}\sum_n c_{n,\lambda}(z)|n;\lambda\rangle = z\sum_n c_{n,\lambda}(z)|n;\lambda\rangle, \tag{3.43}$$

and the expansion coefficients $c_{n,\lambda}(z)$ can be determined through the orthonormalization conditions of the Fock vectors: $\langle m;\lambda|n;\lambda\rangle = \delta_{m,n}$. The resulting recursion relation for the expansion coefficients is

$$c_{m,\lambda}(z) = c_{0,\lambda}(z)\frac{z^m}{\sqrt{\rho_m(\lambda)}} \tag{3.44}$$

where

$$\rho_m(\lambda) = \prod_{i=1}^{m} e_i(\lambda) \tag{3.45}$$

$c_{0,\lambda}(z)$ is ultimately obtained through the normalization condition as

$$c_{0,\lambda}(z) = \left[\sum_n \frac{|z|^{2n}}{\rho_n(\lambda)}\right]^{-1/2}. \tag{3.46}$$

The method of Barut and Girardello was independently generalized by Nieto and Simmons to describe systems with unequal energy spacing.[94] The Barut and Girardello CSs are named annihilation operator CSs (AOCSs).

It is instructive to demonstrate that the canonical CS is not only a DOCS from the group-theoretical method but also an AOCS from the Barut and Girardello method. The boson annihilation operators of the harmonic oscillator acts on the latter's eigenstates as: $\boldsymbol{a}|n\rangle = \sqrt{n}|n-1\rangle$. Comparison with Eq. (3.41) shows that for the harmonic oscillator $e_n(\lambda) = n$. Applying these

Author's personal copy

last results to Eqs. (3.42)–(3.46) and replacing the parameter z with the parameter α yields for the CS $|z;\lambda\rangle = |\alpha\rangle$:

$$\rho_m(\lambda) = m!; \quad c_{0,\lambda}(\alpha) = \left[\sum_n \frac{|\alpha|^{2n}}{n!}\right]^{-1/2} = \exp\left(-\frac{1}{2}|\alpha|^2\right) \tag{3.47}$$

so that

$$|z;\lambda\rangle = |\alpha\rangle = \exp\left(-\frac{1}{2}|\alpha|^2\right)\sum_n \frac{\alpha^n}{\sqrt{n!}}|n\rangle \tag{3.48}$$

that is exactly the canonical CS obtained from the group-theoretic method, Eq. (3.37).

A third method to construct CS sets is the one proposed by Nieto and Simmons.[81,94,100–102] These authors sought to construct CS sets that purposely satisfy property **P4**.[94] Their method starts by casting the classical Hamiltonian of a system in a harmonic oscillator form by introducing a generalized position X_c and a mass-weighted generalized velocity $P_c = m\dot{X}_c$.[81,94,100–102] Notice that in general X_c and P_c are not a pair of conjugate canonical variables. Then, generalized quantum operators are derived from those classical variables as $\hat{X} \equiv X_c$ and $\hat{P}_X \equiv \frac{1}{2}\left[\left(\frac{\mathrm{d}}{\mathrm{d}x}X_c\right)\hat{p}_x + \hat{p}_x\left(\frac{\mathrm{d}}{\mathrm{d}x}X_c\right)\right]$, where x is the usual position and $\hat{p}_x = -\mathrm{i}\mathrm{d}/\mathrm{d}x$ the usual quantum momentum operator.[94] It is well-known that for any two quantum operators $\hat{A}$ and $\hat{B}$, there exists an uncertainty inequality $\Delta A \Delta B = \langle \Delta\hat{A}\rangle\langle\Delta\hat{B}\rangle \geq \frac{1}{2}\langle\hat{G}\rangle$, where $\mathrm{i}\hat{G} = [\hat{A},\hat{B}]$.[103] Then, Nieto and Simmons provided a prescription to construct minimum uncertainty CSs (MUCSs) that saturate the uncertainty inequality for the generalized quantum operators $\hat{X}$ and $\hat{P}_X$ with the restriction that the MUCS set must contain the ground state of the system as a special case. The MUCSs satisfy the CS property **P1** as well as property **P4**. Nieto has provided a further comprehensive study of different MUCS sets derived for various bound and unbound model potentials.[81,100–102]

It is easy to demonstrate that the canonical CS is also a MUCS. With the canonical CS, the generalized operators $\hat{X}_c$ and $\hat{P}_c$ are just the standard position and momentum operators $\hat{x}$ and $\hat{p}_x$; therefore, the MUCS minimum uncertainty relationship for $\hat{X}_c$ and $\hat{P}_c$ should involve the operators $\hat{x}$ and $\hat{p}_x$ in this case. Having the expression of the canonical CS $|\alpha\rangle = \left|\langle\hat{X}\rangle_\alpha\langle\hat{P}\rangle_\alpha\right\rangle$ from Eq. (3.39), it is straightforward to find that its standard deviations for the position and momentum, ΔX_α and ΔP_α, are

Author's personal copy

$$\Delta X_\alpha = \left(\frac{1}{2m\omega}\right)^{1/2};\ \ \Delta P_\alpha = \left(\frac{m\omega}{2}\right)^{1/2}, \tag{3.49}$$

so that the uncertainty inequality is indeed minimized for $\hat{X}$ and $\hat{P}$ (the CS property **P4**)

$$\Delta X_\alpha \Delta P_\alpha = \frac{1}{2}. \tag{3.50}$$

The latter proves that a canonical CS set is also a MUCS with respect to the operators $\hat{x}$ and $\hat{p}_x$.

The fourth and last method to construct CSs that will be reviewed herein is the one proposed by Gazeau and Klauder.[92] These authors sought to construct CS sets that satisfy the primary CS properties **P1** and **P2** as well as the additional properties **P5** and **P6**.[92] These last two properties impart a partial quasi-classical character to their CSs. The construction of Gazeau–Klauder CSs (GKCSs) $\{|z\rangle\}$ starts with the general expression of the AOCS:

$$|z\rangle = N\left(|z|^2\right)\sum_{n\geq 0}\frac{z^n}{\sqrt{\rho_n}}|n\rangle \tag{3.51}$$

where z is a general complex parameter, $N(|z|^2)$ is a normalization constant, ρ_n are the moments of a probability distribution, and $\{|n\rangle\}$ are the eigenstates of the system under study. To impose temporal stability (CS property **P5**), a phase factor $e^{-i\gamma e_n}$ is added in Eq. (3.51) to capture the entire orbit in the complex manifold:[92]

$$|z,\gamma\rangle = N\left(|z|^2\right)\sum_{n\geq 0}\frac{z^n}{\sqrt{\rho_n}}e^{-i\gamma e_n}|n\rangle \tag{3.52}$$

where e_n is the dimensionless reduced energy eigenvalue of the eigenstate $|n\rangle$, with the ground-state reduced energy eigenvalue shifted to $e_0 = 0$, and γ, $-\infty \leq \gamma \leq +\infty$, is a real parameter. Due to this included phase factor, the complex parameter z can, with no loss of generality, be replaced with the real parameter $J = |z|^2 \geq 0$ yielding[92]

$$|J,\gamma\rangle = N(J)\sum_{n\geq 0}\frac{J^{n/2}}{\sqrt{\rho_n}}e^{-i\gamma e_n}|n\rangle \tag{3.53}$$

The GKCS's real parameters J and γ, $J \geq 0$ and $-\infty < \gamma < +\infty$, are conceived as action-angle variables.[54] Equation (3.53) defines GKCSs $\{|J,\gamma\rangle\}$ so far

Author's personal copy

satisfying the CS properties **P1**, **P2**, and **P5**. The specific form of these GKCSs is determined by a particular choice of ρ_n. Requiring that the GKCSs $\{|J,\gamma\rangle\}$ also satisfy action identity in its ideal form (CS property **P6**), $\langle J,\gamma|\hat{H}|J,\gamma\rangle = f(J) = \omega J$ defines ρ_n uniquely as[92]:

$$\rho_0 = 1; \quad \rho_n = \prod_{i=1}^{n\geq 1} e_i \tag{3.54}$$

As mentioned previously, alternative forms of $f(J)$ have been proposed.[82,83,92]

As with the MUCSs, it is easy to demonstrate that a canonical CS is also a GKCS with $f(J)$ in is ideal form. The harmonic oscillator eigenstates $\{|n\rangle\}$ redefined for the above reduced energy eigenvalues satisfy $\hat{H}_{\mathrm{HO}}|n\rangle = \omega n|n\rangle$. Therefore, $e_n = n$ and the GKCSs $\{|J,\gamma\rangle\}$ in Eq. (3.53) become:

$$|J,\gamma\rangle = N(J)\sum_{n\geq 0}\frac{J^{n/2}\mathrm{e}^{-\mathrm{i}n\gamma}}{\sqrt{n!}}|n\rangle. \tag{3.55}$$

By setting $\alpha = J^{1/2}\mathrm{e}^{-\mathrm{i}\gamma}$, the GKCSs $\{|J,\gamma\rangle\}$ in Eq. (3.55) become the usual canonical CSs in Eq. (3.48).

With the exception of the vector CS sets,[84] all the CS sets relevant for the END theory can be constructed by at least one of the four methods reviewed herein. (The canonical CS set is exceptional because it can be equally constructed with any of the four discussed methods.) Having reviewed the construction of CS sets in general, attention will be shifted on the forms, properties, and uses of the specific CS sets relevant for END.

3.3. Nuclear vibrational CS for the vibrational CSQRP

To formulate a CSQRP in SLEND, vibrational and rotational CSs should be associated with the vibrational and rotational parts of the SLEND nuclear wavefunction $|\Psi_{\mathrm{N}}\rangle$, Eq. (3.9), that underlie the SLEND classical dynamics before the application of the zero-width limit to the wave packets in $|\Psi_{\mathrm{N}}\rangle$ (cf. Fig. 3.1). Ideally, the best-suited CSs for that task would be vibrational and rotational CSs rigorously satisfying the quasi-classical properties **P4**–**P7** with the corresponding vibrational and rotational Hamiltonians. As will be seen soon, that ideal is not always reached but good approximations to it are available. Thus, at least five types of vibrational CSs (the canonical CS[16] associated with the harmonic

Author's personal copy

oscillator and four Morse CSs[79–83] associated with the anharmonic Morse oscillator) and one type of rotational CS[26] can be properly utilized in the nuclear CSQRP. Those vibrational CSs will be discussed in detail in this section, while the rotational CS will be explained in the following one. However, before discussing them, it is important to determine two things: (1) how the nuclear SLEND wavefunction $|\Psi_N\rangle$, Eq. (3.9), can be partitioned into translational, vibrational, and rotational parts and (2) how the last two parts can be associated with appropriate CSs. These two questions are answered by the rigorous derivation of the nuclear CSQRP from $|\Psi_N\rangle$ given below. The mentioned partition of $|\Psi_N\rangle$ into degree-of-freedom factors and their subsequent association with CSs must be elucidated despite the fact that the 1D Gaussian frozen wave packets that make up $|\Psi_N\rangle$, Eq. (3.9), are canonical CSs in themselves. This is so because the wave packets in Eq. (3.9) represent the individual motions of the interacting nuclei without explicitly expressing the vibrational and rotational collective motions of those particles. Furthermore, those wave packets are naturally fit for vibrational descriptions but not for rotational ones.

A rigorous derivation of the nuclear CSQRP from the SLEND nuclear wavefunction $|\Psi_N^{AB}\rangle$ for an isolated diatomic molecule AB was presented in Ref. 26 and is outlined herein. In the context of the ion–molecule reactions $I^q + M\left(n_D^i\right) \rightarrow I^{q'} + M^{q''}\left(n_D^f\right)$, Eq. (3.24), discussed in Section 2.4, that isolated diatomic molecule AB can be the pre(post)-collision target $M(n_D^i)$ $\left[M^{q''}\left(n_D^f\right)\right]$, well separated from the incoming(outgoing) projectile I^q ($I^{q'}$), to which the CSQRP is applied at initial (final) time to obtain vibrational and rotational state-to-state dynamical properties. The derivation of the nuclear CSQRP for that diatomic molecule AB starts with its SLEND total wavefunction $|\Psi_{Total}^{AB}\rangle = |\Psi_e^{AB}\rangle|\Psi_N^{AB}\rangle$. By switching into CM and internal coordinates and by assuming rotational–vibrational decoupling and the rigid-rotor approximation,[104,105] the nuclear wavefunction $|\Psi_N^{AB}\rangle$ can be factored into translational $|\Psi_{Trans}^{AB}\rangle$, rotational $|\Psi_{Rot}^{AB}\rangle$, and vibrational $|\Psi_{Vib}^{AB}\rangle$ wavefunctions: $|\Psi_N^{AB}\rangle = |\Psi_{Trans}^{AB}\rangle|\Psi_{Rot}^{AB}\rangle|\Psi_{Vib}^{AB}\rangle$.[22,26] $|\Psi_{Trans}^{AB}\rangle$ is a 3D wave packet centered on the AB CM and describes the translational motion of AB.[22,26] $|\Psi_{Rot}^{AB}\rangle$ is a wavefunction that describes the rotational motion of AB. As revealed by its explicit expression in Ref. 26, $|\Psi_{Rot}^{AB}\rangle$ is not an expected rotational CS, but it can be approximated with a rotational CS as explained in Ref. 26 itself (see also Section 3.5). Finally, $|\Psi_{Vib}^{AB}\rangle$ is exactly a canonical CS describing the vibrational motion of AB:[22,26] $|\Psi_{Vib}^{AB}\rangle = |\alpha\rangle$,

Author's personal copy

Eq. (3.37). Along with the factorization of $|\Psi_N^{AB}\rangle$, the SLEND total energy E_{Total}^{AB} becomes $E_{Total}^{AB} = E_{Trans}^{AB} + E_{Vib}^{AB} + E_{Rot}^{AB} + E_e^{ABEq.}$, where E_{Trans}^{AB}, E_{Rot}^{AB}, and E_{Vib}^{AB} are the classical energies associated with those degrees of freedom, and $E_e^{ABEq.}$ is the electronic energy including nuclear repulsion at the AB equilibrium bond distance $R_{AB}^{Eq.}$, $E_e^{ABEq.} = E_e^{AB}(R_{AB}^{Eq.})$.[22,26] If AB is assumed harmonic, E_{Vib}^{AB} can be approximated as $E_{Vib}^{AB} = (1/2m_{AB})P_{AB}^2 + V_{HO}(R_{AB})$, with $V_{HO}(R_{AB}) = (m_{AB}\omega_{AB}^2/2)(R_{AB} - R_{AB}^{Eq.})^2 = E_e^{AB}(R_{AB}) - E_e^{ABEq.}$, where R_{AB} is the classical vibrational coordinate (A − B separation), P_{AB} the classical vibrational momentum, m_{AB} the reduced mass, and ω_{AB} the angular frequency of AB. Under the harmonic approximation, the canonical CS $|\Psi_{Vib}^{AB}\rangle = |\alpha\rangle$ will quasi-classically evolve exactly as the classical harmonic oscillator analogue of AB (CS property **P7**, cf. Sections 3.1 and 3.2). In an actual SLEND simulation, the zero-width limit is applied to the nuclear wave packets of $|\Psi_N^{AB}\rangle$. That makes those wave packets shrink into Dirac delta functions that represent the nuclei A and B as point particles obeying classical mechanics. However, at any time of the SLEND simulation, it is possible to construct the canonical CS $|\Psi_{Vib}^{AB}\rangle = |\alpha\rangle$ that matches the SLEND classical harmonic vibration of AB. With the constructed $|\Psi_{Vib}^{AB}\rangle = |\alpha\rangle$, it is possible to calculate the probability of finding the molecule AB in its vibrational eigenstate $|n\rangle^{AB}$ via the resolution of the canonical CS $|\Psi_{Vib}^{AB}\rangle = |\alpha\rangle$ into the harmonic oscillator eigenstates $\{|n\rangle\}$, Eq. (3.37). Use of that expression requires finding the value of the parameter α of the $|\Psi_{Vib}^{AB}\rangle = |\alpha\rangle$ matching the SLEND classical vibrational dynamics of AB. From the SLEND simulation data, the values of the classical variables: R_{AB}, P_{AB}, E_{Vib}^{AB}, and ω_{AB} can be easily obtained. R_{AB}, P_{AB}, and ω_{AB} provide the value of α via Eq. (3.40) along with the identifications: $R_{AB} = \langle \hat{X} \rangle_\alpha$, $P_{AB} = \langle \hat{P} \rangle_\alpha$, $\omega_{AB} = \omega$, and $m_{AB} = m$. In addition, it is easy to prove from Eq. (3.40) that

$$\begin{aligned} E_{Vib}^{AB} &= \omega_{AB}|\alpha|^2 \\ &= \frac{1}{2m_{AB}} P_{AB}^2 + \frac{1}{2} m_{AB}\omega_{AB}^2 R_{AB}^2 \end{aligned} \tag{3.56}$$

Notice that $\omega_{AB}|\alpha|^2$ is the classical part E^{cl}, $E^{cl} = \omega_{AB}|\alpha|^2$, of the canonical CS energy since $\langle\alpha|\hat{H}_{HO}|\alpha\rangle = \omega_{AB}|\alpha|^2 + \omega_{AB}/2$.[56] Therefore, the canonical CSQRP probability amplitude A_n^{CCS} and probability $P_n^{CCS} = |A_n^{CCS}|^2$ of finding the molecule AB in its vibrational eigenstate $|n\rangle^{AB}$ from the SLEND variables R_{AB}, P_{AB}, E_{Vib}^{AB}, and ω_{AB} are:

Author's personal copy

$$A_n^{CCS}(R_{AB},P_{AB}) = \exp\left(-\frac{E_{AB}^{Vib}}{2\omega_{AB}}\right) \frac{\left[\sqrt{\frac{m_{AB}\omega_{AB}}{2}}R_{AB} + \frac{i}{\sqrt{2m_{AB}\omega_{AB}}}P_{AB}\right]^n}{\sqrt{n!}}; \quad (3.57)$$

$$P_n^{CCS}\left(\frac{E_{AB}^{Vib}}{\omega_{AB}}\right) = \exp\left(-\frac{E_{AB}^{Vib}}{\omega_{AB}}\right)\frac{\left(\frac{E_{AB}^{Vib}}{\omega_{AB}}\right)^n}{n!}.$$

$P_n^{CCS}(E_{AB}^{Vib}/\omega_{AB})$ is a Poisson distribution function in terms of the variable E_{AB}^{Vib}/ω_{AB}. Notice that when $R_{AB}=P_{AB}=0$ at all times, $E_{AB}^{Vib}=0$ and $A_n^{CCS}=P_n^{CCS}=\delta_{0n}$. The latter implies that a SLEND-simulated molecule AB in its vibrational ground eigenstate $|n=0\rangle^{AB}$ must have a null classical vibrational energy E_{AB}^{Vib}. For the ion–molecule reactions, $I^q + M\left(n_D^i=0\right) \rightarrow I^{q'} + M^{q''}$ discussed in Section 2.4 with a target M = AB, the described canonical CSQRP procedure is applied to M = AB at initial and final times to obtain vibrational state-to-state properties. These reactions start with the target in its vibrational ground eigenstate: $n_{Vib}^i=0 \Rightarrow |n=0\rangle^{AB}$. Therefore, the SLEND simulations of these reactions should start with the target AB having $E_{AB}^{Vib}=0$ so that $A_{n_{Vib}^i=0}^{CCS} = P_{n_{Vib}^i=0}^{CCS} = 1$ (cf. Eq. 3.57). From that initial eigenstate, the probability amplitudes $A_{n_D^i=0\rightarrow n_D^f}$ for the $n_{Vib}^i=0 \rightarrow n_{Vib}^f=0,1,2,\ldots$ transitions $A_{n_D^i=0\rightarrow n_D^f}$ become $A_{n_D^i=0\rightarrow n_D^f} = A_{n_D^f}^{CCS}$ (cf. Eq. 3.57). The obtained probability amplitudes $A_{n_D^i=0\rightarrow n_D^f}$ are subsequently used in the calculation of vibrational state-to-state DCSs and ICSs according to Eqs. (3.25) and (3.28), respectively. Similarly, the final probabilities $P_{n_D^f}^{CCS} = \left|A_{n_D^f}^{CCS}\right|^2$ are used in the calculation of the projectile I^q energy loss spectra (cf. Section 5 and Refs. 25,33).

The explained canonical CSQRP to obtain vibrational state-to-state properties was applied for the first time to SLEND simulations of $H^+ + H_2(v_i=0) \rightarrow H^+ + H_2(v_f)$ at $E_{Lab}=30\,eV$, rendering vibrational state-to-state ICSs for $0 \le v_f \le 6$[23] and vibrational state-to-state DCSs for $0 \le v_f \le 5$[24] in very good agreement with experimental results.[106] The $H^+ + H_2$ SLEND ICSs[23] compared well with their theoretical counterparts

Author's personal copy

obtained with the IOS[107] approximation and did better than ICSs from QCT dynamics calculations.[106] Furthermore, the $H^+ + H_2$ SLEND DCSs[24] matched the experimental data[106] much better than their IOS[107] and QCT[106] counterparts. (The nondirect-dynamics IOS and QCT methods employed diatomics-in-molecules PESs;[106,107] notice that the IOS approximation features a quantum nuclear treatment unlike SLEND and QCT.) More recently, the canonical CSQRP has been applied to SLEND simulation of $H^+ + N_2(v_i = 0) \rightarrow H^+ + N_2(v_f = 0-1)$,[33] $H^+ + CO(v_i = 0) \rightarrow H^+ + CO(v_f = 0-2)$[34] and $H^+ + NO(v_i = 0) \rightarrow H^+ + NO(v_f = 0-2)$[25] all at $E_{Lab} = 30\,eV$, rendering various vibrational state-to-state properties in good agreement with experimental results.[108] Some of those calculated properties are discussed in Section 5.

The rigorous derivation of the nuclear CSQRP from the SLEND nuclear wavefunction $|\Psi_N\rangle$ for an isolated diatomic molecule AB can be easily generalized for the case of an isolated polyatomic molecule P with n_{nm} normal modes of vibration. In this case, the nuclear wavefunction $|\Psi^P_N\rangle$ can be factored into translational $|\Psi^P_{Trans}\rangle$, rotational $|\Psi^P_{Rot}\rangle$, and vibrational $|\Psi^P_{Vib}\rangle$ wavefunctions: $|\Psi^P_N\rangle = |\Psi^P_{Trans}\rangle\,|\Psi^P_{Rot}\rangle\,|\Psi^P_{Vib}\rangle$ that are analogous to their AB counterparts. In particular, $|\Psi^P_{Vib}\rangle$ is the product of n_{nm} canonical CSs, one for each normal mode of vibration in the molecule P. Therefore, the previously described canonical CSQRP applied to the single normal mode of vibration in AB can be applied similarly to each normal mode of vibration in M. Recently, we have completed the first ever application of the canonical CSQRP to a scattering system containing a polyatomic target M: $H^+ + CO_2(v^i_1 v^i_2 v^i_3 = 000) \rightarrow H^+ + CO_2(v^f_1 v^f_2 v^f_3)$ at $E_{Lab} = 29.5\,eV$.[109] Canonical CSQRP proton energy loss spectra of that scattering system are discussed in Section 5.

As discussed in Section 3.2, the canonical CS is constructed for the harmonic potential, satisfying the CS property **P7** (quasi-classical behavior in the weak sense) when evolving with the harmonic oscillator Hamiltonian $\hat{H}_{HO}$. Therefore, a CSQRP based on the canonical CS is best suited for molecular vibrations that can be described adequately within the harmonic approximation. However, in many cases, the harmonic potential poorly describes molecular vibrations and should be substituted for more accurate potentials that include anharmonic effects. The simplest anharmonic potential is the well-known Morse potential. While certainly not being the most accurate anharmonic potential, the Morse potential constitutes a dramatic improvement over its harmonic counterpart and will be adopted to describe vibrational motions hereafter. Once the harmonic potential is substituted for the Morse one, the canonical CS becomes inappropriate to describe

Author's personal copy

molecular vibrations and should be substituted for a CS associated with the Morse potential. For instance, for the above example with an isolated diatomic molecule AB, if the harmonic potential $V_{\mathrm{HO}}(R_{\mathrm{AB}}) = (m_{\mathrm{AB}}\omega_{\mathrm{AB}}^2/2)(R_{\mathrm{AB}} - R_{\mathrm{AB}}^{\mathrm{Eq.}})^2$ is inadequate to describe its SLEND vibrational motions, it can be substituted for the more accurate Morse potential $V_{\mathrm{Morse}}(R_{\mathrm{AB}}) = D_{\mathrm{AB}}^{\mathrm{Eq.}}\{1 - \exp[a_{\mathrm{AB}}(R_{\mathrm{AB}} - R_{\mathrm{AB}}^{\mathrm{Eq.}})]\}^2$ with parameters: $a_{\mathrm{AB}} > 0$, $D_{\mathrm{AB}}^{\mathrm{Eq.}} > 0$ (dissociation energy from the potential well minimum), and $R_{\mathrm{AB}}^{\mathrm{Eq.}}$ (AB equilibrium bond distance). Under that condition, $E_{\mathrm{Vib}}^{\mathrm{AB}} = \frac{1}{2m_{\mathrm{AB}}}P_{\mathrm{AB}}^2 + V_{\mathrm{Morse}}(R_{\mathrm{AB}})$, $V_{\mathrm{Morse}}(R_{\mathrm{AB}}) = E_{\mathrm{e}}^{\mathrm{AB}}(R_{\mathrm{AB}}) - E_{\mathrm{e}}^{\mathrm{ABEq.}}$, and $|\Psi_{\mathrm{Vib}}^{\mathrm{AB}}\rangle$ should be expressed as a CS associated with the Morse Hamiltonian $\hat{H}_{\mathrm{Morse}}$. As mentioned previously, there are at least four types of Morse CS sets[79–83] and three of them have been utilized with the vibrational CSQRP applied to SLEND results[25]: the SU(1,1)[79] and SU(2)[80] Morse CS and the Morse GKCS.[82,83] A concise discussion of these Morse CSs relevant for SLEND is presented in the following paragraphs. Further details are provided in the cited references.

As their names indicate, the SU(1,1) and SU(2) Morse CSs are DOCSs constructed through the group-theoretical approach.[95] For a Morse potential defined as $V_{\mathrm{Morse}}(x) = D(\mathrm{e}^{-2ax} - 2\mathrm{e}^{-ax})$, a set of operators can be defined so that they produce the spectrum-generating algebra of the Morse potential[79]:

$$\left.\begin{matrix}\hat{J}_0 \\ \hat{J}_1\end{matrix}\right\} = \frac{1}{a^2 h(x)}\left(p^2 - 2mE\right) \pm \frac{1}{4}h(x),$$
$$\hat{J}_2 = \frac{\mathrm{i}}{ax}(\mathrm{i}xp + 1) - \frac{\mathrm{i}}{2} \tag{3.58}$$

where

$$h(x) = \frac{(8mD)^{1/2}}{a}\mathrm{e}^{-ax}. \tag{3.59}$$

These operators satisfy the commutation relations:

$$\left[\hat{J}_1, \hat{J}_2\right] = -\mathrm{i}\hat{J}_0; \quad \left[\hat{J}_2, \hat{J}_0\right] = \mathrm{i}\hat{J}_1; \quad \left[\hat{J}_0, \hat{J}_1\right] = \mathrm{i}\hat{J}_2 \tag{3.60}$$

and are therefore the generators of the SU(1,1) Lie algebra. Here, the Morse eigenstates $\{|n,k\rangle^{\mathrm{Morse}}\}$ are labeled with the vibrational quantum number $n = 0, 1, 2, \ldots$ and the Bargmann index k.[79] Then, taking the Morse ground eigenstate $|0,k\rangle^{\mathrm{Morse}}$ as a reference state, SU(1,1) Morse CSs $\{|\xi,k\rangle^{\mathrm{SU(1,1)MCS}}\}$ are constructed using the displacement operator with creation and annihilation operators $\hat{J}_\pm = \hat{J}_1 \pm \mathrm{i}\hat{J}_2$:[79]

Author's personal copy

$$|\xi,k\rangle^{\mathrm{SU(1,1)MCS}} = \exp\left(\xi\hat{J}_+ - \xi^*\hat{J}_-\right)|0,k\rangle^{\mathrm{Morse}} = \left(1-|\xi|^2\right)^k \sum_{n=0}^{\infty}\left[\frac{\Gamma(n+2k)}{n!\Gamma(2k)}\right]^{1/2}\xi^n|n,k\rangle^{\mathrm{Morse}} \tag{3.61}$$

Following the same procedure used with the canonical CS, the probability $P_n^{\mathrm{SU(1,1)MCS}}$ of observing a particular Morse eigenstate $|n,k\rangle^{\mathrm{Morse}}$ in the SU(1,1) Morse CS is:

$$P_n^{\mathrm{SU(1,1)MCS}}\left(E^{\mathrm{cl}}\right) = \left(1-|\xi|^2\right)^{2k}\left[\frac{\Gamma(n+2k)}{n!\Gamma(2k)}\right]|\xi|^{2n} \tag{3.62}$$

where the dependence of $P_n^{\mathrm{SU(1,1)MCS}}$ on the Morse-oscillator classical energy $E^{\mathrm{cl}}<0$ comes through the dependence of $|\xi|^2$ on the Bargmann index, k, and its corresponding dependence upon E^{cl}:[79]

$$|\xi|^2 = \frac{(2mD)^{1/2}-ak}{(2mD)^{1/2}+ak};\quad k=\left[-\frac{2mE^{\mathrm{cl}}}{a^2}\right]^{1/2} \tag{3.63}$$

In the previous example of an isolated diatomic molecule AB, E^{cl} in Eqs. (3.62) and (3.63) is analogous to the classical vibrational energy $E_{\mathrm{Vib}}^{\mathrm{AB}}$ from the SLEND simulation of AB.

To obtain the SU(2) Morse CS, its associated creation and annihilation operators are constructed from the natural coordinate y of the Morse eigenfunctions rather than from x and p.[80] The Morse eigenfunctions are given by[110]:

$$\Psi_n^{\nu}(y) = N_n^{\nu}\mathrm{e}^{-y/2}y^s L_n^{2s}(y) \tag{3.64}$$

where ν and s are[80]:

$$\nu=\left(\frac{8mD}{a^2}\right)^{1/2};\quad s=\left(\frac{-2mE}{a^2}\right)^{1/2}, \tag{3.65}$$

with the constraint that $2s=\nu-2n-1$, N_n^{ν} is a normalization constant, $L_n^{2s}(y)$ is a Laguerre polynomial, and the natural Morse coordinate y is related to the position x via $y=\nu\mathrm{e}^{-ax}$. The creation and annihilation operators in terms of y are[80]

Author's personal copy

$$\hat{K}_+ = \left(\frac{s-1}{s}\right)^{1/2}\left[\frac{\mathrm{d}}{\mathrm{d}y}(2s-1)+\frac{1}{y}s(2s-1)-\frac{v}{s}\right],$$
$$\hat{K}_- = -\left(\frac{s+1}{s}\right)^{1/2}\left[\frac{\mathrm{d}}{\mathrm{d}y}(2s+1)-\frac{1}{y}s(2s+1)+\frac{v}{s}\right]. \tag{3.66}$$

A third operator can be constructed as

$$\hat{K}_0 = -\left[y\frac{\mathrm{d}^2}{\mathrm{d}y^2}+\frac{\mathrm{d}}{\mathrm{d}y}-\frac{s^2}{y}-\frac{y}{4}+n+\frac{1}{2}\right] \tag{3.67}$$

so that the commutation relations of $\hat{K}_+$, $\hat{K}_-$, and $\hat{K}_0$ are

$$\left[\hat{K}_+,\hat{K}_-\right]=2\hat{K}_0;\quad \left[\hat{K}_0,\hat{K}_-\right]=-\hat{K}_-;\quad \left[\hat{K}_0,\hat{K}_+\right]=\hat{K}_+, \tag{3.68}$$

which generate the SU(2) Lie algebra. The Morse eigenstates are the eigenstates of the Casimir operator $\hat{C}$[98,105] of that algebra:

$$\hat{C}=K_0^2+\frac{1}{2}\left(\hat{K}_+\hat{K}_-+\hat{K}_-\hat{K}_+\right) \tag{3.69}$$

with eigenvalues $j(j+1)$, where $j=(v-1)/2$.[80] The SU(2) Morse CSs $\{|\alpha\rangle^{\mathrm{SU(2)MCS}}\}$ are constructed with the corresponding displacement operator as

$$|\alpha\rangle^{\mathrm{SU(2)MCS}}=\exp\left(\alpha\hat{K}_+-\alpha^*\hat{K}_-\right)|0\rangle^{\mathrm{Morse}} \tag{3.70}$$

which can be rewritten in terms of an alternative parameter ζ (see Eq. 3.76 below)

$$|\zeta\rangle^{\mathrm{SU(2)MCS}}=\left(1+|\zeta|^2\right)^{-j}\exp\left(\zeta\hat{K}_+\right)|0\rangle^{\mathrm{Morse}} \tag{3.71}$$

where the reference state is $|0\rangle^{\mathrm{Morse}}=|j,m=-j\rangle^{\mathrm{Morse}}$. The resulting SU(2) Morse CSs $\{|\zeta\rangle^{\mathrm{SU(2)MCS}}\}$ are

$$|\zeta\rangle^{\mathrm{SU(2)MCS}}=\left(1+|\zeta|^2\right)^{-v-1/2}\sum_{n=0}^{n_{\max}}\left[\frac{\Gamma(v-1)}{n!\Gamma(v-n-1)}\right]^{1/2}\zeta^n|n\rangle^{\mathrm{Morse}} \tag{3.72}$$

where $n_{\max}=(v-3)/2$ is the maximum number of bound eigenstates.

Author's personal copy

The average energy of a SU(2) Morse CS is[80]

$$\langle \hat{H} \rangle = -\frac{\omega}{\nu} \left\langle \hat{K}_0^2 \right\rangle \tag{3.73}$$

where $\omega = a^2\nu/2m$ and

$$\begin{aligned} \left\langle \hat{K}_0^2 \right\rangle &= \langle \alpha | \hat{K}_0^2 | \alpha \rangle \\ &= \frac{\nu - 1}{4} \left[\sin^2(2|\alpha|) + (\nu - 1)\cos^2(2|\alpha|) \right]. \end{aligned} \tag{3.74}$$

As with the canonical CS, a classical analogue of Eq. (3.74) is required for the vibrational state analysis. This is obtained by requiring that the bottom of the potential occur when $\zeta = 0$ or equivalently $\alpha = 0$. Those results in Eq. (3.74) give

$$\left\langle \hat{K}_0^2 \right\rangle_{\text{cl}} = \frac{\nu}{4} \left[\sin^2(2|\alpha|) + \nu \cos^2(2|\alpha|) \right]. \tag{3.75}$$

Equation (3.73) in the form of $E^{\text{cl}} = \langle \hat{H} \rangle_{\text{cl}} = -(\omega/\nu) \left\langle \hat{K}_0^2 \right\rangle_{\text{cl}}$ can be solved for $|\alpha|$ with the restriction that $0 \leq |\alpha| \leq \pi/2$. The parameter $|\zeta|^2$ is related to $|\alpha|$ by[95]

$$|\zeta|^2 = \exp\{-2\ln[\cos(|\alpha|)]\} - 1. \tag{3.76}$$

The probability $P_n^{\text{SU(2)MCS}}$ of observing a particular Morse eigenstate $|n\rangle^{\text{Morse}}$ in the SU(2) Morse CS is then given by

$$P_n^{\text{SU(2)MCS}}\left(E^{\text{cl}}\right) = \left(1 - |\zeta|^2\right)^{1-\nu} \left[\frac{\Gamma(\nu - 1)}{n!\Gamma(\nu - n - 1)} \right] |\zeta|^{2n}. \tag{3.77}$$

In the previous example of an isolated diatomic molecule AB, E^{cl} in Eq. (3.77) is analogous to the classical vibrational energy $E_{\text{Vib}}^{\text{AB}}$ from the SLEND simulation of AB.

To construct the Morse GKCS, the alternate form of the Morse potential, $V_{\text{Morse}}^{\text{GK}}(x) = D(1 - e^{-ax})^2$, must be used because the GK prescription adopts the convention that the lowest value of energy obtainable be zero.[92] The energy eigenstate–eigenvalue equation may be written in dimensionless form as[83]

$$\hat{H}_{\text{GK}} |[N], n\rangle = \varepsilon_n |[N], n\rangle^{\text{Morse}} \tag{3.78}$$

Author's personal copy

where

$$\hat{H}_{GK} = \frac{\hat{H}_{Morse} - E_0}{\omega};\ \ \varepsilon_n = \frac{n}{N+1}(N-n);$$
$$N = \left(\frac{8mD}{a^2}\right)^{1/2} - 1;\ \ \omega = \left(\frac{2a^2 D}{m}\right)^{1/2} \tag{3.79}$$

where $\hat{H}_{Morse}$ is the Morse Hamiltonian and $\hat{H}_{GK}$ is a shifted Hamiltonian that produces dimensionless eigenvalues, ε_n, with a minimum possible value of $\varepsilon_0 = 0$. In Eq. (3.78), the symbol [] is the integer-part operator so that $[N]$ returns the integer part of N. From Eq. (3.53), the Morse GKCSs $\{|J,\gamma\rangle^{GKMCS}\}$ are[83]

$$|J,\gamma\rangle^{GKMCS} = N(J)\sum_{n=0}^{[N/2]} \frac{J^{n/2}}{\sqrt{\rho_n}} e^{-i\gamma e_n} |[N],n\rangle^{Morse} \tag{3.80}$$

where now ρ_n is

$$\rho_n = \Gamma(N)\frac{\Gamma(n+1)}{(N+1)^n \Gamma(N-n)} \tag{3.81}$$

and the normalization constant is

$$N(J) = \left(\sum_{n=0}^{[N/2]} \frac{J^n}{\rho_n}\right)^{-1/2}. \tag{3.82}$$

From Eqs. (3.78)–(3.80), the Morse GKCS average energy is as follows:

$$E^{cl} = \langle J,\gamma|^{GKMCS} \hat{H}_{GK} |J,\gamma\rangle^{GKMCS} = N^2(J)\sum_{n=0}^{[N/2]} \frac{J^n}{\rho_n}\varepsilon_n \tag{3.83}$$

As shown above, in a SLEND simulation of a diatomic molecule AB, the corresponding Morse potential is $V_{Morse}(R_{AB}) = D_{AB}^{Eq.}\left\{1 - \exp\left[a_{AB}(R_{AB} - R_{AB}^{Eq.})\right]\right\}^2$ that is of the form of the currently used Morse potential $V_{Morse}^{GK}(x) = D(1 - e^{-ax})^2$. Therefore, the SLEND classical vibrational energy E_{Vib}^{AB} satisfies the presently needed condition that $E_{Vib}^{AB} \geq 0$. However, E_{Vib}^{AB} must be scaled by $\omega_{AB} = \omega$ in order to make it dimensionless and thus compatible with Eq. (3.83) to obtain the parameter J. The probability $P_n^{GKMCS}(E^{cl})$ of observing a particular Morse eigenstate $|[N],n\rangle^{Morse}$ in the Morse GKCS is:

$$P_n^{GKMCS}(E^{cl}) = N^2(J)\frac{(N+1)^n \Gamma(N-n)}{\Gamma(N)\Gamma(n+1)} J^n \tag{3.84}$$

Author's personal copy

In addition to the three Morse CSs previously discussed, Nieto and Simmons have derived a Morse MUCS.[81] That CS has not been implemented for the SLEND CSQRP yet and therefore it will not be reviewed herein; the reader is referred to Ref. 81 for details. The profusion of Morse CSs makes a sharp contrast with the single canonical CS set for the harmonic case. This is so because the group-theoretical, Gazeau–Klauder, and MUCS methods generate completely different CS sets associated with the Morse potential $V_{\text{Morse}}(R)$ but the same canonical CS set with the harmonic potential $V_{\text{HO}}(R)$. Furthermore, with the group-theoretical method, two Lie groups, SU(1,1) and SU(2), producing two different CSs were found in the Morse case but only one Lie group, the Heisenberg–Weyl one, is found in the harmonic case. There is a trade-off in using the Morse CSs. While they incorporate anharmonic effects, they lose some of the CS properties that the canonical CS has. They all have properties **P1** and **P2** by construction. However, only the Morse GKCS have properties **P5** and **P6** by construction, and none of them have property **P7**.

The first ever application of Morse CSs in the CSQRP—and perhaps the first ever application of Morse CSs in chemical dynamics—was conducted on the SLEND simulations of $H^+ + NO(v_i = 0) \rightarrow H^+ + NO(v_f = 0 - 2)$[25] and $H^+ + CO(v_i = 0) \rightarrow H^+ + CO(v_f = 0 - 2)$ both at $E_{\text{Lab}} = 30\,\text{eV}$. In both cases, use of the SU(1,1),[79] SU(2),[80] and GK Morse CS[82,83] rendered various vibrational state-to-state properties in good agreement with experimental results.[25] Some of those calculated properties are presented in Section 5.

3.4. Nuclear rotational CS for the rotational CSQRP

Just as vibrational CSs permitted the calculations of vibrational state-to-state dynamical properties, approximating $|\Psi^{\text{AB}}_{\text{Rot}}\rangle$ and $|\Psi^{\text{M}}_{\text{Rot}}\rangle$ as a rotational CS would permit the calculation of rotational state-to-state dynamical properties. By introducing a modification in the group-theoretical method, Janssen sought to develop a CS suitable for describing abstract tops.[111] For generality, the construction of this rotational CS refers to the Hamiltonian of the asymmetric top:

$$\hat{H}_{\text{Rot}} = \frac{1}{2I_x}\hat{L}_x^2 + \frac{1}{2I_y}\hat{L}_y^2 + \frac{1}{2I_z}\hat{L}_z^2 \tag{3.85}$$

where $I_x \neq I_y \neq I_z$ are the principal moments of inertia and $\{\hat{L}_i : i = x,y,z\}$ are the angular momentum projections onto the body-fixed frame. The total angular momentum in the body-fixed frame is $\hat{L}^2 = \hat{L}_x^2 + \hat{L}_y^2 + \hat{L}_z^2$. The angular momentum in the laboratory frame is given by $\{\hat{J}_i : i = x,y,z\}$.

Author's personal copy

The simultaneous eigenstates $\{|IMK\rangle\}$ of $\hat{L}^2$, $\hat{L}_z$, and $\hat{J}_z$ satisfy

$$\hat{L}^2|IMK\rangle = I(I+1)|IMK\rangle;\ \ \hat{L}_z|IMK\rangle = K|IMK\rangle;\ \ \hat{J}_z|IMK\rangle = M|IMK\rangle,$$
$$I = 0,1/2,1,3/2,\ldots;\ \ M,K = -I,-I+1,\ldots,+I-1,+I \quad (3.86)$$

where Janssen considered the general abstract case with both integer and half-integer quantum numbers. For integer quantum numbers, the eigenstates $\{|IMK\rangle\}$ are the spherical-rotor and symmetric-rotor eigenstates. The space spanned by the eigenstates $\{|IMK\rangle\}$ is the semi-direct product of the direct product $SU(2)\otimes SU(2)$ with an abelian group.[111] The direct product space $SU(2)\otimes SU(2)$ is generated by the creation and annihilation operators of the angular momenta, $\hat{L}_\pm = \hat{L}_x \mp i\hat{L}_y$ and $\hat{J}_\pm = \hat{J}_x \pm i\hat{J}_y$, with the commutation relations

$$\begin{aligned}
\left[\hat{L}_z,\hat{L}_\pm\right] &= \pm\hat{L}_\pm; \left[\hat{L}_-,\hat{L}_+\right] = -2\hat{L}_z;\\
\left[\hat{J}_z,\hat{J}_\pm\right] &= \pm\hat{J}_\pm; \left[\hat{J}_-,\hat{J}_+\right] = -2\hat{J}_z;\\
\left[\hat{L}_i,\hat{J}_l\right] &= 0.
\end{aligned} \quad (3.87)$$

The abelian group $R^{(2\lambda+1)^2}$ is generated by the spherical tensor operators $\left\{\hat{T}^\lambda_{\mu\nu}\right\}$, where $\lambda = 0,1/2,1,3/2,\ldots$ and $\mu,\nu = -\lambda,-\lambda+1,\ldots,+\lambda-1,+\lambda$[26,111,112]; those operators when acting on the eigenstates $\{|IMK\rangle\}$ increase their angular momentum

$$\hat{T}^\lambda_{\mu\nu}|IMK\rangle \rightarrow |I+\lambda\, M+\mu\, K+\nu\rangle. \quad (3.88)$$

The commutation relations between the tensor operators and the angular momentum operators are[26]

$$\begin{aligned}
\left[\hat{L}_z,\hat{T}^\lambda_{\mu\nu}\right] &= \nu\hat{T}^\lambda_{\mu\nu}; \left[\hat{J}_z,\hat{T}^\lambda_{\mu\nu}\right] = \mu\hat{T}^\lambda_{\mu\nu};\\
\left[\hat{L}_\pm,\hat{T}^\lambda_{\mu\nu}\right] &= [(\lambda+1\mp\nu)(\lambda\pm\nu)]^{1/2}\hat{T}^\lambda_{\mu\nu\mp\lambda};\\
\left[\hat{J}\pm,\hat{T}^\lambda_{\mu\nu}\right] &= [(\lambda+1\pm\mu)(\lambda\mp\mu)]^{1/2}\hat{T}^\lambda_{\mu\pm\lambda\nu}
\end{aligned} \quad (3.89)$$

The abelian operators used to form the aforementioned semi-direct product are $\left\{\hat{T}^{1/2}_{\pm1/2\ \pm1/2}\right\}$. Then, the corresponding displacement operator is $D(x,y,z) = \exp\left(x\hat{J}_+\right)\exp\left(z\hat{L}_+\right)\exp\left(y\hat{T}^{1/2}_{-1/2-1/2}\right)$[111] where x, y, and z are generally complex parameters. Although the CSs that result from this displacement operator do not have property **P7**,[111] Janssen introduced a

Author's personal copy

modification into $D(x,y,z)$ in an attempt to obtain rotational CSs $\{|xyz\rangle^{\text{Janssen}}\}$ regaining that property:[111]

$$\begin{aligned}|xyz\rangle^{\text{Janssen}} &= \exp\left[-\frac{1}{2}|y|^2\left(1+|x|^2\right)\left(1+|z|^2\right)\right] \\ &\quad\times \exp\left(x\hat{J}_+\right)\exp\left(z\hat{L}_+\right)\exp\left[y\left(2\hat{I}+\hat{T}^{1/2}_{-1/2-1/2}\right)^{1/2}\right]|000\rangle \\ &= \exp\left[-\frac{1}{2}|y|^2\left(1+|x|^2\right)\left(1+|z|^2\right)\right] \\ &\quad\times\sum_{IMK}\left[\frac{(2I)!}{(I+M)!(I-M)!(I+K)!(I-K)!}\right]^{1/2} x^{I+M}y^{2I}z^{I+K}|IMK\rangle\end{aligned} \tag{3.90}$$

where $\hat{I}$ is defined so that $\hat{I}|IMK\rangle = I|IMK\rangle$. In principle, the CSs of Eq. (3.90) have property **P7** since from the definition $\langle xyz|\hat{L}_i|xyz\rangle = \omega_i/I_i$ one can obtain the equations of motion[111]

$$\begin{aligned}I_x\dot{\omega}_x &= \omega_y\omega_z\left(I_y-I_z\right);\\ I_y\dot{\omega}_y &= \omega_x\omega_z\left(I_x-I_z\right);\\ I_z\dot{\omega}_z &= \omega_x\omega_y\left(I_x-I_y\right),\end{aligned} \tag{3.91}$$

which are the classical Euler equations for a top. The CSs developed by Janssen are suitable to describe abstract molecular tops that admit both half-integer and integer angular momentum quantum numbers. However, Janssen CSs are not suitable for molecular tops that only admit integer angular momentum quantum numbers. A further modification can be used to restrict the angular momentum quantum numbers to integer values thus producing CSs $\{|xyz\rangle\}$ suited for molecular tops[26]

$$\begin{aligned}|xyz\rangle &= \exp\left[-\frac{1}{2}|y|^2\left(1+|x|^2\right)^2\left(1+|z|^2\right)^2\right] \\ &\quad\times \exp\left(x\hat{J}_+\right)\exp\left(z\hat{L}_+\right)\exp\left[y\left(\frac{2\hat{I}^2+\hat{I}}{2\hat{I}-1}\right)^{1/2}\hat{T}^1_{-1-1}\right]|000\rangle \\ &= \exp\left[-\frac{1}{2}|y|^2\left(1+|x|^2\right)^2\left(1+|z|^2\right)^2\right] \\ &\quad\times\sum_{IMK}\left\{\frac{[(2I)!]^2}{(I+M)!(I-M)!(I+K)!(I-K)!}\right\}^{1/2}\frac{x^{I+M}y^Iz^{I+K}}{(I!)^{1/2}}|IMK\rangle\end{aligned} \tag{3.92}$$

Author's personal copy

The CSs of Eq. (3.92) lead to classical Euler equations in the limit of large angular momentum.[26] Both Janssen's CS and its modified version by Morales et al. in Eq. (3.92) have nonpositive measures.[26,111] Furthermore, Irac-Astaud[113] noted that neither the CSs of Eq. (3.90) nor those of Eq. (3.92) satisfy property **P5**, a deficiency that impairs their dynamical properties. However, for spherical and linear rotors, explicit temporal stability can be imposed on the CSs in Eq. (3.92) by following the approach of Gazeau and Klauder.[92] Then, the resulting temporally stable CSs are:

$$|x\xi\tau z\rangle = N_{\text{Sph}} \sum_{IMK} \left\{ \frac{[(2I)!]^2}{(I+M)!(I-M)!(I+K)!(I-K)!} \right\}^{1/2} \frac{x^M \xi^I e^{i\tau I(I+1)} z^K}{\sqrt{I!}} |IMK\rangle \tag{3.93}$$

for the spherical rotor where $|IMK\rangle$ are the spherical-rotor eigenstates, and

$$|x\xi\tau\rangle = N_{\text{Lin}} \sum_{IM} \left\{ \frac{(2I)!}{(I+M)!(I-M)!} \right\}^{1/2} \frac{x^M \xi^I e^{i\tau I(I+1)}}{\sqrt{I!}} |IM0\rangle \tag{3.94}$$

for the linear rotor, where $|IM0\rangle$ are the linear rotor eigenstates. In Eqs. (3.93) and (3.94), x and z are complex parameters, ξ and τ are real parameters, and the normalization constants are

$$\begin{aligned} N_{\text{Sph}} &= \exp\left[-\frac{1}{2} \frac{\xi^2}{|x|^2 |z|^2} \left(1+|x|^2\right)^2 \left(1+|z|^2\right)^2 \right]; \\ N_{\text{Lin}} &= \exp\left[-\frac{1}{2} \frac{\xi^2}{|x|^2} \left(1+|x|^2\right)^2 \right]. \end{aligned} \tag{3.95}$$

The use of temporally stable rotational CSs in the CSQRP to obtain rotational state-to-state dynamical properties is exemplified by determining the probability of a particular eigenstate of a linear rotor. From Eqs. (3.94) and (3.95), the probability P_{IM} of finding a linear rotor in the $|IM0\rangle$ rotational eigenstate is given by

$$P_{IM} = N_{\text{Lin}}^2 \left[\frac{(2I)!}{(I+M)!(I-M)!} \right] \frac{|x|^{2M} \xi^{2I}}{I!} \tag{3.96}$$

The parameters $|x|^2$ and ξ^2 are ultimately determined from the total angular momentum and its z component as follows. First, the total angular momentum is used to determine an intermediate parameter, ζ, as

Author's personal copy

$\langle x\xi\tau|\hat{J}^2|x\xi\tau\rangle = 4\zeta(\zeta+1)$. Then, $|x|^2$ is determined from ζ and the z component of the angular momentum as

$$\langle x\xi\tau|\hat{J}_z|x\xi\tau\rangle = 2\zeta\frac{|x|^2-1}{|x|^2+1}, \tag{3.97}$$

and ξ^2 is determined from ζ and $|x|^2$ as

$$\xi^2 = 2\zeta\frac{|x|^2}{\left(|x|^2+1\right)^2} \tag{3.98}$$

The values of the total angular momentum and its z component are directly obtained from the SLEND simulation data. Generally, the probabilities in Eq. (3.96) provide finer detail than that found in experiments, which generally only resolves the probability of finding the molecule with a particular value of I. To obtain probabilities comparable to the usual experimental results, Eq. (3.96) is summed over all the values of M compatible with I resulting in the less-detailed probability P_I

$$P_I = \mathrm{e}^{-B}\frac{B^I}{I!} \tag{3.99}$$

where $B=(1+|x|^2)^2\xi^2/|x|^2$. The energy of the rotational CS for the linear rotor is

$$E_{\mathrm{Rot}} = \frac{1}{2I_\perp}B(B+2) \tag{3.100}$$

where $I_\perp$ is the moment of inertia of the linear rotor. From Eq. (3.100), B is found as a function of the rotational energy:

$$B = \frac{-2+\sqrt{4+8I_\perp E_{\mathrm{Rot}}}}{2}, \tag{3.101}$$

which, when used with Eq. (3.99), gives the probability as a function of the rotational energy.

3.5. Electronic CS

The SLEND and SLEND/KSDFT methods utilize a bilinear fermion CS to define the electronic trial wavefunction due to the desirable characteristics of the CS parameters as discussed in Section 2.1. The bilinear fermion CS, originally developed by Thouless[15] and commonly referred to as the

Author's personal copy

Thouless CS, can be formulated as a DOCS following the group-theoretical approach. Fermion annihilation, b_i, and creation, $b_i^\dagger$, operators, which satisfy the anticommutation relationships

$$\begin{aligned}\left[b_j, b_k^\dagger\right]_+ &= \delta_{jk};\\ \left[b_j, b_k\right]_+ &= \left[b_j^\dagger, b_k^\dagger\right]_+ = 0,\end{aligned} \tag{3.102}$$

are used to construct the operators $b_i^\dagger b_j$ that have the commutation relation

$$\left[b_i^\dagger b_j, b_k^\dagger b_l\right] = \delta_{jk} b_i^\dagger b_l - \delta_{li} b_k^\dagger b_j \tag{3.103}$$

For a system of r single-fermion states and k fermions, $k < r$, the operators $b_i^\dagger b_j$ span the algebra of the $\mathbf{U}(r)$ group, and the appropriate reference state for defining the CSs is $|\psi_0\rangle = |1,1,\ldots,1,0,0,\ldots,0\rangle$ where k states are occupied. The set of operators $b_i^\dagger b_j$ where $1 \le j \le k$ or $k+1 \le i \le r$ forms the subgroup $\mathbf{U}(k) \otimes \mathbf{U}(r-k)$. Displacement operators are constructed from the irreducible representations of the quotient space $\mathbf{U}(r)/\mathbf{U}(k) \otimes \mathbf{U}(r-k)$ yielding the Thouless CSs $\{|\eta\rangle\}$

$$|\eta\rangle = \exp\left(\sum_{\substack{k+1 \le i \le r\\ 1 \le j \le k}} \eta_{ij} b_i^\dagger b_j - \eta_{ij}^* b_j^\dagger b_i\right)|\psi_0\rangle, \tag{3.104}$$

which may be rewritten using the BCH formula as (3.98)

$$|z\rangle = N(z) \exp\left(\sum_{\substack{k+1 \le i \le r\\ 1 \le j \le k}} z_{ij} b_i^\dagger b_j\right)|\psi_0\rangle \tag{3.105}$$

where $N(z) = \det(\mathbf{I} + \mathbf{z}^\dagger \mathbf{z})^{-1/2}$ is the normalization constant and $\{z_{ij}\}$ is the set of Thouless parameters. The use of the Thouless CS in SLEND and SLEND/KSDFT has been discussed in detail in Sections 2.1 and 2.2, respectively.

While the Thouless CS has been integral to the SLEND framework, additional electronic CSs have been and continue to be developed in order to achieve other research goals, as discussed in Section 3.1. Morales has suggested an electronic valence bond CS (VB/CS)[51] in association with a generalized charge-equilibration model that predicts correct ET processes

Author's personal copy

at dissociations. Moreover, Deumens et al. have used the concept of vector CSs[84] to derive multiconfigurational CSs (MCCSs).[39] The MCCSs provide a numerically efficient way of implementing the multiconfigurational self-consistent field (MCSCF) electronic structure method in the END framework.[39] While an END multiconfigurational description promises a greater accuracy for simulations, it also involves a significant computational cost.

4. IMPLEMENTATION: CSDYN AND PACE

All the present SLEND developments have been implemented in two successive codes: CSDYN (Coherent-States DYNamics, 2008–present)[114] and PACE (2010–present).[52] Earlier results presented in this chapter were produced with CSDYN, whereas more recent results presented herein were produced with PACE. At the beginning of this year, 2013, PACE has superseded CSDYN as our main computational tool to perform SLEND simulations.

CSDYN was developed from the ENDyne 2.7 and 2.8 codes by the Deumens and Öhrn group.[115] CSDYN has implementations for SLEND, SLEND/KSDFT, and for their respective BODD limiting cases: BODD/HF and BODD/KSDFT, respectively. The four methods are furnished with the ECP method in CSDYN. In addition, CSDYN possesses various auxiliary codes to prepare visualizations ("movies") of the produced simulations, to perform the CSQRP, and to calculate ET probabilities. The auxiliary code performing the last task is an independent component called Resolve. Like ENDyne 2.7 and 2.8, CSDYN was written in FORTRAN for serial use with 32-bit processors. Due to its coding style, CSDYN was not amenable for implementing new theoretical and computational methods into it. In addition, its serial nature made CSDYN computationally slow in terms of modern performance standards, and its failure to fully utilize modern 64-bit processors limited the size of systems which CSDYN could simulate. To overcome these deficiencies and resolve some details of END simulation techniques, the new code PACE has been developed.[52]

PACE[52] is a highly sophisticated code that exploits various state-of-the-art techniques in computational science such as a mixed language approach,[116–118] which combines Python for overall controlling logic and FORTRAN and C++ languages for intensive numerical computations, intranode and internode parallel programming for computer clusters, and Compute Unified Device Architecture (CUDA) parallel implementations

Author's personal copy

(only for ECP evaluations at the moment). In addition, PACE incorporates the fast atomic integral package developed by Lotrich et al.[119] (This atomic integral package was originally used in the CC code ACES III of the Bartlett group.[120]) Currently, PACE features the same methods and the same (rewritten) auxiliary codes of CSDYN, but now running at much higher speeds. Due to its structure, PACE will soon undergo further developments to incorporate new methods like CCEND, which can be incorporated much easier into PACE than in CSDYN. Some of the distinctive features of PACE, such as its mixed language approach and parallel programming, deserve further elucidation and therefore those are explained in detail in the following paragraphs.

In regard to PACE's mixed language approach,[116–118] it is well recognized that computationally intensive calculations should be implemented in a low-level compiled language, minimizing the impact of operations such as compiler-generated object-oriented programming constructs. However, low-level tools are ungainly in the development of controlling logic and data manipulation such as the interpretation of the user's input and construction of atomic orbital basis sets and nuclear geometries. These are best left to a high-level language as these procedures take only a very small fraction of the total run time, typically being performed only rarely. For these reasons, PACE is being developed using Python for the controlling logic and C++ and for computationally intensive routines. The integration of Python and C++ is accomplished through SWIG wrapping code.[121] A benefit of this approach is that new theoretical and computational methods can be rapidly implemented in Python, validated, and when so, the computational bottlenecks can be migrated to C++. Additionally, the high-level syntax simplifies maintenance, as the conceptual underpinning of the code is more transparent to subsequent researchers.

The mixed language design of PACE has further facilitated the incorporation of advanced computational techniques. Among these are the ability to use general-purpose graphical processing units (specifically those adhering to the CUDA) to supplement the available CPU cores in the evaluation of ECP integrals, intranodal parallelization via the Threading Building Blocks (TBB) template library for C++,[122] and internodal parallelization via the message passing interface (MPI) wrapped by the PyPar package.[123]

Three parallel constructs from TBB are used in PACE. The first and most common is the "parallel for" loop over a range where each item is independent of the others. The second construct is parallel reduction in which, given an associative "join" operation, a range is split, the computations performed,

Author's personal copy

and the final result is obtained from joining the results of the range divisions. An example of parallel reduction is in the computation of the nuclear gradient of energy wherein each spawned thread loops over the range of electronic integrals, building up a set of contributions to structures private to each thread, which are then summed to produce the final complete gradient. The third construct is a pipeline methodology, novel in the evaluation of the DFT integrals. The pipeline consists of a set of three filters connected in series. The first filter generates tokens containing grid points and quadrature weights. The second filter receives the tokens from the first filter and contributes to the weights of the grid points with the partitioning scheme according to either Becke's fuzzy weights[124] or Voronoi polyhedra. The final filter constructs the density and evaluates the functionals. The parallelism is made finer-grained by splitting each nuclear grid into several smaller tokens. Formally, all grid points are independent, but the overhead of constructing a token in practice sets a lower limit on the size of the token. This pipeline runs all three filters in parallel: when work piles up at a filter, threads migrate to work on that filter. Thus, the evaluation balances itself without applying empirical heuristics.

As stated previously, internode parallelization is achieved with MPI via PyPar, which provides a Python interface to the MPI API. Typically, MPI is used to provide communications between sets of processes running in tandem so that there is one process per core and all processes communicate using MPI whether they are physically located on the same node or not. However, the use of TBB allows PACE to use the more efficient multithreading model for all cores on a node. To enable the use of that efficiency over multiple nodes, a master process coordinates the interpretation of the user's input and delegates, via MPI, computations to slave processes running on all nodes. That is, rather than spawning one process per core, one slave process per node is created plus a single master process. When run using MPI, PACE itself differentiates processes of rank greater than zero into a server that waits to be contacted by the master process. The range concept from TBB is recycled: the master process breaks up the iteration space and delegates those ranges to the slave processes, which in turn subdivide the given range for threads created with TBB.

In addition to the aforementioned computational technologies, PACE uses a flexible input language, the General Atomic Instruction Transform (GAIT), which is easily extended to accept new commands. The code evaluating GAIT is based on the open-source package asteval[125] which avoids

Author's personal copy

the inherent security holes of a Python input file by parsing input into abstract syntax trees and disallowing "dangerous" statements. GAIT allows the PACE input file to handle execution control, variable assignment and array slicing procedures, function definitions, and data structure construction. It also permits the use of a large library of math functions from numpy[126] as well as all PACE-specific functions in the input file.

Analysis of the simulations is performed both within PACE and using auxiliary codes. PACE can currently provide visualizations of the dynamics as well as use the auxiliary code Resolve for calculating ET probabilities by computing the overlaps of single determinants of orthogonal orbitals (i.e. HF or KSDT states) with the single Thoules determinant of nonorthogonal DSO produced by the SLEND dynamics. CS analysis for vibrational and rotational state resolved properties is currently performed with auxiliary codes; however, the previously mentioned characteristics of PACE and GAIT will facilitate the migration of those CS analysis routines into PACE.

5. APPLICATIONS

SLEND, with its new developments discussed herein, has been successfully applied to a variety of systems. Most prevalent is its application to ion–molecule collisions. These collisions play a critical role in interstellar chemistry, atmospheric chemistry, plasma dynamics, particle accelerators, and ion cancer therapies. These collisions occur at energies E_{Lab} broadly ranging from 10 eV to 1.0 MeV. At the lower range of energies, SLEND has successfully modeled various proton–molecule collisions at $E_{\mathrm{Lab}} = 30\,\mathrm{eV}$ reporting vibrational state-to-state dynamical properties.[25,33,34] Through employing the vibrational CSQRP along with SLEND, proton energy loss spectra, vibrational state probabilities, and vibrational state-to-state DCSs have been calculated in good agreement with experiments.[25,33,34] In addition, SLEND/KSDFT has been used to calculate accurate vibrational frequencies for a set of representative molecules and to study additional proton–molecule reactions.[49] At the higher range of energies, the keV range, SLEND has been used to study proton collisions with water clusters and nucleobases (i.e., DNA and RNA bases) as an initial step in a theoretical chemistry study of PCT. All those applications are discussed in the following subsections. While SLEND has been most often used to study ion–molecule collisions, it is not limited to these types of collisions. For instance, recent

Author's personal copy

SLEND simulations of a Diels–Alder 2 + 4 cycloaddition and SLEND + ECP simulation of a S_N2 reaction are presented in the following subsections.

5.1. Vibrational state-to-state and ET total dynamical properties

The vibrational canonical CSQRP discussed in Section 3.3 has been applied to several systems to obtain proton energy loss spectra, vibrational state-to-state DCSs and ICSs, and state probabilities from SLEND simulations. As discussed in Section 3.3, the vibrational canonical CSQRP was applied for the first time to SLEND simulations of $H^+ + H_2$ at $E_{Lab} = 30\,eV$[23,24] by Morales et al. Those studies provided results in good agreement with experimental data[106] as has been discussed in Section 3.3 and in Refs. 23,24. More recently, the vibrational canonical CSQRP has been successfully applied to various SLEND simulations to calculate proton energy loss spectra in $H^+ + N_2(v_i = 0) \rightarrow H^+ + N_2(v_f = 0 - 1)$ at $E_{Lab} = 30\,eV$[33] and vibrational state-to-state DCS in $H^+ + N_2(v_i = 0) \rightarrow H^+ + N_2(v_f = 0 - 1)$[33] and $H^+ + CO(v_i = 0) \rightarrow H^+ + CO(v_f = 0 - 2)$[34] at $E_{Lab} = 30\,eV$, *inter alia*. Those SLEND studies were conducted with our code CSDYN. Figures 3.2 and 3.3 show proton energy loss spectra and the vibrational DCS with $v_f = 0$, respectively, for $H^+ + N_2(v_i = 0) \rightarrow H^+ + N_2(v_f = 0 - 1)$ at $E_{Lab} = 30\,eV$. Proton energy loss spectra tend to be a more sensitive measurement than the DCS

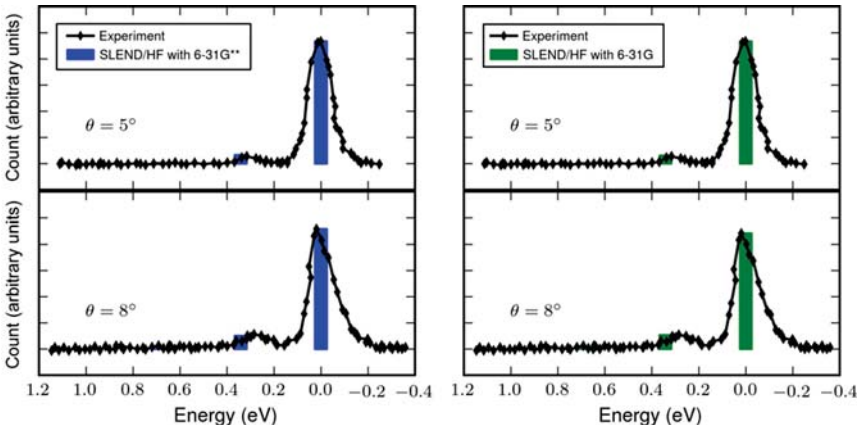

Figure 3.2 H^+ energy loss spectra computed at $\theta_{Lab} = 5^\circ$ and 8° for $H^+ + N_2$ at $E_{Lab} = 30\,eV$. Results from SLEND using the 6-31G and 6-31G** bases are compared with the experimental results of Krutein and Linder.[108] *Reprinted with permission from Ref. 33. Copyright 2011, American Institute of Physics.*

Author's personal copy

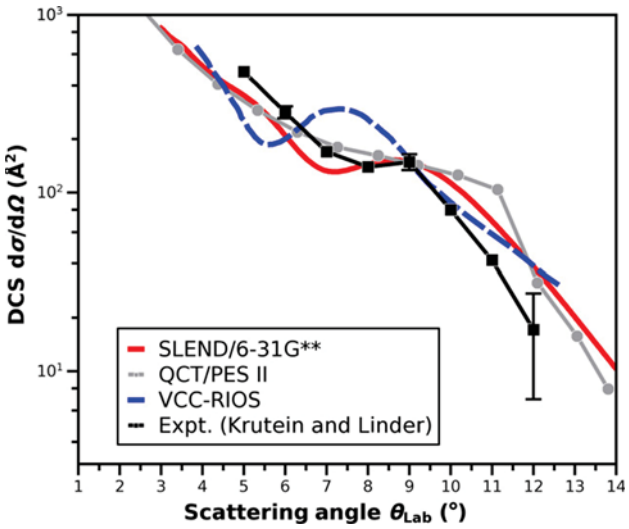

Figure 3.3 Differential cross sections for the $H^+ + N_2(v_i = 0) \rightarrow H^+ + N_2(v_f = 0)$ elastic channel at $E_{Lab} = 30$ eV versus scattering angle: SLEND with the 6-31G** basis, VCC-RIOS,[127] QCT,[128] and experimental[108] results. The last three results reported in arbitrary units are normalized to the absolute SLEND DCS at the experimental rainbow angle $\theta_{Lab}^{Expt} = 9^\circ$. *Reprinted with permission from Ref. 33. Copyright 2011, American Institute of Physics.*

since it is on a linear scale rather than a logarithmic one. Nonetheless, it is evident from Fig. 3.2 that the vibrational canonical CSQRP in conjunction with SLEND simulations produces spectra in good agreement with experiment.[108] Furthermore, comparison of DCS results from the vibrational close-coupling rotational infinite-order sudden (VCC-RIOS) approximation,[127] QCT[128] dynamics, SLEND,[33] and experiment[108] shown in Fig. 3.3 indicates that SLEND models the projectile–target interaction accurately, reproducing the overall DCS profile in good agreement with the experimental result. Both VCC-RIOS and QCT fail to predict the correct rainbow angle at $\theta_{Lab} = 9^\circ$, with VCC-RIOS predicting a rainbow angle a full 2° lower than the experiment at $\theta_{Lab}^{VCC\text{-}RIOS} = 7^\circ$, while QCT produces a rainbow angle 2°–3° higher than experiment in the range $11^\circ \leq \theta_{Lab}^{QCT} \leq 12^\circ$ (QCT DCS values were computed at discrete angle values that do not include its own rainbow angle). In contrast, SLEND produces the correct rainbow angle at $\theta_{Lab}^{SLEND} = 9^\circ$. Similar results are obtained for $H^+ + CO$ at $E_{Lab} = 30$ eV. The DCSs for the final vibrational states $v_f = 0, 1, 2$ are shown in Fig. 3.4. As with the $H^+ + N_2$ system, SLEND reproduces the DCS with $v_f = 0$ in good agreement with the

Author's personal copy

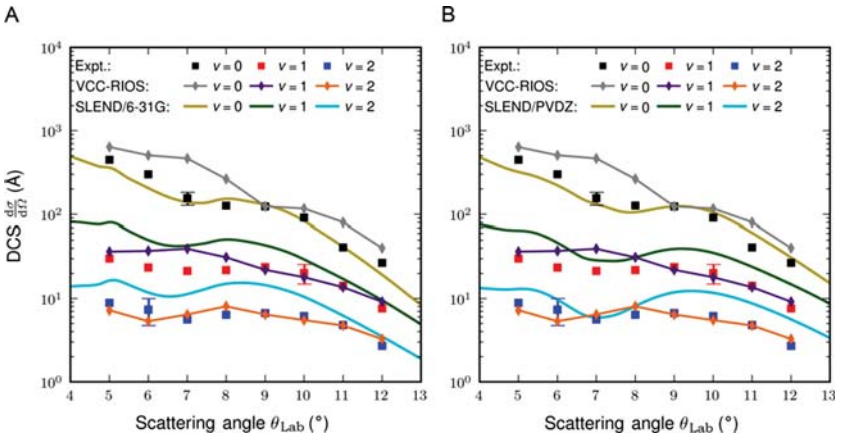

Figure 3.4 (A) Vibrational state-to-state differential cross section for $H^+ + CO(v_i = 0) \rightarrow H^+ + CO(v_f = 0, 1, 2)$ at $E_{Lab} = 30$ eV versus scattering angle: SLEND using the 6-31G basis analyzed with the canonical CS compared with VCC-RIOS[129] and experimental[108] results. VCC-RIOS and experimental results are normalized to the $v_f = 0$ SLEND results at $\theta_{Lab} = 9°$. (B) Same as (A) using SLEND with the cc-pVDZ basis. *Reprinted with permission from Ref. 34. Copyright 2012, American Institute of Physics.*

experimental result[108] and predict a rainbow angle at $\theta_{Lab}^{SLEND} = 9°$ in agreement with the experimental result and superior to the rainbow angle produced by VCC-RIOS $\theta_{Lab}^{VCC\text{-}RIOS} = 7°$. However, DCSs with $v_f = 1$ and $v_f = 2$ obtained from SLEND are generally larger than those obtained from the experiment. This is largely due to the amount of energy transferred from the proton to the CO shown in Fig. 3.5A. Clearly, SLEND produced more energy transfer than observed in the experiment. This is in contrast to the amount of energy transferred in the SLEND simulations of $H^+ + N_2$, shown in Fig. 3.5B, which was in better agreement with experiment. It has been shown by calculation[34] that if the energy transferred in the $H^+ + CO$ simulations was closer to the experimental values, then the final vibrational state-to-state DCS would also be in significantly better agreement with the experiment.[108] It is expected that as higher levels of theory are used to model the electronic wavefunction, the amount of energy transferred will improve because of the improved modeling of the projectile–target interaction.

The initial application of the vibrational canonical CSQRP to diatomic molecules was due to the simplicity of these systems insofar as they only have one normal mode. However, there is no inherent restriction in this procedure that would limit it to such systems, as discussed in Section 3.3. Indeed, the vibrational canonical CSQRP has also been applied to triatomic systems

Author's personal copy

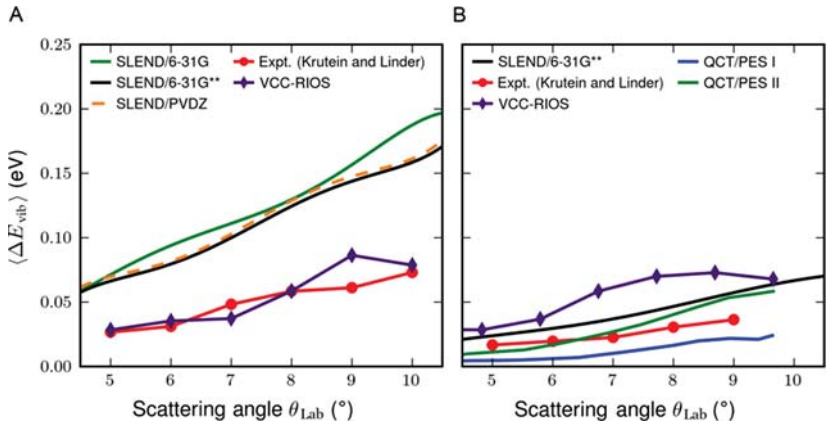

Figure 3.5 (A) Average CO vibrational energy transfer in $H^+ + CO$ at $E_{Lab} = 30\,eV$ computed with SLEND using the 6-31G, 6-31G**, and cc-pVDZ bases compared with VCC-RIOS[129] and experimental[108] results. (B) Average N_2 vibrational energy transfer in $H^+ + N_2$ at $E_{Lab} = 30\,eV$ computed with SLEND using the 6-31G** basis compared with VCC-RIOS, QCT, and experimental results. *Panel (A): Reprinted with permission from Ref. 34. Copyright 2012, American Institute of Physics. Panel (B): Reprinted with permission from Ref. 33. Copyright 2011, American Institute of Physics.*

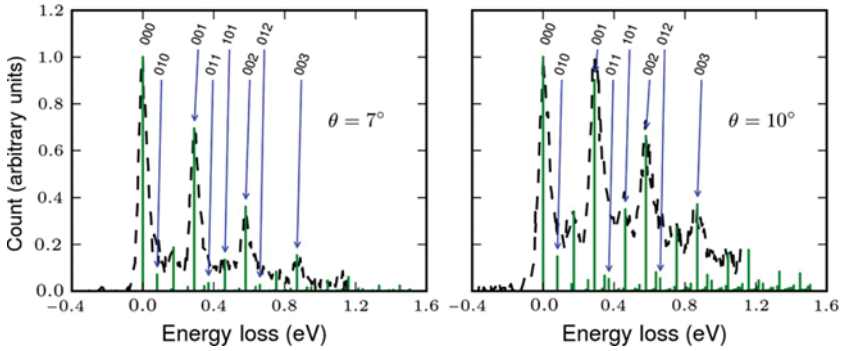

Figure 3.6 Proton energy loss spectrum for $H^+ + CO_2$ at $E_{Lab} = 29.5\,eV$ from experiments (dotted curves)[130] and SLEND[109] (green peaks) using the DZ basis set and obtained with the canonical CS.

simulated with CSDYN. Figure 3.6 presents proton energy loss spectra of $H^+ + CO_2(\nu_1^i \nu_2^i \nu_3^i = 000) \rightarrow H^+ + CO_2(\nu_1^f \nu_2^f \nu_3^f)$ at $E_{Lab} = 29.5\,eV$ for the scattering angles of 7° and 10° obtained from experiments[130] and from the vibrational canonical CSQRP on CO_2 from SLEND simulations with the DZ basis set.[109] Although this is the first application of the vibrational

Author's personal copy

canonical CSQRP to polyatomic molecules, it is clear that this procedure can successfully predict accurate transition probabilities for polyatomic molecules. Not only do the SLEND results stand in excellent agreement with the experiment,[130] they are also of finer-grained detail, thus providing a guide for future experiments. Further SLEND studies of $H^+ + CO_2$ system are currently under way.[130]

Some systems may not be sufficiently harmonic for the canonical CS to adequately model the systems' behavior. For those systems, the Morse CS's incorporation of anharmonic effects suggests that they can provide a more accurate state resolution. For this reason, they have been used to analyze SLEND results with CSDYN for $H^+ + NO(v_i = 0) \rightarrow H^+ + NO(v_f = 0 - 2)$[25] and $H^+ + CO(v_i = 0) \rightarrow H^+ + CO(v_f = 0 - 2)$[34] at $E_{Lab} = 30\,eV$. For each of those systems, the Morse potential parameters were determined from a nonlinear least squares fit to the molecular vibration from SLEND. In the case of $H^+ + NO$, quantum DCSs were obtained from SLEND with the cc-pVDZ basis set using the partial wave analysis.[76] The vibrational Morse CSQRP was used to resolve the quantum DCS[25] for the first three vibrational eigenstates using each of the three Morse CS sets: the SU(1,1),[79] SU(2),[80] and GK[82,83] Morse CS sets, as discussed in Section 3.3. The rms percent difference between the DCSs obtained from each of the three CSs are 0.84%, 0.58%, and 1.4% for SU(1,1) and SU(2), SU(1,1) and GKCS, and SU(2) and GKCS, respectively.[25] Figure 3.7 shows the proton energy loss spectrum for $H^+ + NO$ at $E_{Lab} = 30\,eV$ at the scattering angle of 5°. That figure indicates that the GK Morse CS provides a small improvement over the canonical CS compared with the experimental results.[108] This was anticipated since the anharmonic constant of NO is 0.74% of its vibrational frequency, allowing NO to be modeled well by the harmonic approximation. It was also anticipated that the Morse CSs would only provide a small improvement over the canonical CS in the case of CO as the anharmonic constant of CO is 0.61% of its vibrational frequency. Figure 3.8 compares vibrational state-to-state DCS results from the vibrational SU(1,1) Morse and canonical CSQRP and from experiment.[108] The SLEND DCSs were obtained using the methodologies discussed in Section 2.4. Figure 3.8 indeed shows that the SU(1,1) Morse CS provides a small improvement in the DCS over the canonical CS. To the best of our knowledge, these are the first applications of the Morse CS sets in chemical dynamics. However, the anharmonicity of the selected systems is not high enough to reveal the full advantages of the anharmonic Morse CSs. Despite that, the vibrational Morse CSQRP not only produce results in good agreement with the experiment but also show an expected modest improvement over the results obtained with the

Author's personal copy

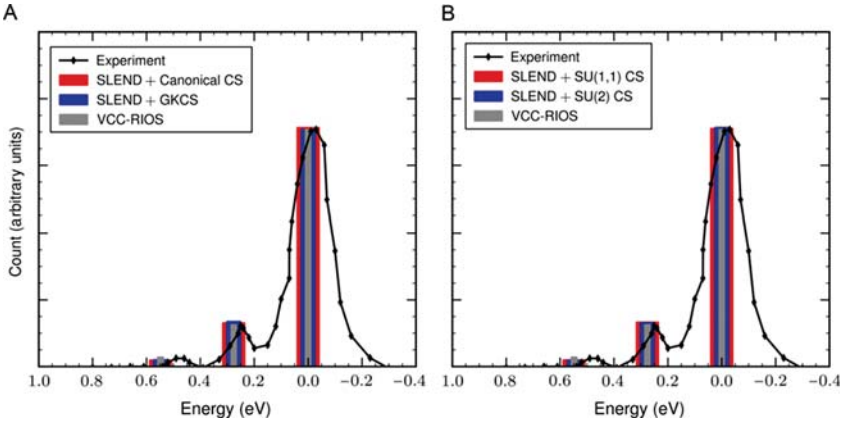

Figure 3.7 Proton energy loss spectra from experiment, the canonical CS analysis, and three Morse CS analyses obtained at the scattering angle $\theta_{Lab} = 5^\circ$ for $H^+ + NO$ at $E_{Lab} = 30$ eV. Simulations performed with SLEND using the cc-pVDZ basis set. A) Compares canonical CS, GKCS, VCC-RIOS, and experiment. B) Compares SU(1,1) CS, SU(2) CS, VCC-RIOS, and experiment. *Reprinted from Ref. 25. Copyright 2012, with permission from Elsevier.*

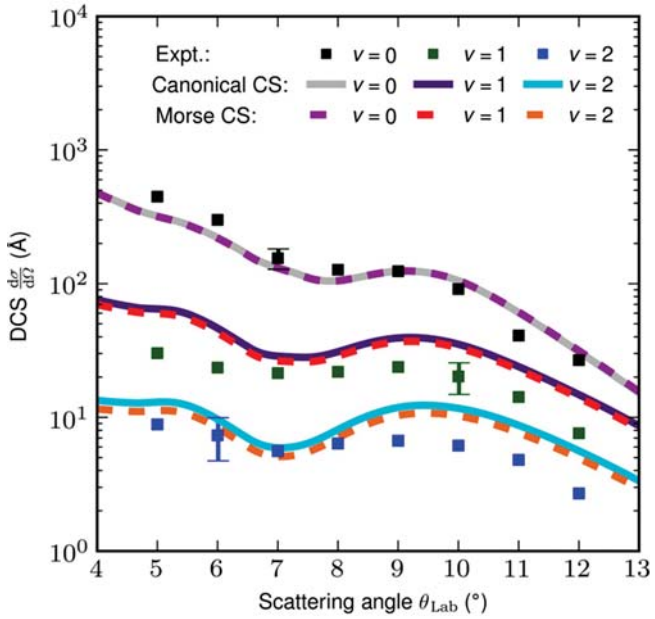

Figure 3.8 Vibrational state-to-state differential cross sections for $H^+ + CO$ at $E_{Lab} = 30$ eV from experiments[108] and from SLEND simulations with the cc-pVDZ basis set and using the canonical and the SU(1,1) Morse CSs.

Author's personal copy

vibrational canonical CSQRP. Current research efforts concentrate on the application of the vibrational Morse CSQRP to systems exhibiting higher levels of anharmonicity.

In addition to nuclear state-to-state dynamical properties, it was stated in Sections 2.4 and 4 that charge-transfer (CT) probabilities (formerly named ET probabilities) can be obtained from SLEND simulations using the auxiliary code Resolve. The success of this procedure is demonstrated in Fig. 3.9 for $H^+ + O_2$ at $E_{Lab} = 23.7\,eV$, which compares the one-electron CT $[H^+ + O_2(v_i = 0) \rightarrow H + O_2^+(v_f = \text{all})]$ and the noncharge transfer (NCT) $[H^+ + O_2(v_i = 0) \rightarrow H^+ + O_2(v_f = \text{all})]$ total DCSs obtained with SLEND using the 6-31++G* basis set and partial wave analysis[76] with the corresponding DCSs obtained from experiments.[131] The SLEND simulations were performed with CSDYN. The experimental NCT and CT total DCSs reported in relative units were normalized with respect to the NCT SLEND result. Also, the SLEND CT total DCS result was scaled by 0.01 to account for the lower 1% probability of the experimental H detection relative to the

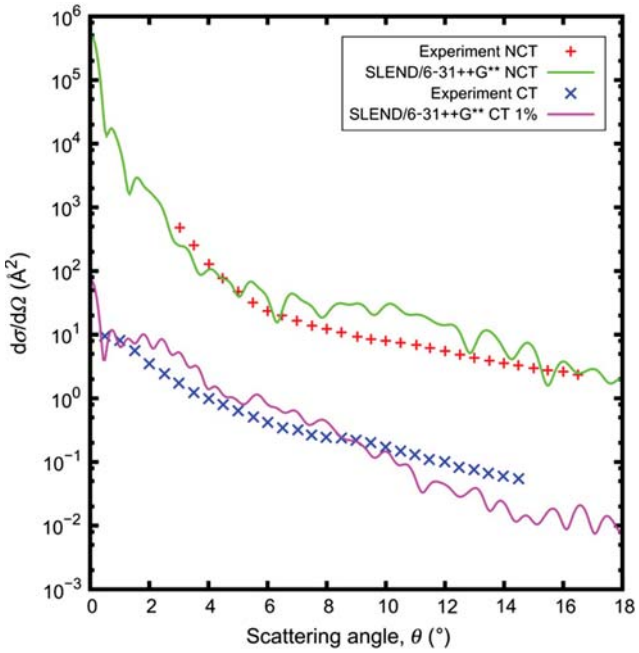

Figure 3.9 Charge transfer (CT) and noncharge transfer (NCT) total DCS for $H^+ + O_2(v_i = 0) \rightarrow H^{+/0} + O_2^{0/+}(v_f = \text{all})$ at $E_{Lab} = 23.7\,eV$. SLEND results obtained with the 6-31++G** basis set in comparison with experimental results.[131]

Author's personal copy

H^+ detection.[131] Our theoretical results were scaled rather than the experimental CT results in order to maintain good separation between the CT and NCT total DCSs plots, thus facilitating comparison between SLEND and the experiments. From Fig. 3.9, it is evident that SLEND predicts CT total DCSs in good agreement with the experimental results and can thus be used as an accurate predictive tool for determining CT properties of other systems.

5.2. Applications of SLEND/KSDFT and SLEND + ECP

The aforementioned difficulty in predicting the correct energy transfer in $H^+ + CO$ has been attributed to the lack of electron correlation in SLEND. It is further thought that improving the electronic wavefunction used in SLEND will improve the overall quality of the results. To this end, the electron correlation description was improved by incorporating TD KSDFT procedures into SLEND as discussed in Section 2.2. This recently developed SLEND/KSDFT method was first used to simulate normal mode vibrations of H_2, HF, H_2O, NH_3, and CH_4 with CSDYN to determine dynamically their periods/frequencies.[49] Those simulations used the B3LYP hybrid functional and the 6-31G** basis set. In each case, the molecules were perturbed only slightly from their equilibrium geometry in order to ensure the vibration would be sufficiently harmonic to allow comparison with periods/frequencies obtained from a standard normal mode analysis (NMA). The results of those studies are shown in Table 3.1, where the DFT NMA results were obtained using the code GAMESS[132] and the HF NMA and experimental values were taken from the National Institute of Standards and Technology's online databases. The SLEND/KSDFT vibrational periods, *T*, are in excellent agreement with those obtained from the DFT NMA indicating that SLEND/KSDFT is able to correctly simulate molecular vibrations. Furthermore, SLEND/KSDFT generally produces frequencies in better agreement with experiment than the HF NMA. This is expected since KSDFT predicts better vibrational wavenumbers than HF.[133] The improvement in the vibrational description by SLEND/KSDFT is highly relevant for a more accurate application of the CSQRP.

Following the normal modes' simulations, SLEND/KSDFT was used to simulate the $C_2H_4 + C_4H_6 \rightarrow C_8H_{10}$ Diels–Alder reaction with a relative translational energy of 2.602 eV.[78] For that simulation, the PBE functional in conjunction with the STO-3G basis set was used. A minimal basis set was chosen due to the size of the system, 46 electrons and 16 nuclei, and the previously discussed limitations of CSDYN. The results of that simulation are depicted in Fig. 3.10, which contains snapshots of the nuclear positions

Author's personal copy

Table 3.1 Periods (T) and frequencies ($\widetilde{\nu}$) obtained from SLEND/KSDFT simulations of small amplitude vibrations for H_2, HF, H_2O, NH_3, and CH_4 molecules compared with KSDFT and HF normal mode analysis (NMA) and experimental harmonic frequencies

	$T \pm 1$ a.u. (fs)		$\widetilde{\nu}$ (cm^{-1})			
Molecule-NM IRep	**SLEND/ KSDFT**	**DFT NMA**	**SLEND/ KSDFT**	**DFT NMA**	**HF NMA**	**Exp**
H_2-A_1	310 (7.5)	309 (7.5)	4448	4462	4635	4401
HF-A_1	339 (8.2)	338 (8.2)	4068	4084	4493	4138
H_2O-A_1	832 (20.1)	832 (20.1)	1657	1665	1770	1595
H_2O-A_1	365 (8.8)	363 (8.8)	3778	3797	4148	3657
H_2O-B_2	355 (8.6)	353 (8.6)	3885	3910	4265	3756
NH_3-A_1	1272 (30.8)	1266 (30.6)	1084	1090	1142	950
NH_3-E	815 (19.7)	814 (19.7)	1692	1693	1811	1627
NH_3-E	815 (19.7)	814 (19.7)	1692	1693	1811	1627
NH_3-A_1	399 (9.7)	399 (9.7)	3456	3458	3705	3337
NH_3-E	386 (9.3)	385 (9.3)	3573	3586	3843	3444
NH_3-E	386 (9.3)	385 (9.3)	3573	3586	3843	3444
CH_4-T_2	1018 (24.6)	1012 (24.5)	1354	1363	1469	1306
CH_4-T_2	1018 (24.6)	1012 (24.5)	1354	1363	1469	1306
CH_4-T_2	1018 (24.6)	1012 (24.5)	1354	1363	1469	1306
CH_4-E	874 (21.1)	870 (21.0)	1577	1585	1685	1534
CH_4-E	874 (21.1)	870 (21.0)	1577	1585	1685	1534
CH_4-A_1	452 (10.9)	453 (11.0)	3050	3045	3174	2917
CH_4-T_2	436 (10.5)	436 (10.5)	3166	3165	3285	3019
CH_4-T_2	436 (10.5)	436 (10.5)	3166	3165	3285	3019
CH_4-T_2	436 (10.5)	436 (10.5)	3166	3165	3285	3019

Normal modes are identified by molecule and irreducible representation symbol (Molecule-NM IRep).

and the electron density at select times during the simulation, and in Fig. 3.11, which contains plots of the C—C and C═C bonds as well as of the potential energy as a function of time. Figure 3.10 clearly shows the spatial overlap of the electron density followed by the formation of C—C bonds between the diene and the dienophile. Furthermore, the electron density isosurfaces have been colored so that the red isosurfaces indicate

Author's personal copy

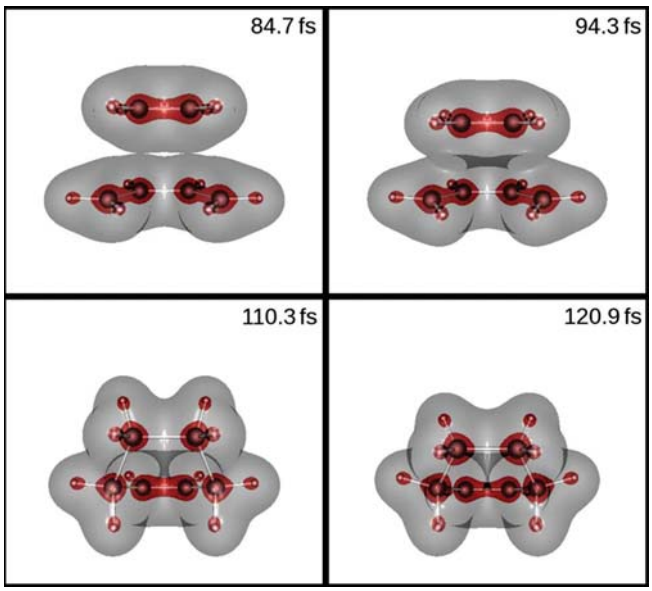

Figure 3.10 Snapshots of the $C_2H_4 + C_4H_6$ Diels–Alder reaction with 2.602 eV of relative translational energy showing the location of the nuclei (spheres) and two electron density isosurfaces (gray and red clouds). Simulation conducted with SLEND/KSDFT with the PBE functional and the STO-3G basis set.

regions of high electron density and therefore the location of C—C and C═C bonds by its absence or presence between carbon atoms, respectively. It is thus evident from Fig. 3.10 that the expected formation/breakage of C—C and C═C bonds occurs during the SLEND/KSDFT simulation. This is further supported by Fig. 3.11 that shows that by the end of the simulation the initial values of the C═C bonds have elongated to values of C—C bonds while the initial values of the C—C bonds have contracted toward values of C═C bonds. Furthermore, Fig. 3.11 indicates that SLEND/KSDFT/PBE/STO-3G predicts a reaction barrier of 19.55 kcal/mol, which is to be compared with the range of experimental activation energies from 27.5 to 34.3 kcal/mol.[134]

While SLEND/KSDFT was implemented to improve electron correlation effects, SLEND + ECP and SLEND/KSDFT + ECP were implemented to allow the study of larger systems. Furthermore, as was previously discussed in Section 4, the performance and code development limitations of CSDYN have prompted the design of our new code PACE using various state-of-the-art techniques in computer science. Due to its so recent development, there are few applications demonstrating the capabilities and

Author's personal copy

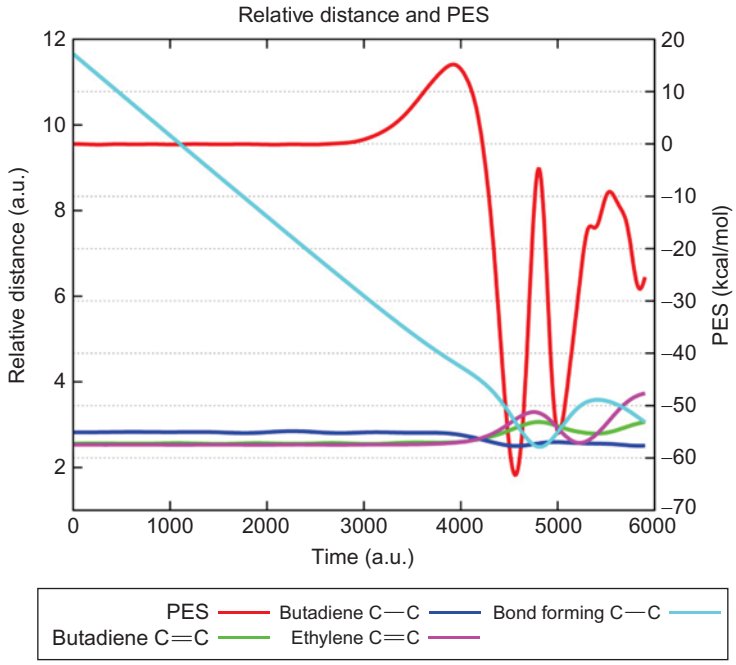

Figure 3.11 Potential energy (kcal/mol) and various C—C bond distances (a.u.) during the simulation of the $C_2H_4 + C_4H_6$ Diels–Alder reaction with 2.602 eV of relative translational energy. Simulation conducted with SLEND/KSDFT with the PBE functional and the STO-3G basis set.

features of PACE; however, it has been used to simulate the $CH_3Br + F^- \rightarrow CH_3F + Br^-$ S_N2 reaction at $E_{Lab} = 20\,eV$ of relative translational energy using SLEND + ECP with the SBKJC basis set.[75] That simulation was found to be too costly for CSDYN to complete; however, this was not so for PACE. Figure 3.12 shows snapshots at selected times during the S_N2 reaction simulation demonstrating that PACE is indeed capable of fully simulating that reaction. While there have been other direct-dynamics studies of S_N2 reactions,[135] we want to emphasize herein that the BODD methods used in those studies lacked the electron–nuclear coupling and the nonadiabatic effects present in SLEND. Therefore, those BODD methods will become less accurate as the reaction energy increases.

5.3. Applications to PCT

The successful simulation of the S_N2 and the Diels–Alder reactions opens the door for the use of SLEND and SLEND/KSDFT to elucidate reactive mechanisms of more complex organic chemistry and biochemical reactions.

Author's personal copy

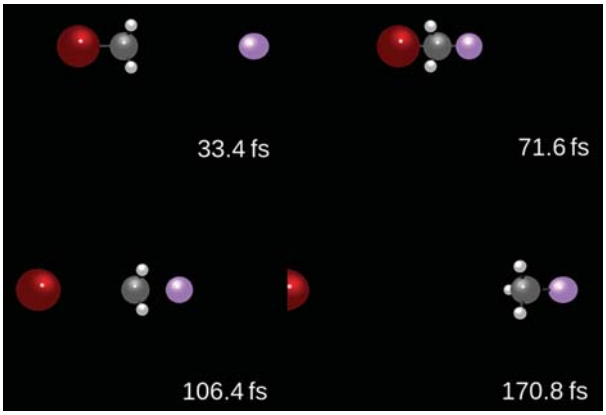

Figure 3.12 Snapshots of the $CH_3Br + F^- \rightarrow CH_3F + Br^-$ S_N2 reaction with 20 eV of relative translational energy. Simulation conducted with SLEND + ECP with the SBKJC basis set. The computation was performed with PACE.

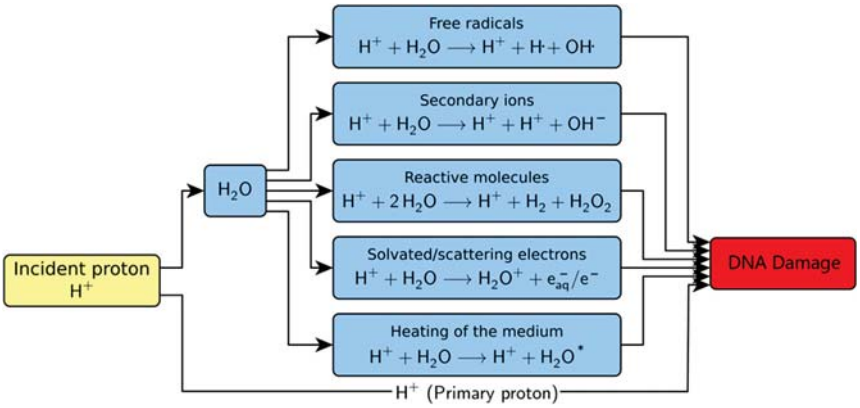

Figure 3.13 Principal physical processes and chemical reactions involved in proton cancer therapy.

Of particular interest are those reactions that play key roles in PCT. The basic physical processes and chemical reactions involved in PCT are schematized in Fig. 3.13. PCT uses high-energy proton (H^+) projectiles (from an initial energy of 200–430 MeV down to 1–100 keV in deep tissues) to destroy cancerous tumors with minimum damage to healthy tissues and without the side effects of X-ray therapy.[136,137] The therapeutic action of H^+ projectiles results from the damage they cause to the cellular DNA of both cancerous and healthy cells; however, due to their higher rate of

Author's personal copy

division and reduced ability to repair damaged DNA, cancerous cells are killed at a much higher rate than healthy cells during H^+ irradiation.[136,137] The present consensus[136,137] is that the high-energy H^+ projectiles mostly collide with the water molecules that comprise ~70% of the human body mass. As shown in Fig. 3.13, the initial high-energy H^+ collisions with cellular H_2O molecules produce secondary reactive species such as radicals (e.g., OH and H), ions (e.g., secondary H^+ and HO^-), reactive molecules (e.g., H_2 and H_2O_2), and solvated/free electrons as well as localized heating. These products can react with additional H_2O molecules initiating cascade reactions that produce analogous tertiary, quaternary, etc., reactive species. Regardless of the stage they are produced, those reactive species diffuse through the cellular medium, reach the cellular DNA, and damage it via both single- and double-strand breaks, the latter exhibiting a much higher cellular lethality than the former (cf. Fig. 3.13).

Based on previous scattering applications,[23–25,27,28,30–34,49] SLEND and SLEND/KSDFT are well suited for studying these types of PCT reactions due to their versatility to accurately describe various processes of the PCT reactions such as ions' scattering, collision-induced fragmentations, and ETs. Noteworthy, the high energies employed in PCT are such that the nuclear dynamics can be described accurately with classical mechanics as is done in SLEND and SLEND/KSDFT. The initial foray into PCT studies with SLEND has been the study of high-energy $H^+ + (H_2O)_n$ reactions featuring water clusters $(H_2O)_n$ with $n = 2$[138] and $n = 3 - 4$[78] as an approximation to the bulk water radiolysis reactions discussed in the previous paragraph. Those studies concentrated on the elucidation of the reactions' mechanisms and on the calculation of reaction cross sections. In fact, SLEND has the potential to describe accurately at least three types of PCT reactions (cf. Fig. 3.13): (1) the aforesaid water radiolysis reactions, (2) H^+ collisions with DNA units (either by primary or secondary H^+), and (3) damage (strand breaks) of DNA units by electrons produced during water radiolysis. Examples of SLEND simulations of the first two types of reactions are given here. For instance, Fig. 3.14 presents the results from the collision of a H^+ projectile with $(H_2O)_4$ at $E_{Lab} = 1$ keV simulated at the SLEND + ECP/SBKJC level with CSDYN. That simulation predicts the collision of the H^+ projectile with a H_2O molecule's oxygen atom resulting in the cleavage of both O—H bonds of this H_2O molecule and producing in total from the water cluster two H, one O, one OH, one H_2O, and one H_3O species. Figure 3.15 presents the collision of a H^+ projectile with $(H_2O)_3$ at $E_{Lab} = 1$ keV simulated at the SLEND/6-31G** level. That figure shows the H^+ projectile traversing the

Author's personal copy

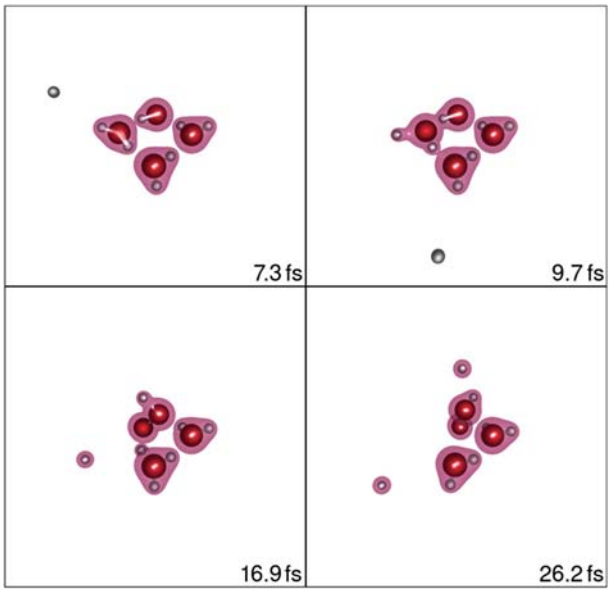

Figure 3.14 Snapshots of $H^+ + (H_2O)_4$ collision at $E_{Lab} = 1$ keV from a SLEND + ECP simulation with the SBKJC basis set. O and H nuclei are represented by red and white spheres, respectively, and a selected electron density isosurface by a pink cloud.

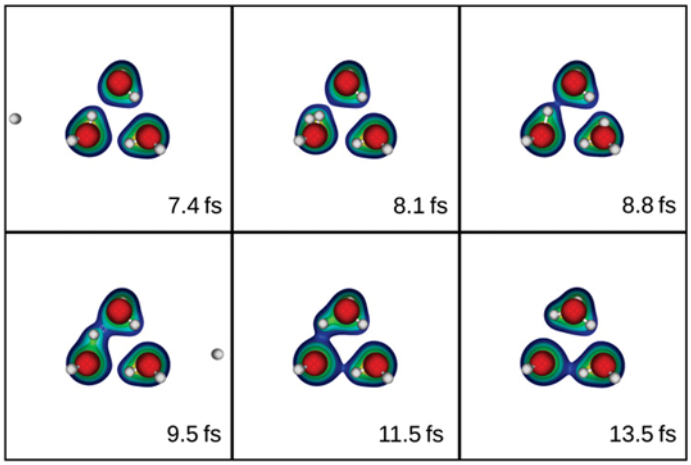

Figure 3.15 Snapshots of $H^+ + (H_2O)_3$ collision at $E_{Lab} = 1$ keV from a SLEND simulation using with the 6-31G** basis set. O and H nuclei are represented by red and white spheres, respectively, and selected electron density isosurfaces by different colored clouds.

Author's personal copy

space between the upper H_2O and the lower $(H_2O)_2$, colliding with and transferring one H from the left lower H_2O to the upper H_2O, and producing a $(H_3O)(OH)(H_2O)$ final cluster. It is equally clear from Figs. 3.14 and 3.15 that no appreciable ET occurs between the projectiles and the clusters.

Primary and secondary H^+ collisions on DNA provide another mechanism by which PCT can work. Due to the size of DNA molecules, SLEND simulations starting with a well-separated and noninteracting pair of reactants H^+ and DNA and ending up with well-separated and noninteracting products are wholly intractable at this time, even with PACE. However, as with H^+ collisions with the water medium, H^+ collisions with DNA may be approximately modeled by H^+ collisions with DNA units such as single nucleobases, nucleobase pairs, nucleosides, nucleotides, etc. Indeed, other research groups have used this approach to calculate ET and ionization cross sections using single center basis methods[139,140] and fixed target nuclei.[136,139,141–144] Though there have been studies of the dynamical fragmentation processes as well,[145] they were conducted without the presence of the proton and with an assumed initial ionized state from which to start the dynamics calculations, thus ultimately limiting the accuracy of the results. In contrast, the SLEND simulations would entail the actual collision of a H^+ projectile with a DNA unit. Figure 3.16 shows snapshots from the collision between a 1-keV H^+ projectile and the DNA nucleobase cytosine taken from a SLEND/STO-3G simulation. The latter started with the cytosine molecule at its UHF ground-state equilibrium geometry at rest having its CM on the origin of the laboratory frame and with the H^+ projectile travelling rectilinearly toward the O atom of cytosine. That simulation was performed with CSDYN. Figure 3.16 shows the breaking of the C—O bond of cytosine upon collision and substantial electron transfer from cytosine to the H^+ projectile.

The satisfactory simulation of a H^+ collision with cytosine at $E_{Lab} = 1\,keV$ with the resulting molecular fragmentation encourages using SLEND with large DNA-related systems. Toward that end, a SLEND/STO-3G simulation of a H^+ collision with the cytosine–guanine (CG) nucleobase pair at $E_{Lab} = 1\,keV$ was performed with CSDYN. As with the H^+-cytosine simulation, the CG pair was initialized at its UHF ground-state equilibrium geometry at rest having its CM at the origin of the laboratory frame. Additionally, the H^+ projectile was initialized with its momentum vector on the CG (nearly) plane and directed at the O of cytosine and through the CG bridge. Select snapshots from this simulation are shown in Fig. 3.17. Like the cytosine case, Fig. 3.17 shows substantial

Author's personal copy

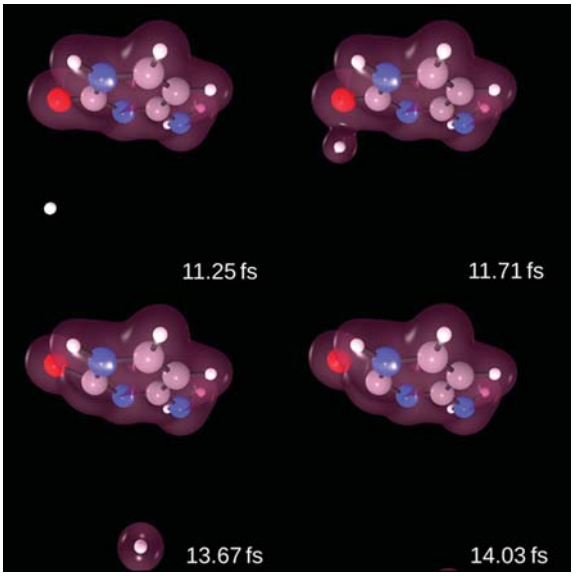

Figure 3.16 Snapshots of a $H^+ +$ cytosine collision at $E_{Lab} = 1$ keV from a SLEND simulation using the STO-3G basis set. O, C, N, and H nuclei are represented by red, gray, blue, and white spheres, respectively, and a selected electron density isosurface by a purple cloud.

electron transfer from the CG pair to the H^+ projectile. Furthermore, while there is no evidence of a violent dissociation, on close inspection it is revealed that the central hydrogen on the pair bridge migrates away from the N(3) atom of cytosine and toward the N(1) atom of guanine. Unfortunately, the duration of the $H^+ +$ CG simulation was insufficient to draw any definitive conclusion about what final process that H atom migration leads to. It may be the beginning of the CG pair splitting into cytosine and guanine or it may simply be a vibration of that H atom between the cytosine N(3) and guanine N(1) atoms.

Although the PCT studies presented herein have been qualitative, they nevertheless suggest that SLEND can be successfully used to model H^+ collisions with water and biomolecules that are relevant for PCT. Toward that end, quantitative studies of H^+ collisions with aqueous clusters $(H_2O)_n$, $n = 1 - 6$, and various nucleobases are in progress. Those quantitative studies have become tractable through the use of our new program PACE. It is expected that those ongoing studies will accurately predict dynamical properties such as ET ICSs *inter alia*.

Author's personal copy

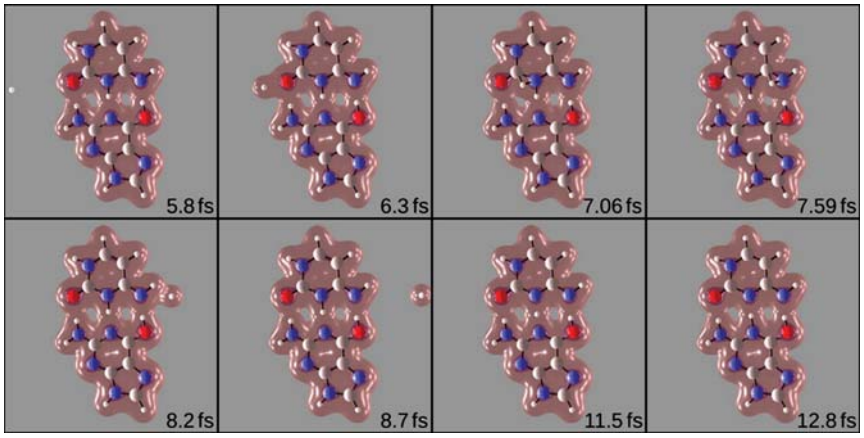

Figure 3.17 Snapshots of a $H^+ + CG$ collision at $E_{Lab} = 1$ keV from a SLEND simulation using the STO-3G basis set. O, C, N, and H nuclei are represented by red, gray, blue, and white spheres, respectively, and a selected electron density isosurface by a purple cloud.

6. SUMMARY

Recent developments in the SLEND method conducted in the Morales research group have been presented and discussed in detail. As an END realization, SLEND is a time-dependent, variational, direct, and nonadiabatic dynamics method that describes the nuclei and electrons of a molecular system simultaneously. Being at the lowest end of the hierarchy of END realizations, SLEND adopts nuclear classical dynamics and an electronic Thouless single-determinantal state. Due to its computational feasibility, SLEND has become the *de facto* END version at the time to perform applications to chemical systems. In that regard, SLEND has proved quite accurate for the simulation of various types of gas-phase chemical reactions at intermediate and high collision energies. Despite that success, SLEND may perform unsatisfactorily whenever its restriction to nuclear classical dynamics and/or its insufficient levels of electron correlation in its single-determinantal representation become inadequate to treat more demanding system. High-level END realizations can overcome the SLEND shortcomings through the adoption of a nuclear quantum description and more correlated electronic wavefunctions, but those solutions come at a very high computational cost. With a view toward ultimately treating large systems of biochemical relevance, we pursued more practical solutions that

Author's personal copy

retain SLEND's feasibility due to its classical dynamics and single-determinantal representation but nevertheless overcome its limitations. Therefore, to improve the SLEND electronic description, we developed a novel SLEND/KSDFT method wherein appropriate electron correlation is included within a feasible single-determinantal representation through TD KSDFT procedures. In addition, to improve the SLEND nuclear description, we augmented a CSQRP to recover quantum state-to-state transition probability amplitudes from the SLEND nuclear classical dynamics. This improved CSQRP features vibrational canonical (harmonic), vibrational Morse, rotational, and electronic CS sets, with the first two sets being fully implemented and the last two in advanced stages of theoretical development and testing. Finally, we improved the SLEND computational performance by incorporating ECPs in its framework and implementing our models in our new code PACE. PACE is a sophisticated code that utilizes state-of--the-art techniques in computer science and electronic structure computations such as the Python language for logical operations, FORTRAN and C++ languages for intensive numerical computations, intra- and inter-node code parallelization, a CUDA implementation, and the fast atomic integral package by Lotrich et al.[119] The new SLEND developments have been applied to a vast array of scattering systems and chemical reactions in the gas phase at intermediate and high collision energies. SLEND in conjunction with CSQRP has been applied with the canonical CS to study $H^+ + N_2$, $H^+ + CO$, and $H^+ + CO_2$ at/near $E_{Lab} = 30\,eV$ and with various Morse CSs to $H^+ + CO$ and $H^+ + NO$ at $E_{Lab} = 30\,eV$. Those simulations produced reconstructed quantum vibrational state-to-state properties in very good agreement with results from experiments and from theoretical methods utilizing onerous quantum nuclear treatments and/or high-level PESs. SLEND/KSDFT has been successfully applied to the simulation of molecular vibrations and the archetypical Diels–Alder reaction $C_2H_4 + C_4H_6 \rightarrow C_8H_{10}$. The power of the ECP implementation has been illustrated with a SLEND + ECP simulation of the S_N2 reaction: $CH_3Br + F^- \rightarrow CH_3F + Br^-$ at $E_{Lab} = 20\,eV$. However, the most promising applications of our new SLEND developments concern reactions in PCT. For instance, SLEND simulations of $H^+ + (H_2O)_3$ and $H^+ + (H_2O)_4$ at $E_{Lab} = 1\,keV$ were conducted as prototypes of the water radiolysis reactions in PCT; these simulations predicted the formation of DNA-damaging species such as OH radicals. In addition, SLEND simulations of $H^+ +$ cytosine and $H^+ +$ cytosine − guanine at $E_{Lab} = 1\,keV$ were conducted as prototypes of the DNA damage reactions by primary or secondary H^+'s in PCT. Present

Author's personal copy

research efforts concentrate on the full implementation and testing of the rotational and electronic VB CS sets into the CSQRP and on systematic SLEND and SLEND/KSDFT investigations of additional reactions in PCT.

ACKNOWLEDGMENTS

The authors would like to thank Prof. John R. Sabin (University of Florida) for his kind invitation to submit this chapter to *Advances in Quantum Chemistry*. The authors are indebted to Dr. S. Ajith Perera (University of Florida and Texas Tech University: TTU) for many useful discussions on electronic structure theory (electron correlation effects, DFT, ECPs, etc.) and on high-performance programming. All the present calculations have been conducted at the TTU High Performance Computer Center (TTU HPCC) and the TTU Chemistry Computer Cluster (TTU CCC). This material is based upon work partially supported by the National Science Foundation under grants CHE-0645374 (CAREER) and CHE-0840493 (Instrumentation: TTU CCC), by the Robert A. Welch Foundation under grant D-1539, and by an award from the Research Corporation. In addition, acknowledgment is made to the donors of the American Chemical Society Petroleum Research fund for partial support of this research.

REFERENCES

1. Deumens, E.; Diz, A.; Longo, R.; Öhrn, Y. Time-Dependent Theoretical Treatments of the Dynamics of Electrons and Nuclei in Molecular Systems. *Rev. Mod. Phys.* **1994**, *66*, 917–983.
2. Deumens, E.; Ohrn, Y. Wavefunction Phase Space: An Approach to the Dynamics of Molecular Systems. *J. Chem. Soc., Faraday Trans.* **1997**, *93*, 919–929.
3. Deumens, E.; Öhrn, Y. Complete Electron Nuclear Dynamics. *J. Phys. Chem. A* **2001**, *105*, 2660–2667.
4. Wang, I. S. Y.; Karplus, M. Dynamics of Organic Reactions. *J. Am. Chem. Soc.* **1973**, *95*, 8160–8164.
5. Leforestier, C. Classical Trajectories Using the Full Ab Initio Potential Energy Surface $H^- + CH_4 \rightarrow CH_4 + H^-$. *J. Chem. Phys.* **1978**, *68*, 4406–4410.
6. Car, R.; Parrinello, M. Unified Approach for Molecular Dynamics and Density-Functional Theory. *Phys. Rev. Lett.* **1985**, *55*, 2471–2474.
7. Bolton, K.; Hase, W. L.; Peslherbe, G. H. Direct Dynamics Simulations of Reactive Systems. In *Multidimensional Molecular Dynamics Methods*; Thompson, D. L., Ed.; World Scientific Publishing: London, 1998; pp 143–189.
8. Sun, L.; Hase, W. L. Born-Oppenheimer Direct Dynamics Classical Trajectories Simulations. In Lipkowitz, K. B., Larter, R., Cundari, T. R., Eds.; Reviews in Computational Chemistry, Vol. 19; Wiley: New York, 2003; pp 79–146.
9. Schatz, G. C. Quasiclassical Trajectory Studies of State to State Collisional Energy Transfer in Polyatomic Molecules. In Bowman, J. M., Ed.; Molecular Collision Dynamics, Vol. 33; Springer: Berlin Heidelberg, 1983; pp 25–60.
10. Schinke, R.; McGuire, P. Combined Rotationally Sudden and Vibrationally Exact Quantum Treatment of Proton-H2 Collisions. *Chem. Phys.* **1978**, *31*, 391–412.
11. Kramer, P.; Saraceno, M. *Geometry of the Time-Dependent Variational Principle in Quantum Mechanics*; Springer-Verlag: New York, 1981.
12. Meyer, H. D.; KuCar, J.; Cederbaum, L. S. Time-Dependent Rotated Hartree: Formal Development. *J. Math. Phys.* **1988**, *29*, 1417–1430.

Author's personal copy

13. Kay, K. G. The Matrix Singularity Problem in the Time-Dependent Variational Method. *Chem. Phys.* **1989**, *137*, 165–175.
14. Kay, K. G. Hamiltonian Formulation of Quantum Mechanics with Semiclassical Implications. II. Variational Treatment. *Phys. Rev. A* **1992**, *46*, 1213–1232.
15. Thouless, D. J. Stability Conditions and Nuclear Rotations in the Hartree-Fock Theory. *Nucl. Phys.* **1960**, *21*, 225–232.
16. Klauder, J. R.; Skagerstam, B.-S. *Coherent States: Applications in Physics and Mathematical Physics*; World Scientific: Singapore, 1985.
17. Schrödinger, E. Der Stetige Übergang von der Mikro-zur Makromechanik. *Naturwissenschaften* **1926**, *14*, 664–666.
18. Heller, E. J. Time-Dependent Approach to Semiclassical Dynamics. *J. Chem. Phys.* **1975**, *62*, 1544–1555.
19. Herman, M. F.; Kluk, E. A Semiclassical Justification for the Use of Non-spreading Wavepackets in Dynamics Calculations. *Chem. Phys.* **1984**, *91*, 27–34.
20. Miller, W. H. On the Relation Between the Semiclassical Initial Value Representation and an Exact Quantum Expansion in Time-Dependent Coherent States. *J. Phys. Chem. B* **2002**, *106*, 8132–8135.
21. Giese, C. F.; Gentry, W. R. Classical Trajectory Treatment of Inelastic Scattering in Collisions of H^{+} with H_{2}, HD, and D_{2}. *Phys. Rev. A* **1974**, *10*, 2156–2173.
22. Morales, J. A. Some Coherent-States Aspects of the Electron Nuclear Dynamics Theory: Past and Present. *Mol. Phys.* **2010**, *108*, 3199–3211.
23. Morales, J. A.; Diz, A. C.; Deumens, E.; Öhrn, Y. Molecular Vibrational State Distributions in Collisions. *Chem. Phys. Lett.* **1995**, *233*, 392–398.
24. Morales, J.; Diz, A.; Deumens, E.; Ohrn, Y. Electron Nuclear Dynamics of $H^+ + H_2$ Collisions at E_{lab}=30 eV. *J. Chem. Phys.* **1995**, *103*, 9968–9980.
25. Stopera, C.; Maiti, B.; Morales, J. A. $H^+ + NO(vi=0) = H^+ + NO(vf=0\text{-}2)$ at E_{Lab}=30 eV with Canonical and Morse Coherent States. *Chem. Phys. Lett.* **2012**, *551*, 42–49.
26. Morales, J. A.; Deumens, E.; Ohrn, Y. On Rotational Coherent States in Molecular Quantum Dynamics. *J. Math. Phys.* **1999**, *40*, 766–786.
27. Jacquemin, D.; Morales, J. A.; Deumens, E.; Ohrn, Y. Electron Nuclear Dynamics of Proton Collisions with Methane at 30 eV. *J. Chem. Phys.* **1997**, *107*, 6146–6155.
28. Hedström, M.; Morales, J. A.; Deumens, E.; Öhrn, Y. Electron Nuclear Dynamics of $H^+ + H_2O$ Collisions. *Chem. Phys. Lett.* **1997**, *279*, 241–246.
29. Malinovskaya, S. A.; Cabrera-Trujillo, R.; Sabin, J. R.; Deumens, E.; Ohrn, Y. Dynamics of Proton-Acetylene Collisions at 30 eV. *J. Chem. Phys.* **2002**, *117*, 1103–1108.
30. Morales, J. A.; Maiti, B.; Yan, Y.; Tsereteli, K.; Laraque, J.; Addepalli, S.; Myers, C. Coherent-States Dynamics of the $H^+ + C_2H_2$ Reaction at $E_{Lab} = 30$ eV: A Complete Electron Nuclear Dynamics Investigation. *Chem. Phys. Lett.* **2005**, *414*, 405–411.
31. Maiti, B.; Sadeghi, R.; Austin, A.; Morales, J. A. Coherent-States Dynamics of the $H^+ + HF$ Reaction at $E_{Lab} = 30$eV: A Complete Electron Nuclear Dynamics Investigation. *Chem. Phys.* **2007**, *340*, 105–119.
32. Maiti, B.; McLaurin, P. M.; Sadeghi, R.; Ajith Perera, S.; Morales, J. A. Dynamics for the Dynamic Frank Harris: Exploring $H^+ + CF_4$ at $E_{lab} = 20$ and 30 eV. *Int. J. Quantum Chem.* **2009**, *109*, 3026–3035.
33. Stopera, C.; Maiti, B.; Grimes, T. V.; McLaurin, P. M.; Morales, J. A. Dynamics of $H^+ + N_2$ at $E_{Lab} = 30$ eV. *J. Chem. Phys.* **2011**, *134*, 224308.
34. Stopera, C.; Maiti, B.; Grimes, T. V.; McLaurin, P. M.; Morales, J. A. Dynamics of $H^+ + CO$ at $E_{Lab} = 30$ eV. *J. Chem. Phys.* **2012**, *136*, 054304.
35. Cabrera-Trujillo, R.; Öhrn, Y.; Deumens, E.; Sabin, J. R. Application of the END Theory to the $H + D_2 \rightarrow HD + D$ Reaction. *J. Phys. Chem. A* **2004**, *108*, 8935–8940.

Author's personal copy

36. Coutinho-Neto, M.; Deumens, E.; Öhrn, Y. Selective Bond Breaking in H+HOD Reaction. *Int. J. Quantum Chem.* **2000**, *77*, 301–304.
37. Coutinho-Neto, M.; Deumens, E.; Öhrn, Y. Abstraction and Exchange Mechanisms for the $D_2 + NH_3^+$ Reaction at Hyperthermal Collision Energies. *J. Chem. Phys.* **2002**, *116*, 2794–2802.
38. McWeeny, R. *Methods of Molecular Quantum Mechanics*; 2nd ed.; Academic Press: London, 1992.
39. Deumens, E.; Ohrn, Y.; Weiner, B. Coherent State Formulation of Multiconfiguration States. *J. Math. Phys.* **1991**, *32*, 1166–1175.
40. Nest, M. The Multi-Configuration Electron–Nuclear Dynamics Method. *Chem. Phys. Lett.* **2009**, *472*, 171–174.
41. Ulusoy, I. S.; Nest, M. Remarks on the Validity of the Fixed Nuclei Approximation in Quantum Electron Dynamics. *J. Phys. Chem. A* **2012**, *116*, 11107–11110.
42. Ulusoy, I. S.; Nest, M. The Multi-Configuration Electron-Nuclear Dynamics Method Applied to LiH. *J. Chem. Phys.* **2012**, *136*, 054112–054116.
43. Pedersen, T. B.; Koch, H. On the Time-Dependent Lagrangian Approach in Quantum Chemistry. *J. Chem. Phys.* **1998**, *108*, 5194–5204.
44. Bartlett, R. J.; Musiał, M. Coupled-Cluster Theory in Quantum Chemistry. *Rev. Mod. Phys.* **2007**, *79*, 291–352.
45. Chakraborty, A.; Pak, M. V.; Hammes-Schiffer, S. Development of Electron-Proton Density Functionals for Multicomponent Density Functional Theory. *Phys. Rev. Lett.* **2008**, *101*, 153001.
46. Nakai, H.; Sodeyama, K. Many-Body Effects in Nonadiabatic Molecular Theory for Simultaneous Determination of Nuclear and Electronic Wave Functions: Ab Initio NOMO/MBPT and CC Methods. *J. Chem. Phys.* **2003**, *118*, 1119–1127.
47. Webb, S. P.; Iordanov, T.; Hammes-Schiffer, S. Multiconfigurational Nuclear-Electronic Orbital Approach: Incorporation of Nuclear Quantum Effects in Electronic Structure Calculations. *J. Chem. Phys.* **2002**, *117*, 4106–4118.
48. Solov'yov, A. V.; Surdutovich, E.; Scifoni, E.; Mishustin, I.; Greiner, W. Physics of Ion Beam Cancer Therapy: A Multiscale Approach. *Phys. Rev. E* **2009**, *79*, 011909.
49. Perera, S. A.; McLaurin, P. M.; Grimes, T. V.; Morales, J. A. Time-Dependent Density-Functional Theory Method in the Electron Nuclear Dynamics Framework. *Chem. Phys. Lett.* **2010**, *496*, 188–195.
50. Runge, E.; Gross, E. K. U. Density-Functional Theory for Time-Dependent Systems. *Phys. Rev. Lett.* **1984**, *52*, 997–1000.
51. Morales, J. A. Valence-Bond/Coherent-States Approach to the Charge Equilibration Model I. Valence-Bond Models for Diatomic Molecules. *J. Phys. Chem. A* **2009**, *113*, 6004–6015.
52. Grimes, T. V.; Morales, J. A. *PACE: Python Accelerated Coherent-States Electron Nuclear Dynamics, 1.0*; Texas Tech University: Lubbock, TX, 2010.
53. Flocke, N.; Lotrich, V. Efficient Electronic Integrals and Their Generalized Derivatives for Object Oriented Implementations of Electronic Structure Calculations. *J. Comput. Chem.* **2008**, *29*, 2722–2736.
54. Goldstein, H. *Classical Mechanics*; 2nd ed.; Addison-Wesley: Reading, MA, 1980.
55. Thouless, D. J. *The Quantum Mechanics of Many-Body Systems*; 2nd ed.; Academic Press: New York and London, 1972.
56. Cohen-Tannoudji, C.; Diu, B.; Laloë, F. *Quantum Mechanics*. Vol. 1. Wiley-VCH: Singapore, 1977; Vol. 1–2.
57. Grimes, T. V.; Privett, A.; Morales, J. A. PACE: Python Accelerated Coherent-States Electron Nuclear Dynamics. J. Chem. Phys. 2013, in preparation.
58. Longo, R.; Diz, A.; Deumens, E.; Ohrn, Y. Influence of Electronic Nuclear Coupling on Dynamics. *Chem. Phys. Lett.* **1994**, *220*, 305–311.

Author's personal copy

59. Gross, E. K. U.; Kohn, W. Time-Dependent Density-Functional Theory. In Per-Olov, L., Ed.; Advances in Quantum Chemistry, Vol. 21; Academic Press: New York, 1990; pp 255–291.
60. Gross, E. K. U.; Dobson, J. F.; Petersilka, M. Density Functional Theory of Time-Dependent Phenomena. In Nalewajaki, R. F., Ed.; Topics in Current Chemistry, Vol. 181; Springer: Berlin, 1996; pp 81–172.
61. Marques, M. A. L.; Gross, E. K. U. Time-Dependent Density Functional Theory. *Annu. Rev. Phys. Chem.* **2004**, *55*, 427–455.
62. Theilhaber, J. Ab Initio Simulations of Sodium Using Time-Dependent Density-Functional Theory. *Phys. Rev. B.* **1992**, *46*, 12990–13003.
63. Hohenberg, P.; Kohn, W. Inhomogeneous Electron Gas. *Phys. Rev.* **1964**, *136*, 864–871.
64. Kohn, W.; Sham, L. J. Self-Consistent Equations Including Exchange and Correlation Effects. *Phys. Rev.* **1965**, *140*, A1133–A1138.
65. van Leeuwen, R. Causality and Symmetry in Time-Dependent Density-Functional Theory. *Phys. Rev. Lett.* **1998**, *80*, 1280–1283.
66. van Leeuwen, R. Key Concepts in Time-Dependent Density-Functional Theory. *Int. J. Mod. Phys. B* **2001**, *15*, 1969–2023.
67. Parr, R. G.; Yang, W. *Density-Functional Theory of Atoms and Molecules*; Oxford University Press: New York, 1989.
68. Szabo, A.; Ostlund, N. S. *Modern Quantum Chemistry: Introduction to Advanced Electronic Structure Theory*; 1st rev ed.; Dover Publications, Inc.: Mineola, NY, 1989.
69. Rajagopal, A. K. Time-Dependent Variational Principle and the Effective Action in Density-Functional Theory and Berry's Phase. *Phys. Rev. A* **1996**, *54*, 3916–3922.
70. Mukamel, S. Generalized Time-Dependent Density-Functional-Theory Response Functions for Spontaneous Density Fluctuations and Nonlinear Response: Resolving the Causality Paradox in Real Time. *Phys. Rev. A* **2005**, *71*, 024503.
71. Vignale, G.; Kohn, W. Current-Dependent Exchange-Correlation Potential for Dynamical Linear Response Theory. *Phys. Rev. Lett.* **1996**, 77, 2037–2040.
72. Skylaris, C.-K. ; Gagliardi, L.; Handy, N. C.; Ioannou, A. G.; Spencer, S.; Willetts, A.; Simper, A. M. An Efficient Method for Calculating Effective Core Potential Integrals Which Involve Projection Operators. *Chem. Phys. Lett.* **1998**, *296*, 445–451.
73. Krauss, M.; Stevens, W. J. Effective Potentials in Molecular Quantum Chemistry. *Annu. Rev. Phys. Chem.* **1984**, *35*, 357–385.
74. McMurchie, L. E.; Davidson, E. R. Calculation of Integrals Over Ab Initio Pseudopotentials. *J. Comput. Phys.* **1981**, *44*, 289–301.
75. Grimes, T. V.; McLaurin, P. M.; Morales, J. A. Evaluation of Effective Core Potential Integrals Optimized for Dynamics. J. Comput. Chem. 2013, in preparation.
76. Child, M. S. *Molecular Collision Theory*; 1st ed.; Academic Press, Inc.: New York, 1974.
77. Connor, J. N. L.; Farrelly, D. Theory of Cusped Rainbows in Elastic Scattering: Uniform Semiclassical Calculations Using Pearcey's Integral. *J. Chem. Phys.* **1981**, *75*, 2831–2846.
78. McLaurin, P. M. New Applications of the Electron Nuclear Dynamics Theory to Scattering Processes and Chemical Reactions: Tool Development, Method Validation, and Computer Simulation. PhD Thesis, Texas Tech University, Lubbock, 2012.
79. Kais, S.; Levine, R. D. Coherent States for the Morse Oscillator. *Phys. Rev. A* **1990**, *41*, 2301–2305.
80. Dong, S. H. The SU(2) Realization for the Morse Potential and Its Coherent States. *Can. J. Phys.* **2002**, *80*, 129–139.
81. Nieto, M.; Simmons, L. M., Jr. Coherent States for General Potentials. III. Nonconfining One-Dimensional Examples. *Phys. Rev. D* **1979**, *20*, 1342–1350.

Author's personal copy

82. Roy, B.; Roy, P. Gazeau–Klauder Coherent State for the Morse Potential and Some of Its Properties. *Phys. Lett. A* **2002**, *296*, 187–191.
83. Popov, D. Gazeau–Klauder Quasi-Coherent States for the Morse Oscillator. *Phys. Lett. A* **2003**, *316*, 369–381.
84. Hecht, K. T. *The Vector Coherent State Method and Its Applications to Problems of Higher Symmetries*; Springer: New York, 1987.
85. Bowen, J. P.; Allinger, N. L. Molecular Mechanics: The Art and Science of Parameterization. In Lipkowitz, K. B., Boyd, D. B., Eds.; Reviews in Computational Chemistry, Vol. 2; VCH Publishers, Inc.: New York, 1991; pp 81–97.
86. Warshel, A.; Levitt, M. Theoretical Studies of Enzymic Reactions: Dielectric, Electrostatic and Steric Stabilization of the Carbonium Ion in the Reaction of Lysozyme. *J. Mol. Biol.* **1976**, *103*, 227–249.
87. Warshel, A. *Computer Modeling of Chemical Processes in Enzymes and Solutions*; 1st ed.; Wiley: New York, 1991.
88. Field, M. J.; Bash, P. A.; Karplus, M. A Combined Quantum Mechanical and Molecular Mechanical Potential for Molecular Dynamics Simulations. *J. Comput. Chem.* **1990**, *11*, 700–733.
89. Day, P. N.; Jensen, J. H.; Gordon, M. S.; Webb, S. P.; Stevens, W. J.; Krauss, M.; Garmer, D.; Basch, H.; Cohen, D. An Effective Fragment Method for Modeling Solvent Effects in Quantum Mechanical Calculations. *J. Chem. Phys.* **1996**, *105*, 1968–1986.
90. Rappé, A. K.; Goddard, W. A., III. Charge Equilibration for Molecular Dynamics Simulations. *J. Phys. Chem.* **1991**, *95*, 3358–3363.
91. Itskowitz, P.; Berkowitz, M. L. Chemical Potential Equalization Principle: Direct Approach from Density Functional Theory. *J. Phys. Chem. A* **1997**, *101*, 5687–5691.
92. Gazeau, J. P.; Klauder, J. R. Coherent States for Systems with Discrete and Continuous Spectrum. *J. Phys. A Math. Gen.* **1999**, *32*, 123–132.
93. Barut, A. O.; Girardello, L. New "Coherent" States Associated with Non-Compact Groups. *Commun. Math. Phys.* **1971**, *21*, 41–55.
94. Nieto, M. M.; Simmons, L. M., Jr. Coherent States from General Potentials. I. Formalism. *Phys. Rev. D* **1979**, *20*, 1321–1331.
95. Perelomov, A. *Generalized Coherent States and Their Applications*. Springer-Verlag: Berlin, 1986, p 320.
96. Gilmore, R. Geometry of Symmetrized States. *Ann. Phys.* **1972**, *74*, 391–463.
97. Zhang, W. M.; Feng, D. H.; Gilmore, R. Coherent States: Theory and Some Applications. *Rev. Mod. Phys.* **1990**, *62*, 867–927.
98. Gilmore, R. *Lie Groups, Lie Algebras, and Some of Their Applications*; Wiley & Sons: New York, 1974.
99. Popov, D.; Pop, N.; Chiritoiu, V.; Luminosu, I.; Costache, M. Generalized Barut-Girardello Coherent States for Mixed States with Arbitrary Distribution. *Int. J. Theor. Phys.* **2010**, *49*, 661–680.
100. Nieto, M.; Simmons, L. M., Jr. Coherent States for General Potentials. II. Confining One-Dimensional Examples. *Phys. Rev. D* **1979**, *20*, 1332–1341.
101. Nieto, M. M. Coherent States for General Potentials. IV. Three-Dimensional Systems. *Phys. Rev. D* **1980**, *22*, 391–402.
102. Nieto, M. M.; Gutschick, V. P. Coherent States for General Potentials. V. Time Evolution. *Phys. Rev. D* **1980**, *22*, 403–418.
103. Robertson, H. P. The Uncertainty Principle. *Phys. Rev.* **1929**, *34*, 163–164.
104. Wilson, B. E.; Decius, J. C.; Cross, P. *Molecular Vibrations*; 1st ed.; Dover Publications, Inc.: New York, 1955.
105. Iachello, F.; Levine, R. D. *Algebraic Theory of Molecules*. Oxford University Press: New York, 1995.

Author's personal copy

106. Niedner, G.; Noll, M.; Toennies, J. P.; Schlier, C. Observation of Vibrationally Resolved Charge Transfer in $H^+ + H_2$ at E_{CM}=20 eV. *J. Chem. Phys.* **1987**, *87*, 2685–2694.
107. Baer, M.; Niednerschatteburg, G.; Toennies, J. P. A 3-Dimensional Quantum-Mechanical Study of Vibrationally Resolved Charge-Transfer Processes in $H^+ + H_2$ at E_{CM}=20 eV. *J. Chem. Phys.* **1989**, *91*, 4169–4182.
108. Krutein, J.; Linder, F. Measurements of Vibrational Excitation of N_2, CO, and NO by Low Energy Proton Impact. *J. Chem. Phys.* **1979**, *71*, 599–604.
109. McLaurin, P. M.; Morales, J. A. Dynamics of $H^+ + CO_2$ at E_{Lab} = 30 eV. *J. Chem. Phys.* **2013**, to be submitted.
110. Nieto, M. M.; Simmons, L. M., Jr. Eigenstates, Coherent States, and Uncertainty Products for the Morse Oscillator. *Phys. Rev. A* **1979**, *19*, 438–444.
111. Janssen, D. Coherent States of the Quantum-Mechanical Top. *Sov. J. Nucl. Phys.* **1977**, *25*, 479.
112. Zare, R. N. *Angular Momentum, Understanding Spatial Aspects in Chemistry and Physics*; Wiley-Interscience Publication: New York, 1988.
113. Irac-Astaud, M. Molecular-Coherent-States and Molecular-Fundamental-States. *Rev. Math. Phys.* **2001**,*13*, 1437–1457.
114. Perera, S. A.; Grimes, T. V.; Morales, J. A. CSDYN; Department of Chemistry and Biochemistry, Texas Tech University: Lubbock, TX, 2008–2012.
115. Deumens, E. ENDyne: Electron Nuclear Dynamics Simulations, Version 2 Release 8, 2.8. *Quantum Theory Project*; University of Florida: Gainesville, FL, 1997.
116. Cai, X.; Langtangen, H. P.; Moe, H. On the Performance of the Python Programming Language for Serial and Parallel Scientific Computations. *Sci. Program.* **2005**, *13*, 31–56.
117. Hinsen, K. High-Level Scientific Programming with Python Computational Science—ICCS 2002. In Sloot, P., Hoekstra, A., Tan, C., Dongarra, J., Eds.; Vol. 2331; Springer: Berlin/Heidelberg, 2002; pp 691–700.
118. Beazley, D. M.; Lomdahl, P. S. Building Flexible Large-Scale Scientific Computing Applications with Scripting Languages. In *Eighth SIAM Conference on Parallel Processing for Scientific Computing, March 14–17, 1997*, SIAM: Hyatt Regency Minneapolis on Nicollet Mall Hotel: Minneapolis, Minnesota, USA, 1997.
119. Lotrich, V.; Flocke, N.; Ponton, M.; Yau, A. D.; Perera, A.; Deumens, E.; Bartlett, R. J. Parallel Implementation of Electronic Structure Energy, Gradient, and Hessian Calculations. *J. Chem. Phys.* **2008**, *128*, 194104.
120. Lotrich, V.; Ponton, M.; Perera, S. A.; Deumens, E.; Bartlett, R. J.; Sanders, B. Super Instruction Architecture of Petascale Electronic Integrals and Their Generalized Derivatives for Object Oriented Implementations of Electronic Structure Calculations. *J. Comput. Chem.* **2010**, *29*, 3323–3330.
121. SWIG Simplified Wrapper and Interface Generator. http://www.swig.org/.
122. Intel Threading Building Blocks.
123. PyPar. http://code.google.com/p/pypar/.
124. Becke, A. D. A Multicenter Numerical Integration Scheme for Polyatomic Molecules. *J. Chem. Phys.* **1988**, *88*, 2547–2553.
125. Newville, M. *asteval*, 0.9, 2012.
126. Oliphant, T. E. Python for Scientific Computing. *Comput. Sci. Eng.* **2007**, *9*, 10–20.
127. Gianturco, F. A.; Kumar, S.; Ritschel, T.; Vetter, R.; Zulicke, L. Interaction Anisotropy and Vibrotational Excitation in Proton Scattering from $N_2\left(^1\sum_g^+\right)$. *J. Chem. Phys.* **1997**, *107*, 6634–6645.
128. Ritschel, T.; Mahapatra, S.; Zülicke, L. Quasiclassical Dynamics of Proton Scattering by $N_2(^1\Sigma_g^+)$ on an Improved Ab Initio Potential Energy Surface. *Chem. Phys.* **2001**, *271*, 155–164.

Author's personal copy

129. Kumar, T. J. D.; Kumar, S. Vibrationally Inelastic Collisions in H^+ + CO System: Comparing Quantum Calculations with Experiments. *J. Chem. Phys.* **2004**, *121*, 191–203.
130. Krutein, J.; Linder, F. Differential Scattering Experiments on Vibrational Excitation in Low-Energy H^+-CO_2 Collisions. *J. Phys. B At. Mol. Phys.* **1977**, *10*, 1363.
131. Noll, M.; Toennies, J. P. Vibrational State Resolved Measurements of Differential Cross Sections for H^+ + O_2 Charge Transfer Collisions. *J. Chem. Phys.* **1986**, *85*, 3313–3325.
132. Schmidt, M. W.; Baldridge, K. K.; Boatz, J. A.; Elbert, S. T.; Gordon, M. S.; Jensen, J. H.; Koseki, S.; Matsunaga, N.; Nguyen, K. A.; Su, S.; Windus, T. L.; Dupuis, M.; Montgomery, J. A. General Atomic and Molecular Electronic Structure System. *J. Comput. Chem.* **1993**, *14*, 1347–1363.
133. Levine, I. N. *Quantum Chemistry*, 6th ed.; Pearson Prentice Hall: Upper Saddle River, NJ, 2008.
134. Houk, K. N.; Lin, Y. T.; Brown, F. K. Evidence for the Concerted Mechanism of the Diels-Alder Reaction of Butadiene with Ethylene. *J. Am. Chem. Soc.* **1986**, *108*, 554–556.
135. Manikandan, P.; Zhang, J.; Hase, W. L. Chemical Dynamics Simulations of X^- + $CH_3Y \rightarrow XCH_3 + Y^-$ Gas-Phase S_N2 Nucleophilic Substitution Reactions. Nonstatistical Dynamics and Nontraditional Reaction Mechanisms. *J. Phys. Chem. A* **2012**, *116*, 3061–3080.
136. Pichl, L.; Kimura, M.; Yan, L.; Buenker, R. J. Branching Ratios for Secondary Processes of Water Ions Induced by Proton Beams in Radiation Therapy of Cancer. *IEEE Trans. Nucl. Sci.* **2004**, *51*, 1407–1411.
137. Surdutovich, E.; Gallagher, D. C.; Solov'yov, A. V. Calculation of Complex DNA Damage Induced by Ions. *Phys. Rev. E* **2011**, *84*, 051918.
138. Quinet, O.; Deumens, E.; Öhrn, Y. Proton Collisions with the Water Dimer at keV Energies. *Int. J. Quantum Chem.* **2008**, *109*, 259–265.
139. Lüdde, H. J.; Spranger, T.; Horbatsch, M.; Kirchner, T. Nonperturbative, Quantum-Mechanical Approach to Ion Collisions from Molecular Targets. *Phys. Rev. A* **2009**, *80*, 060702.
140. Dal Cappello, C.; Hervieux, P. A.; Charpentier, I.; Ruiz-Lopez, F. Ionization of the Cytosine Molecule by Protons: Ab Initio Calculation of Differential and Total Cross Sections. *Phys. Rev. A* **2008**, *78*, 042702.
141. Lekadir, H.; Abbas, I.; Champion, C.; Hanssen, J. Total Cross Sections for Ionizing Processes Induced by Proton Impact on Molecules of Biological Interest: A Classical Trajectory Monte Carlo Approach. *Nucl. Instrum. Methods Phys. Res., Sect. B* **2009**, *267*, 1011–1014.
142. Illescas, C.; Errea, L. F.; Méndez, L.; Pons, B.; Rabadán, I.; Riera, A. Classical Treatment of Ion-H_{2}O Collisions with a Three-Center Model Potential. *Phys. Rev. A* **2011**, *83*, 052704.
143. Dubois, A.; Carniato, S.; Fainstein, P. D.; Hansen, J. P. Ionization of Water Molecules by Fast Charged Projectiles. *Phys. Rev. A* **2011**, *84*, 012708.
144. Bacchus-Montabonel, M.-C. ; Tergiman, Y. S. Radiation Damage on Biomolecular Systems: Dynamics of Ion Induced Collision Processes. *Comput. Theor. Chem.* **2012**, *990*, 177–184.
145. López-Tarifa, P.; Hervé du Penhoat, M. A.; Vuilleumier, R.; Gaigeot, M. P.; Tavernelli, I.; Le Padellec, A.; Champeaux, J. P.; Alcamí, M.; Moretto-Capelle, P.; Martín, F.; Politis, M. F. Ultrafast Nonadiabatic Fragmentation Dynamics of Doubly Charged Uracil in a Gas Phase. *Phys. Rev. Lett.* **2011**, *107*, 023202.